

Structural and functional characterization of PhzO and TcpA, two members of the two-component flavin-diffusible monooxygenase family

DISSERTATION

zur Erlangung des akademischen Grades
eines Doktors der Naturwissenschaften (Dr. rer. nat.)
des Fachbereichs Chemie der Technischen Universität Dortmund

angefertigt am Max-Planck-Institut für molekulare Physiologie
Dortmund

vorgelegt von

Emerich Mihai Gazdag

Dortmund 2011

Die vorliegende Arbeit wurde in der Zeit von Januar 2007 bis Dezember 2010 am Max-Planck-Institut für Molekulare Physiologie in Dortmund unter der Anleitung von Prof. Dr. Wulf Blankenfeldt und Prof. Dr. Roger S. Goody durchgeführt.

1. Gutachter: Prof. Dr. W. Blankenfeldt

2. Gutachter: Prof. Dr. R. Winter

TABLE OF CONTENTS

TABLE OF CONTENTS..... I

SYMBOLS AND ABBREVIATIONS V

1. INTRODUCTION 1

 1.1 GENERAL ASPECTS 1

 1.2 MONOOXYGENASES A CLASS OF ENZYMES WITH GREAT POTENTIAL..... 2

 1.2.1 Monooxygenases..... 2

 1.2.2 Activation mode 4

 1.3 BIOCATALYSIS 7

 1.4 BACTERIA PSEUDOMONAS AND CUPRIAVIDUS 8

 1.4.1 Pseudomonas sp. 8

 1.4.2 Cupriavidus necator..... 9

 1.5 POLYCHLOROPHENOLS 10

 1.5.1 PCPs 10

 1.5.2 TCP..... 11

 1.6 BIODEGRADATION..... 12

 1.7 PHENAZINES, PCA AND ITS DERIVATIVES..... 13

 1.7.1 Phenazines 13

 1.7.2 Phenazine biosynthesis 15

 1.8 THE BIOCATALYSTS PHZO AND TCPA..... 17

 1.8.1 PhzO 17

 1.8.2 TcpA 19

 1.9 4-HYDROXYPHENYLACETATE 3-MONOOXYGENASE - HPAB 21

3. AIMS OF THIS WORK 23

4. MATERIALS AND METHODS..... 24

 4.1 MATERIALS 24

 4.1.1 Chemicals..... 24

 4.1.2 Other materials 26

4.1.3	Instruments.....	27
4.1.4	Buffers and growth media.....	28
4.2	MOLECULAR CLONING METHODS	30
4.2.1	General aspects	30
4.2.2	Plasmids and bacterial strains.....	30
4.2.2.1	Expression vector.....	30
4.2.2.2	Bacterial strains	31
4.2.3	Polymerase chain reaction (PCR)	32
4.2.4	Preparative PCR	32
4.3	SUBCLONING	33
4.3.1	Restriction	33
4.3.2	Ligation of DNA fragments into a vector.....	34
4.3.3	Transformation	35
4.3.4	Colony PCR screen	35
4.3.5	Isolation of plasmid DNA.....	36
4.3.6	DNA sequencing.....	36
4.3.7	Glycerol stock	37
4.4	PROTEIN CHEMICAL METHODS	38
4.4.1	Protein expression strategies.....	38
4.4.2	Expression of PhzO and TcpA.....	39
4.4.2.1	Expression of native proteins	39
4.4.2.2	Expression of selenium-L-methionine labeled proteins	39
4.4.3	Cell disruption.....	40
4.4.4	Nickel Affinity Chromatography	41
4.4.5	Preparative gel filtration.....	42
4.4.6	Analytical size exclusion chromatography	42
4.4.7	Concentration of the proteins	43
4.4.8	Determination of protein concentration	44
4.5	BIOPHYSICAL METHODS.....	45
4.5.1	Isothermal Titration Calorimetry (ITC)	45
4.5.2	Mass Spectrometry.....	49
4.5.2.1	ESI-MS.....	49

4.5.2.2	HPLC - APCI - MS Measurements.....	50
4.6	PROTEIN CRYSTALLOGRAPHY	54
4.6.1	Introduction.....	54
4.6.2	Crystallization	55
4.6.3	Cryo-protection	57
4.6.4	Data collection and processing	57
4.6.5	Solving the phase problem.....	59
4.6.5.1	Molecular replacement (MR)	60
4.6.5.2	Singular or multiple anomalous dispersion (SAD/MAD)	60
4.6.6	Model building and refinement	61
5.	RESULTS AND DISCUSSION.....	63
5.1	EXPRESSION OF THE PROTEINS.....	63
5.1.1	Preliminary tests for the expression	63
5.1.2	Expression and purification of PhzO.	63
5.1.2.1	Wildtype PhzO	63
5.1.2.2	Selenium-L-methionine labeled PhzO	65
5.1.3	Expression and purification of TcpA.	66
5.1.3.1	Wildtype TcpA	66
5.1.3.2	Selenium-L-methionine labeled TcpA	67
5.1.4	Expression and purification of Fre.	69
5.2	CHARACTERIZATION BY ESI MASS SPECTROMETRY	70
5.3	CRYSTALLIZATION.....	71
5.3.1	Crystallization of native and selenium labeled PhzO.....	71
5.3.2	Crystallization of TcpA and selenium-L-methionine labeled TcpA	72
5.3.3	Substrate and cofactor soaks and co-crystallization of PhzO.....	73
5.3.4	Substrate and cofactor soaks and co-crystallization of TcpA.....	75
5.4	STRUCTURE DETERMINATIONS	76
5.4.1	Sequence alignment of PhzO, TcpA and HpaB	76
5.4.2	Data collection, solving and refinement of PhzO.....	76
5.4.3	Data collection, solving and refinement for PhzO complexed with FAD.....	78
5.4.4	Data collection, structure determination and refinement of TcpA.....	79
5.5	STRUCTURAL AND FUNCTIONAL ANALYSIS OF THE MONOOXYGENASES	81

5.5.1	Structure of PhzO.....	81
5.5.2	Structure of PhzO in complex with FAD	82
5.5.3	Structure of TcpA.....	86
5.6	MODELING.....	88
5.7	LIGAND AFFINITY MEASUREMENTS.....	95
5.7.1	Preliminary test for buffer contribution.....	95
5.7.2	Preliminary tests for determining the titration parameters.....	95
5.7.3	Binding affinity measurements with FAD, FMN, ADP, AMP and PCA.....	96
5.8	ENZYME ASSAY AND HPLC-APCI-MS MEASUREMENTS.....	101
5.8.1	Measurements for PhzO.....	101
5.8.2	Measurements for TcpA.....	105
5.9	PART OF DISCUSSION	106
6.	SUMMARY AND OUTLOOK	109
6.1	PHZO.....	109
6.2	TCPA	110
6.3	OUTLOOK	111
6.4	ZUSAMMENFASSUNG.....	112
6.4.1	PhzO.....	113
6.4.2	TcpA.....	114
6.5	AUSBLICK.....	114
7.	REFERENCES.....	116
8.	APPENDICES	127
9.	ACKNOWLEDGMENTS	131

SYMBOLS AND ABBREVIATIONS

2OHPHZ	2-hydroxy phenazine
2OHPCA	2-hydroxy phenazine 1-carboxylic acid
4HPA	4-hydroxyphenylacetate
Å	Angstrom (1 Å = 0.1 nm = 10 ⁻¹⁰ m)
AA	Amino acid
AcA	Acetic acid
ACN	Acetonitrile
ADIC	2-amino-2-deoxychorismic acid
APCI	Atmospheric Pressure Controlled Ionization
bp	base pair
<i>C. necator</i>	<i>Cupriavidus necator</i>
CBR	C-terminus binding region
C-terminus	Carboxyterminus
Da	Dalton
DMSO	Dimethyl Sulfoxide
DNA	Deoxyribonucleic acid
DTE	1,4-Dithioerythritol
DTT	Dithiothreitol
<i>E. coli</i>	<i>Escherichia coli</i>
EDTA	Ethylendiaminetetraacetate
ESI-MS	Electrospray Ionisation Mass Spectroscopy
FAD	Falvin Adenine Dinucleotide
F _{calc} , F _{obs}	Structure-factor amplitudes (calc:calculated, obs: observed)
GF	Gel filtration
HpaB	4HPA 3-monooxygenase
HPLC	High performance liquid chromatography
IPTG	Isopropyl-β-D-1-thiogalactopyranosid
ITC	Isothermal Titration Calorimetry
kb	kilo-base pair
kDa	kilo-Dalton
kJ	kilo-Joule
LB	Luria-Bertani
LC-MS	Liquid chromatography-mass spectrometry
MAD	Multiple Wavelength Anomalous Dispersion
MALDI	Matrix Assisted Laser Desorption/Ionization
Min	Minute
MIR	Multiple Isomorphous Replacement

SYMBOLS AND ABBREVIATIONS

mM	Millimolar
MR	Molecular Replacement
Mw	Molecular Weight
MWCO	Molecular weight cut off
NADH	Nicotinamide Adenine Dinucleotide
NADPH	Nicotinamide Adenine Dinucleotide Phosphate
NCS	Non-Crystallographic Symmetry
Nm	Nanometer
NMR	Nuclear Magnetic Resonance
N-terminus	Aminotermminus
OD600	Optical density at 600 nm
<i>P. aureofaciens</i>	<i>Pseudomonas aureofaciens</i>
<i>P.aeruginosa</i>	<i>Pseudomonas aeruginosa</i>
PCA	Phenazine-1-carboxylic acid
PCP	Polichlorophenol
PCR	Polymerase Chain Reaction
PDB	Protein Data Bank
PDC	Phenazine-1,6-dicarboxylic acid
PEG	Polyethelene glycol
PhzO	PCA 2-monooxygenase
PMSF	Phenylemethylsulphonyl fluoride
Pyo	Pyocyanin
<i>R. eutropha</i>	<i>Ralstonia eutropha</i>
Rmsd	Root mean square deviations
RNA	Ribonucleic acid
RP-HPLC	Reversed-phase high performance liquid chromatography
RT	Room temperature
SAD	Single-Wavelength Anomalous Dispersion
SAM	S-Adenosyl methionine
SDS	Sodium dodecyl sulfate
SDS-PAGE	Sodiumdodecylsulphate-Polyacrylamide Gel Electrophoresis
Se	Selenium
SeMet	Seleno-L-Methionine
TB	Terrific Broth
TCP	2,4,6 trichlorophenol
TcpA	TCP monooxygenase
TEMED	N,N,N,N -Tetramethyl-Ethylenediamine
TEV	Tobacco Etch Virus
TFA	Trifluoroacetic acid
TRIS	Tris-(hydroxymethyl)-aminomethane

SYMBOLS AND ABBREVIATIONS

U	Units
UV	Ultraviolet
V	Volt
λ	Wavelength, Lambda
μ l	Microliter
μ M	Micromolar

Amino Acids Abbreviations

Amino Acids	3-letter-code	1-letter Code
Alanine	Ala	A
Arginine	Arg	R
Asparagine	Asn	N
Aspartate	Asp	D
Cysteine	Cys	C
Glutamine	Glu	E
Glutamate	Gln	Q
Glycine	Gly	G
Histidine	His	H
Isoleucine	Ile	I
Leucine	Leu	L
Lysine	Lys	K
Phenylalanine	Phe	F
Methionine	Met	M
Proline	Pro	P
Serine	Ser	S
Threonine	Thr	T
Tryptophane	Trp	W
Tyrosine	Tyr	Y
Valine	Val	V

1. INTRODUCTION

1.1 General aspects

Microorganisms, though hardly noticed in everyday life, form an integral part of our existence and are omnipresent. They adapt to constantly changing environmental conditions. As a matter of fact, in case of pathogens such adaptive behavior, may pose major problems for humans and other species. On the other hand for beneficial microorganisms that kind of adaptation is most desirable, offering many advantages. Amongst the most studied microorganisms belong the genera of *Pseudomonas* and *Cupriavidus*. Characteristic for some species of these genera is the production of compounds with antibiotic properties and others having biodegradation properties. For example the species *Pseudomonas putida* and *Cupriavidus necator* are able to carry out hydroxylation of organic substances and are therefore involved in the biological degradation of pollutants and xenobiotics. On the other hand, *Pseudomonas aureofaciens* is known to produce a wide spectrum of organic compounds with antibiotic properties. In order to maximize the benefits of these microorganisms, either a whole cell system, the enzyme complex or the particular enzyme that catalyses the reaction of interest is used. The use of natural catalysts such as whole cell systems and enzymes in order to perform chemical transformations of organic compounds is termed biocatalysis. Many reactions that are either difficult or nearly impossible to achieve with chemical methods are done with ease by biocatalysts (oxygenases/ hydroxylases), e.g. the stereo- and regioselectivity hydroxylation and oxygenation reactions.

Oxygenases are widely distributed in animals, plants and micro-organisms and play a key role in very important biochemical pathways, being a target for drugs and are thus directly involved in drug metabolism^[2]. It has been shown that most of oxygenases are specific and some of them even have unique biological functions. For example, indoleamine dioxygenase (IDO) is an immunomodulatory enzyme that is involved in immunological activities; prolyl monooxygenase serves as an oxygen sensor; nitric oxide

synthase converts L-arginine to nitric oxide (NOS); prostaglandin cyclo-oxygenase (COX) is involved in the biosynthesis of various prostaglandins, monoamine oxidase (MAO) catalyzes the oxidation of monoamines, cytochrome P-450 (CYP450) metabolizes various lipids^[1-5].

The great variety of enzymes that catalyze reactions with molecular oxygen as a substrate or cofactor are broadly classified into- oxidases, oxygenases, dioxygenases and monooxygenases (hydroxylases). **Oxidases** are membrane bound or soluble enzymes that catalyze the transfer of electrons to O₂. **Oxygenases** catalyze the incorporation of O₂ into the substrates and are subdivided in the classes of dioxygenases and monooxygenases. **Dioxygenases** catalyse the cleavage of molecular oxygen with subsequent incorporation of both oxygen atoms into organic substrates, while **monooxygenases** insert only one oxygen atom of O₂ into the substrate^[6].

1.2 Monooxygenases, a class of enzymes with great potential

1.2.1 Monooxygenases

Reactions catalyzed by oxygenase enzymes (mono- or dioxygenases) are interesting from a synthetic chemists perspective^[8-10]. The advantages of the reaction catalyzed by oxygenases are: high regio- and stereoselectivity and the absence of competing side reactions. Biological systems include numerous examples of mono- and dioxygenase reactions and a handful of chemical catalysts are known to compete with biocatalysts^[11-13, 20]. Chemical procedures used to obtain the same end products often use toxic chemical oxidants, in contrast to biocatalysts like monooxygenases, which use molecular oxygen as an environmentally benign oxidant^[14-18]. In the reaction catalyzed by monooxygenases, one oxygen atom of an oxygen molecule (O₂) is transferred to the substrate while the second oxygen atom is reduced to water.

Monooxygenases catalyze reactions such as heteroatom oxidation, Baeyer-Villiger oxidation, aromatic and aliphatic hydroxylation and epoxidation (**Figure 1**). Often,

these enzymes contain heme B or non-heme iron at the active site. The iron or the heme B binds and reduces molecular Oxygen to generate a reactive oxygen species intermediate which is required for the hydroxylation of the substrate^[26,27]. Cytochrome P450 is a heme B containing monooxygenase. Another example is Fe(II)/ α -ketoglutarate (α KG) - dependent monooxygenase which catalyses a variety of reactions that result in biodegradation of pollutants, biosynthesis of antibiotics, repair of alkylated DNA/RNA and protein side-chain modifications^[126].

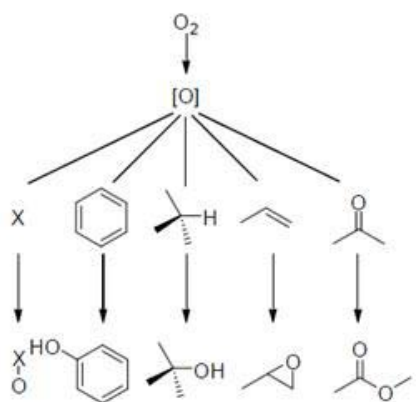


Figure 1: Examples of reactions catalyzed by monooxygenases. From left to the right: heteroatom oxidations, aromatic and aliphatic hydroxylations, epoxidations and Baeyer-Villiger oxidations (figure adopted from [127])

In addition to cofactors like heme B and non-heme iron, some of the oxygenases are able to use oxido-reduction cofactors such as NAD(P)H or $FADH_2$. To maintain the oxidation/reduction cycle *in vivo*, these redox cofactors must be recycled by various metabolic processes of a whole cell system. In the first step of a catalytic cycle, monooxygenases carry out the reduction of molecular oxygen, followed by the substrate oxidation and the release of hydrogen peroxide and other side products of the reaction generated from spent oxidation/reduction cofactors (**Figure 2**).

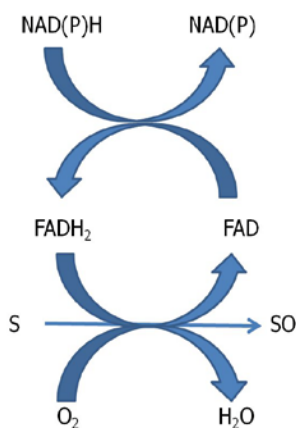


Figure 2: Two step catalysis: FAD-dependent oxygenases use molecular oxygen to insert one oxygen atom into a substrate (S). NAD(P)H and $FADH_2$ are the electron donors which subsequently reduce the second oxygen atom to water.

As shown in **Figure 2**, the overall reaction occurs in two steps. In the first step, FAD as substrate is reduced to FADH₂, and then subsequently is used as a cofactor in the actual hydroxylation / oxygenation reaction. From this point of view, there are monooxygenases able to perform both steps but others must be supplemented with FADH₂ by a flavin reducing enzyme. Given this fact, monooxygenases are divided into two classes: single-component flavin-diffusible and two-component flavin-diffusible monooxygenases (TC-FDM). The last is a class of yet understudied enzymes from the crystallography perspective, with just a few characterized crystal structures. Studies concerning the crystal structure of the monooxygenases would provide insights into their substrate specificity, making them more interesting for biotechnological processes.

1.2.2 Activation mode

The oxygenating agent that activates flavin-dependent monooxygenases is the C-4- α (hydro)peroxyflavin intermediate^[52-56]. This instable intermediate is the product of a general oxido-reduction cycle in which NAD(P)H reduces the flavin and the reduced flavin reacts with O₂ (**Figure 3, steps I-II**). As mentioned above, oxygenases are able to transfer the atomic oxygen on the substrate by two pathways: independent of any other enzyme or in complex with a flavin reductase^[28,29] e.g. two-component flavin-diffusible monooxygenase (TC-FDM). In order to fulfill this complex catalytic process, several requirements must be accomplished by a single site of the enzyme. In the first pathway, the enzymes undergo significant conformational changes during the catalysis. These changes are associated with flavin dynamics^[56] and are coordinated by the protein itself during catalysis^[57-59].

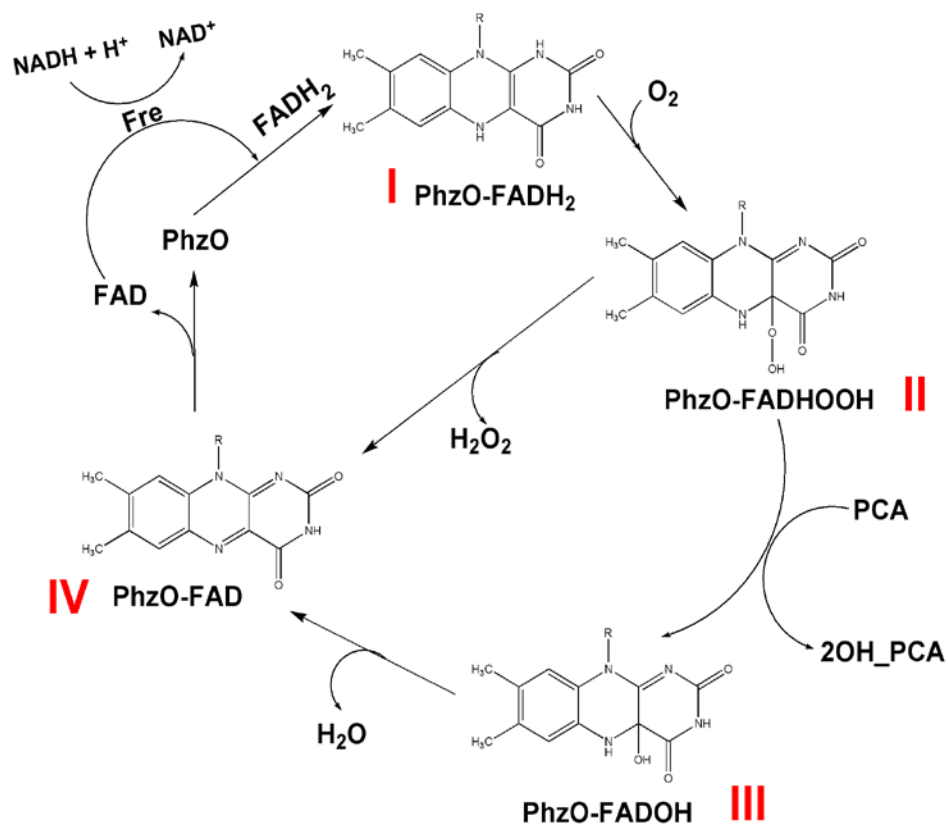


Figure 3: Mechanistic scheme of the FAD oxido-reduction single component flavin diffusible monooxygenases and two component flavin diffusible monooxygenases.

Single-component flavoprotein monooxygenases have a unique catalytic cycle in which cofactors define the reaction velocity more than substrates (**Figure 3**)^[65]. In the open conformation, monooxygenases move the isoalloxazine ring complex of FAD towards the solvent, exposing its N5 for hydride delivery from NAD(P)H (**I**)^[66]. Molecular oxygen binds the reduced flavin and C-4-α peroxyflavin intermediate is formed (**II**). This species is stable for several hours because the monooxygenase is in the closed conformation. This conformation offers protection against the solvent which may destabilize it and C-4-α hydroperoxyflavin intermediate will complex the enzyme until substrate binding^[64]. The enzyme complex will form a substrate access channel that allows passing of substrates. The ability of substrates to pass through this channel depends on their size and charge state^[66,67]. When a substrate enters the active site through the substrate access channel, its nucleophilic moiety can react with the C-4-α hydroperoxyflavin intermediate (**III**). An oxygen atom is then incorporated into the

substrate and a water molecule is released (**IV**). In the last step, NADP leaves the active site closing the catalytic cycle ^[64-66]. Example for such a single-component monooxygenase is PhzS from *P. aeruginosa*^[125].

The second pathway uses two enzymes: a reductase that catalyzes the reduction of FAD to FADH⁻ and an oxygenase that uses the reduced flavin (FADH⁻) as a substrate rather than a cofactor to react with oxygen and finally to hydroxylate the organic substrate^[63]. This two-component flavin-diffusible monooxygenase system (TC-FDM) is able to transfer reduced flavin (FADH⁻) from the reductase component to the oxygenase and stabilize the C-4- α peroxyflavin intermediate until a substrate binds to be hydroxylated (**Figure 3**) ^[56,57,60-62]. This is an example that for successful reaction catalysis, protein complex dynamics play an important role.

The first step (**I**) in **Figure 3** depicts the binding of flavin reductase delivered FADH₂ by the monooxygenase. This will behave as a substrate rather than a cofactor and will bind O₂ in the second step (**II**), leading to the formation of the C-4- α hydroperoxyflavin intermediate. At this stage, the hydroperoxyflavin intermediate is acting as a cofactor shaping conformational changes in the tertiary structure of the monooxygenase which makes the real substrate bind. After product release, the third step (**III**) is finished, while the enzyme remains complexed by the C-4- α hydroxyflavin intermediate. This complex is very unstable and will spontaneously dissociate releasing FAD and water (**IV**)^[57-59]. The oxidized form of FAD will enter a new redox cycle, first being reduced by the flavin reductase (Fre) and then delivered to the monooxygenase.

1.3 Biocatalysis

For several decades already, scientists have understood the extraordinary potential of microorganisms and macromolecules for transforming and producing compounds in a “natural” way without using harmful chemical intermediates. New scientific fields were created in order to develop and/or modify enzymes given by the necessity to optimize biotechnological processes. In order to modify the conditions under which an enzyme is most effective in catalyzing a certain chemical reaction, the methods of protein engineering are used as most common methods. After a detailed biochemical and structural characterization of the enzyme, its effectiveness and its affinity towards substrates or compounds similar to the substrate can be increased by changing certain amino acids in its catalytically active site. The exchange of amino acids is brought about by creating mutations in the gene that encodes the enzyme.

Biocatalysis can be defined as the acceleration of chemical reactions achieved by biological catalysts (enzymes). Enzymes consist entirely or predominantly out of one or more proteins and partly also a cofactor. Most of the biochemical reactions in living organisms are catalyzed by specific enzymes. From the onset of biocatalysis in industrial applications (biotechnology), enzymes, either isolated or in the living cell, are used to catalyze chemical reactions. Oxidation reactions are difficult to achieve using chemical approaches, making oxygenases interesting biocatalysts for biotechnological applications. Oxidation reactions in chemistry are followed in many cases by a high number of side products, low yield and mixed with racemic products. Enzyme catalyzed oxidation reactions are clean, efficient and able to provide stereo selective oxygenation products.

Developments in the biotechnology have been extremely rapid in the last couple of decades, these being coupled to the progress achieved in the recombinant DNA technology but also because of the new applications of biocatalysts, which have been routinely applied in chemistry, leading to naturally obtained products.

1.4 Bacteria *Pseudomonas* and *Cupriavidus*

1.4.1 *Pseudomonas* sp.

Microorganisms are ubiquitous, but often unnoticed, because most of them are not pathogenic, or because they bring benefits to the organisms with which they live in symbiosis. A very much studied genus of microorganism is *Pseudomonas*. Because of their low life claims *Pseudomonads* are widespread, in soil and in water, wastewater and air. Many species of the genus *Pseudomonas* are characterized by the formation of colored or fluorescent pigment, so that they are easy to spot. Some species have thoroughly useful properties. *P. putida*, enters into a symbiosis with mycorrhizal fungi which promotes faster plant growth^[33]. Another useful type is *P. denitrificans*, which denitrifies biological wastewater. However, there are also some harmful species in the genus *Pseudomonas*. *P. aeruginosa* is for example a human pathogen that is responsible for various infections such as wound and chronic lung infections in patients suffering on cystic fibrosis. Generally, the cause of the pathogenicity consists in the excretion of an arsenal of various virulence factors that also include phenazines. About phenazines and their biosynthesis many details are still unknown, so that they represent a great interest for scientific research.

Pseudomonas aeruginosa is a yellowish, aerobic, gram-negative, motile, polar flagellated, rod bacterium isolated for the first time from clay near the river Maas^[30].

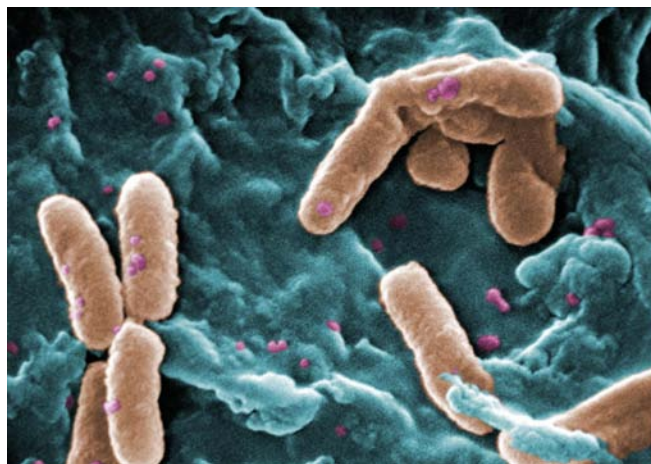


Figure 4 *Pseudomonas aeruginosa* (figure adopted from [30])

Other representatives of *Pseudomonas* include the strains *P. aureofaciens* 30-84, *P. fluorescens* 2-79 and *P. chlororaphis* PCL1391. Based on 16S rRNA analysis, *P. aureofaciens* has been placed in the group of *P. chlororaphis*. All these strains produce more or less the same small molecules but can differ in their biosynthetic properties with respect to phenazine derivatization. For example, *P. aureofaciens* possesses the monooxygenase PhzO, which was shown to convert the common phenazine precursor phenazine-1-carboxylic acid (PCA) into 2-hydroxy-phenazine-1-carboxylic acid (2OHPCA), a orange pigment (**Figure 5**). *P. chlororaphis* on the other hand expresses the transamidase PhzH, which converts PCA into phenazine-1-carboxamide (PCN), a green pigment^[36, 37].

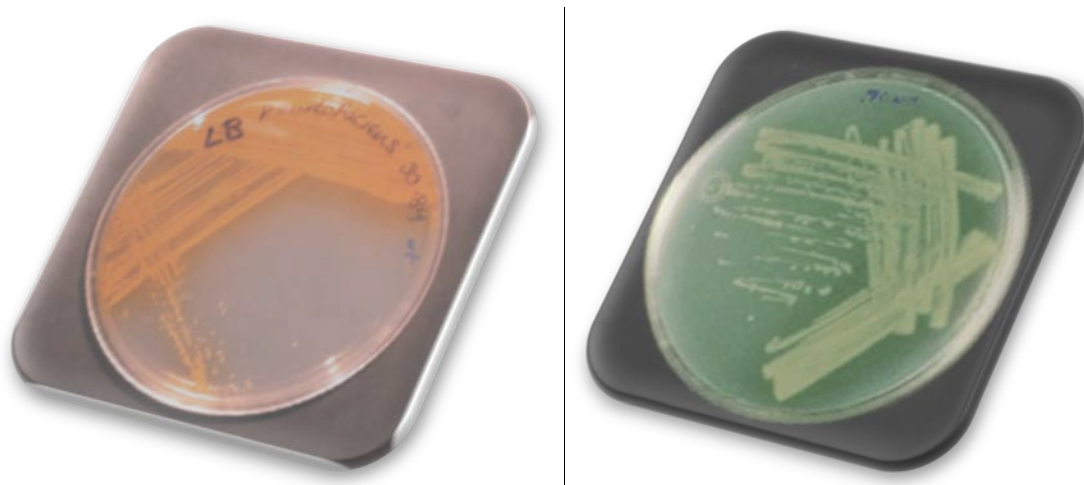


Figure 5 *P. aureofaciens* expressing 2-OHPCA, a orange pigment.^[47] and *P. chlororaphis* expressing PCN, a green pigment^[36-37]

1.4.2 *Cupriavidus necator*

Cupriavidus necator (formerly *Ralstonia eutropha*)^[82] is a gram-negative soil β -proteobacterium that can be found in both soil and water. It was originally isolated based on its ability to use 2,4 dichlorophenoxyacetic acid (2,4-D) as a sole carbon source of energy. *Cupriavidus necator* is a non-pathogenic bacterium, facultatively aerobe, which means they can live in both aerobic and anaerobic environments.

Cupriavidus necator require non-halophilic environment and the optimal growth temperature is 30 °C [83].



Figure 6 *Cupriavidus necator* (formerly *Ralstonia eutropha*) (figure adopted from [86])

Cupriavidus sp. was shown to have a great potential for use in bioremediation, because of its ability to degrade chlorinated aromatic compounds which are often used as pesticides, but also for chemically related pollutants^[84,85]. This bacterium became a model for studying microbial chemolithoautotrophic metabolism and for production of polyhydroxyalkanoates^[86]. The latter ones are part of a divers spectrum of biodegradable polymers used as raw material for production of biodegradable plastics. This bacterial species is also capable of developing on hydrogen, thus contributing to the development of hydrogen-based biotechnological processes concerning various metabolites, polymers and other compounds^[38-40].

1.5 Polychlorophenols

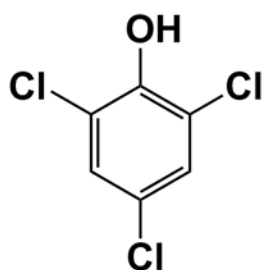
1.5.1 PCPs

Polychlorophenols (PCPs) are a commonly applied general biocide, used for many years as a bactericide, wood preservative, herbicide or precursor in the synthesis of herbicides, defoliant and detergent supplement in soaps^[68-70]. PCP contamination of

soil, ground and sea waters is common and its concentration tends to increase among many other hydrophobic xenobiotics, since they are highly hydrophobic, barely soluble in water and very resistant to biotic and abiotic attack^[71-73]. An example of this kind of toxic compound is the 2,4,6 tri-chlorophenol (TCP), which can be found in soil and fresh water as a result of extensive usage of herbicides, fungicide, insecticide and other agrochemicals.

1.5.2 TCP

TCP is a chlorinated phenol, a yellow solid with a strong, sweet odor. It is carcinogenic, causing liver cancer, leukemia and/or lymphomas via oral exposure.



2,4,6 TCP

Figure 7 Structure of 2,4,6, TCP

A complete mineralization of these toxins requires the involvement of bacteria and bacterial consortia, which are gaining importance for toxicologists, biochemists, microbial genetics and microbial ecologists^[75].

Polychlorophenols such as TCP are involved in the uncoupling of mitochondrial oxidative phosphorylation and in discharging the chemo-osmotic gradient generated by electron transport to drive the phosphorylation of ADP^[74-76]. This is the main reason why PCPs are toxic to a variety of aerobic organisms, but there are some which are able to use PCPs as a carbon source, breaking them down chemically via biodegradation processes. In case of 2,4,6 trichlorophenol (TCP), this is dechlorinated stepwise to 2,6, dichloroquinone (2,6-DCHQ) and 6 chloroquinol (6-CHQ) respectively, as it is depicted in **Figure 8**.

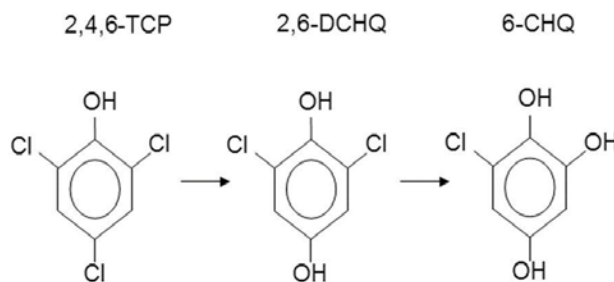


Figure 8 Subsequent dechlorination of 2,4,6, trichlorophenol (TCP) to 6 chloroquinol (6-CHQ)

1.6 Biodegradation

The definition of biodegradation has been given as a chemical breakdown of a certain compound by a physiological environment. This process became the major mechanism for the removal of spilled pollutant from aquatic environments, as well from the soil. To develop the process of biodegradation, a large volume of research on the biochemistry and genetics is involved turning this process into an important tool in the control of soil and water pollution. The physiological environment able to break certain toxins down chemically contains organism like bacteria, fungi or enzymes and protein complexes for *in vitro* biodegradation processes. In case of *in vitro* biodegradation, the reactions may be catalyzed by various groups of enzymes, for example oxygenases, dioxygenases, monooxygenases, methyltransferases or dehalogenases. An important role is played by cytochrome P-450 monooxygenases, which are present in microorganisms, plants and animals. These groups of enzymes are capable of dehalogenation, dealkylation, epoxydation, hydroxylation of xenobiotics^[77]. The present work focuses in part on the biodegradation of chlorinated pollutants such as TCP. As for dehalogenation, this process involves a multi-step reaction. Biodegradation of polychlorophenols may occur in many different ways. One of them is the subsequent dechlorination by removal of the chlorine atoms or reductive dechlorination and insertion of hydroxyl groups to the aromatic ring^[78]. Another way would be the transformation of polychlorophenols to a less toxic substrate without chlorine removal. The most common transformation in aerobic conditions is methylation or ethylation of the hydroxyl group in PCP compounds.

These reactions lead to the formation of chloroanisoles. They are less reactive and less toxic compounds than their substrates because of their higher hydrophobicity. Formation of anisoles was observed in *Phanerochaete sp.* cultures^[79, 80], but also in higher organisms^[81].

1.7 Phenazines, PCA and its derivatives

1.7.1 Phenazines

The concerted work of small molecules and macromolecules is the basis of the chemical machine that promotes life. Macromolecules like lipids, carbohydrates, nucleic acids and proteins are conventional biopolymers, essential in functions that are defined as life. Processes like storing and passing on genetic information, gene expression regulation, cell to cell communication, intercellular signaling and many other processes are strongly dependent on small molecules, also called metabolites. But not all of the small molecules play crucial roles in cellular functions. Some of them are not directly involved in the normal growth, development and reproduction of organisms and therefore they belong to the group of the so-called secondary metabolites.

Many of the small molecules known before as secondary metabolites with unidentified roles gained importance in the survival of the living cell. Over the past couple of decades, secondary metabolites became an extensively researched domain since many of them are found to have interesting biological and chemical properties, such as antioxidant activities, antitumor, anti-inflammation and last but not least antibiotic activities.

Phenazines form a well studied class of secondary metabolites,^[34] and have been of great interest to pharmaceutical and clinical research groups for several years. Phenazines are nitrogen-containing aromatic compounds which have an antibiotic effect. Currently more than 100 naturally occurring phenazine derivatives are known, some of which are shown in **Figure 9**. The various compounds all have the same

skeletal structure and only differ in the substituents on the hetero-cycle, which affects the physical properties and biological activity.

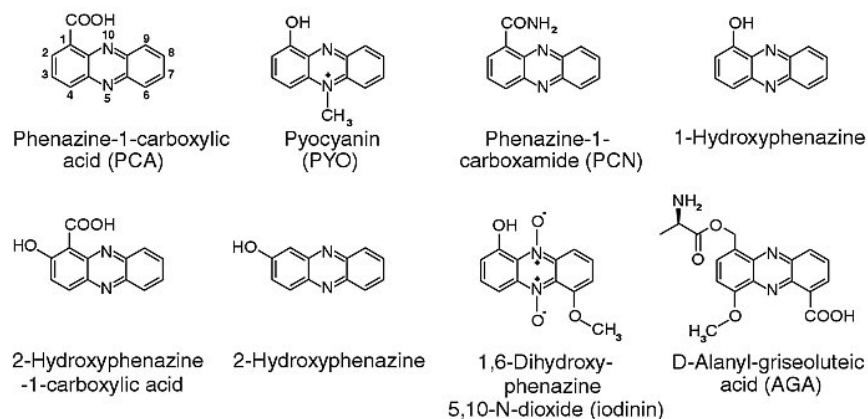


Figure 9:

Some of the natural phenazine derivatives (figure adopted from [31])

Phenazines are synthesized almost exclusively by a variety of bacterial genera, including *Pseudomonas*, *Burkholderia*, *Streptomyces*, *Pelagibacteria*, *Brevibacterium*, *Burkholderia* and *Xanthomonas*. Phenazines are generally water soluble and show distinctive coloration depending on the substitution groups (**Figure 10**)^[49-50].

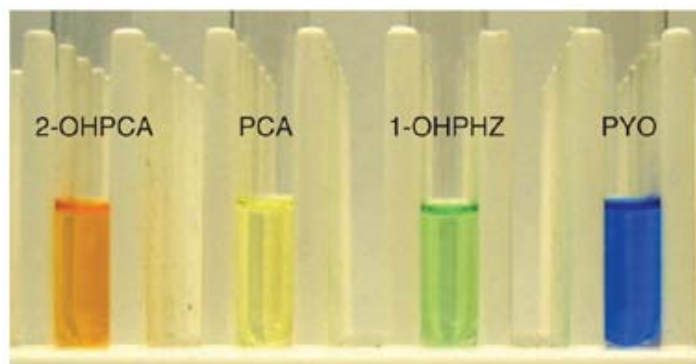


Figure 10: Some of the phenazine derivatives produced by various *Pseudomonas* strains (figure adopted from [50])

Due to this coloration, phenazines are also used as pigments and in addition to this many of them exhibit broad spectrum antibiotic activity^[48,49] and others are also involved in supplying the bacteria with iron. Through their strong redox activity, the phenazines are able to reduce insoluble Fe^{3+} occurring in the environment to the better soluble Fe^{2+} , which then can be incorporated by the bacteria by the use of specific transport molecules. The antibiotic action is based on the redox activity of phenazines

where O_2 is reduced to superoxide O_2^- and hydrogen peroxide H_2O_2 . These two are very reactive oxygen species and have a toxic effect on sensitive cells. Examples of the defense of the habitat are the two phenazine derivatives 2-hydroxy-phenazine-1-carboxylic acid (2OHPCA) and 2-hydroxy-phenazine (2OHPHZ), which have a very broad antibacterial and antifungal activity. These compounds are synthesized by *P. aureofaciens*, which colonizes the roots of plants and protect these against various plant pathogens. These phenazines are not dangerous for mammals, fish or insects, but this is not true for all of phenazine derivatives. In fact, some are of a great importance in bacterial infectious diseases. *P. aeruginosa*, which produces pyocyanin a blue phenazine pigment (**Figure 10**), causes chronic lung infection with about 90% of patients suffering from cystic fibroses. As was shown in a mouse model, the infection of *P. aeruginosa* can be better combated by the immune system when the synthesis of pyocyanin is limited or completely interrupted. Therefore, phenazines and the enzymes that synthesize them represent a particular interest to scientific research in the efforts to intervene effectively in reducing their harmful effects by controlling the biosynthesis of these compounds^[31, 32, 33]. On the other hand, the antibiotic properties of phenazine derivatives such as 2OHPCA and 2OHPHZ and the enzymes involved in their synthesis, constitute an interesting research target. The precursor of naturally occurring phenazine derivatives 2OHPCA and 2OHPHZ is the structurally simple phenazine-1-carboxylic acid (PCA).

1.7.2 Phenazine biosynthesis

The biosynthesis of phenazines is shown in **Figure 11**. According to the current understanding of phenazine biosyntheses, in most cases phenazine-1-carboxylic acid (PCA) is the common precursor of naturally occurring phenazine derivatives, but in some it may be phenazine-1,6-dicarboxylic acid instead. These basic structures are resulting from a synthesis catalyzed by several enzymes encoded in the conserved *phz* operon. First, chorismate is transformed by PhzE into 2-amino-2-desoxyisochorismat (ADIC). This is the substrate for PhzD, which will turn it into trans-2,3-dihydro-3-hydroxyanthranilate (DHHA); then PhzF will catalyse the

[1,5]-proton shifting to the ketone 6-amino-5-oxocyclohex-2-en-1-carboxylic acid, followed by isomerization. This ketone can dimerize spontaneously *in vitro* and a tricyclic phenazine precursor is formed. *In vivo*, the heterodimer PhzA/B will catalyze the double condensation^[41]. The mechanism of the subsequent production of the precursors of PCA, which involves an oxidative decarboxylation and further oxidation is not yet clear^[32, 41, 42].

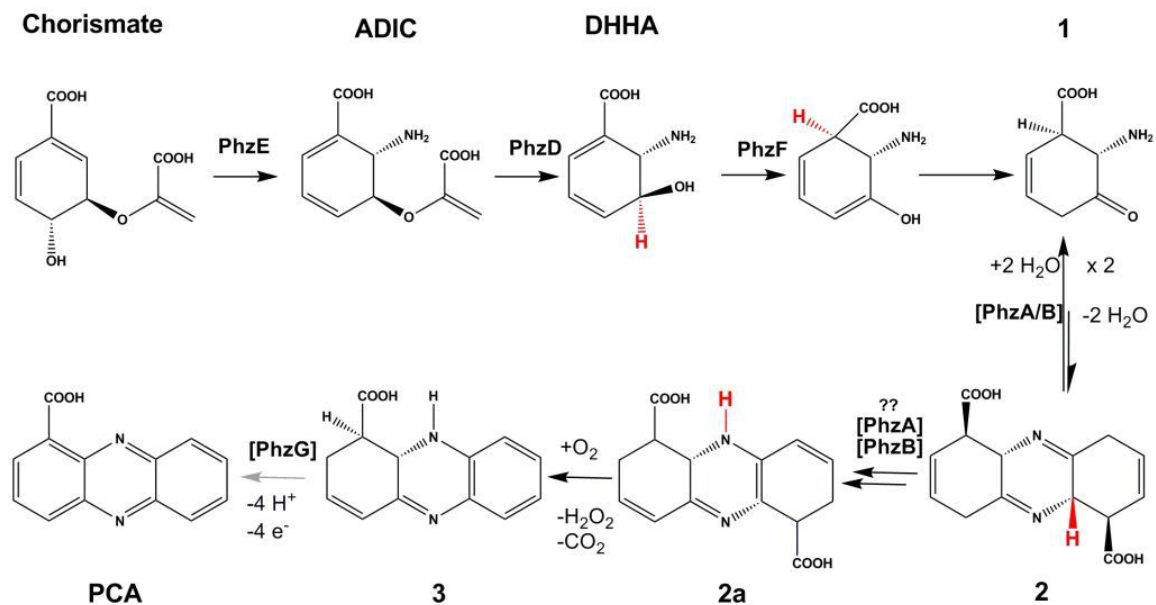


Figure 11: The biosynthesis pathway of phenazine-1-carboxylic acid

PCA can be further modified to strain-specific derivatives. *P. aureofaciens*, for example, has the phenazine-hydroxylating enzyme PhzO, which was investigated in this work. This enzyme converts PCA to 2OHPCA. The hydroxylated phenazine derivative 2OHPCA and its decarboxylated variant, the resulting 2OHPHZ, have stronger antibacterial and antifungal effects compared to the non-hydroxylated phenazine. A better understanding of the phenazine biosyntheses pathway responsible for the production of various phenazine derivatives can help to modify the relevant genes and enzymes so that new phenazine derivatives can be produced which show a significantly improved activity against pathogens and are at the same time safe for the fauna and flora. This could contribute to the development of new pharmaceutical products^[33].

1.8 The biocatalysts PhzO and TcpA

1.8.1 PhzO

The antibiotic activities of naturally derived phenazines have gained the interest in developing synthetic analogues for particular therapeutic applications, but synthesis of substituted phenazines turned to be difficult because of the lack of efficient methods^[50].

PhzO from *Pseudomonas aureofaciens* is a monooxygenase that hydroxylates phenazines^[33] and consists of 491 amino acids with a molecular weight of 55.1 kDa. PhzO catalyzes the reaction shown in **Figure 12** where PCA is transformed to 2OHPCA, which can spontaneously decarboxylate forming 2OHPHZ. The oxygen atom transferred to PCA comes from the molecular oxygen O_2 , whose second oxygen atom is converted to water. For the oxygen transfer on the substrate, the cofactor $FADH_2$ is essential as electron donor. $FADH_2$ is consumed and transformed into its oxidized form FAD during the reaction^[33]. Since $FADH_2$ is a very unstable compound in aerobic conditions and cannot regenerate itself, it must be synthesized in situ by a flavin reductase (Fre), which requires NAD(P)H as a cofactor.

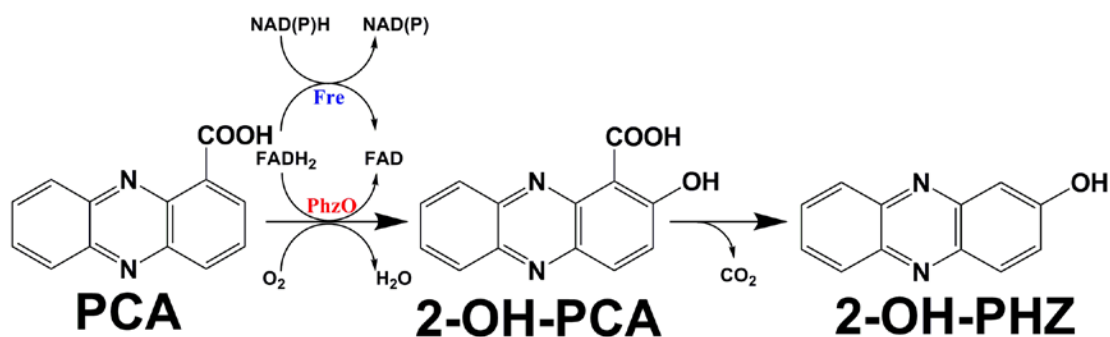


Figure 12: The conversion of PCA to 2-OH-PCA catalysed by PhzO

The gene coding for PhzO is located in *phz* operon, 271 nucleotides downstream of the *phzG* gene (**Figure 13**) and is preceded by a highly-conserved ribosome binding site GAGG^[33].

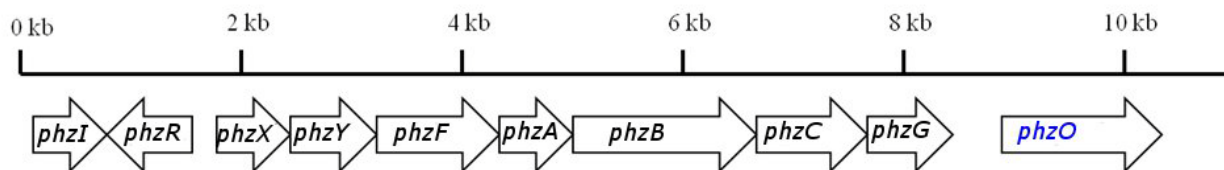


Figure 13: Position of the *phzO* in the *phz* operon (*phzIRXYFABCG*) in *P. aureofaciens* 30-84

Homology comparison of the known amino acid sequence of PhzO shows that this enzyme has a similarity to bacterial aromatic hydroxylases and monooxygenases. PhzO belongs to the 4-hydroxyphenylacetate 3-hydroxylase (*hpaB*) family. The comparison points to the oxygenase component (*hpaB*) of the 4-hydroxyphenylacetate 3-monooxygenase from *Thermus thermophilus*, which has an identity of 25.7% and a similarity of 43.7% to PhzO (EMBOSS protein alignment) and it was predicted to have nearly identical tertiary and quaternary structure. The phylogenetic relationships between PhzO and different bacterial aromatic monooxygenases are shown in **Figure 14**.

Since the hydroxylation activity of the enzymes including PhzO is dependent on the presence of a reductase component, these enzymes belong to the so-called TC-FDM family, the "two-component flavin-diffusible monooxygenase family"^[43].

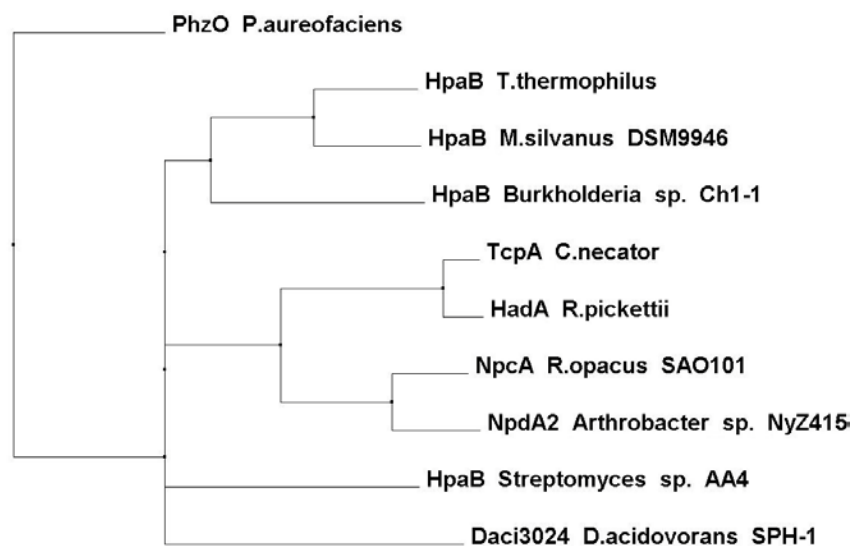


Figure 14: Phylogenetic relationships between different bacterial aromatic monooxygenases and PhzO. The Neighbor-Joining tree was created by using CLUSTAL W

It is assumed that PhzO may be responsible for the generation of a large variety of hydroxylated phenazine derivatives that is produced by *P. aureofaciens*^[33]. The heterocyclic structure of PCA allows nucleophilic substitution reactions at some of its carbon atoms. Substitution with hydroxyl groups leads to the following PCA derivatives: 2-hydroxy-phenazine-1-carboxylic acid (2OH-PCA); 6-hydroxy-phenazine-1-carboxylic acid (6OH-PCA); 2,3-dihydroxy-phenazine-1-carboxylic acid (2,3OH-PCA); 2,6-dihydroxy-phenazine-1-carboxylic acid (2,6OH-PCA); 2,4,6-trihydroxy-phenazine-1-carboxylic acid (2,4,6OH-PCA) and others.

The chemical syntheses of PCA derivatives is very difficult to achieve especially when taking the regioselectivity in account. There are several examples of how nature is handling these difficulties, for instance by using enzymes or enzyme complexes managing the stereo and regioselectivity properties of the catalyzed reaction.

1.8.2 TcxA

The *tcpABC* genes from *Cupriavidus necator* JMP134(pJP4) were shown to encode the enzymes that are involved in the degradation pathway of 2,4,6-trichlorophenol (2,4,6-TCP) converting it into maleylacetate (MA)^[87-90]. These genes are located adjacent to four other open reading frames: *tcpY*, *tcpD*, *tcpR*, and *tcpX* resembling them in a putative catabolic *tcpRXABCYD* operon (**Figure 15**)^[89].

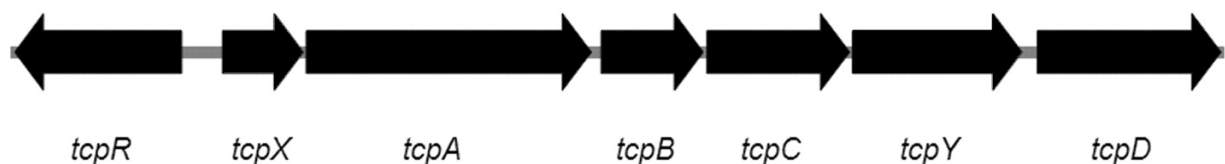


Figure 15 The genetic organization of *tcp* genes in *C.necator* JMP134, *tcpRXABCYD*

Partner flavin reductases are usually located in the same operon^[92-95]. Indeed, the *tcpX* gene is 54% identical to another flavin reductase TftC from *Burkholderia cepacia*, which performs the same reductase process in the degradation of 2,4,5-TCP^[91, 92].

The catabolic pathway for 2,4,6-TCP (**Figure 16**) was suggested to start with the conversion of 2,4,6-TCP to 2,6-dichloro-p-hydroquinone(2,6-DCHQ) followed then by its conversion into 6-chlorohydroxyquinol (6-CHQ-ol). Both reactions are catalyzed by flavin adenine dinucleotide (FAD)-dependent 2,4,6-TCP monooxygenase (TCP-MO). The next steps include the transformation of 6-CHQ-ol to 2-chloromaleylacetate (2-CMA) by 6-chlorohydroxyquinol-1,2-dioxygenase (HQDO) and the conversion of 2-CMA to β -ketoadipate by NADH-dependent maleylacetate reductase (MAR) [87, 88, 96, 97].

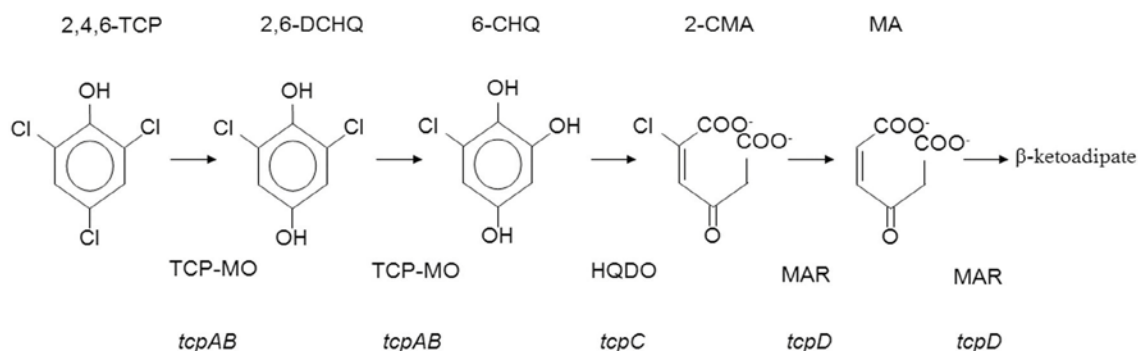


Figure 16 Degradation pathway proposed for 2,4,6-TCP in *C. necator* JMP134. TCP-MO (monooxygenase), HQDO (hydroxyquinol 1,2-dioxygenase) and MAR (maleylacetate reductase) catalyze the conversion of 2,4,6-trichlorophenol (TCP) to 2,6-dichlorohydroquinone, 6-chlorohydroxyquinol, 2-chloromaleylacetate, maleylacetate, and β -ketoadipate, respectively (figure adopted from [89]).

The reaction catalyzed by *TcpA* is shown in **Figure 17**, where an oxygen atom will displace the chlorine from the para position followed by hydroxylation under reductive conditions.

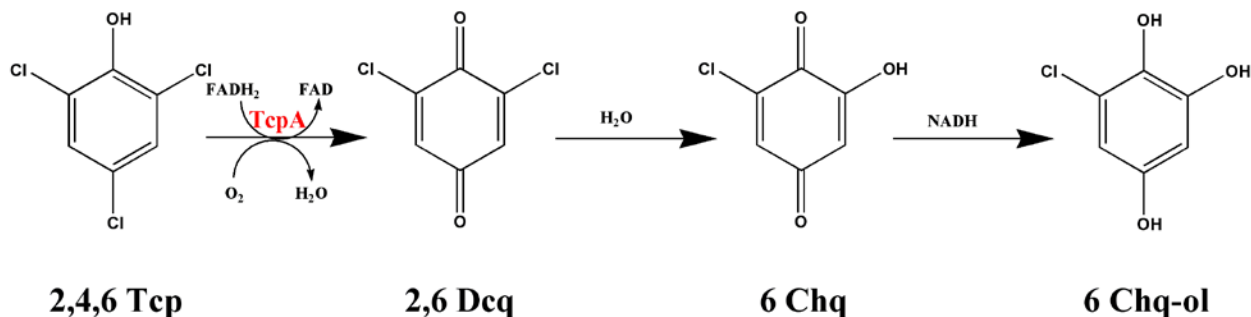


Figure 17 Reaction catalysed by *TcpA*. Molecular oxygen and reduced FAD are used to transform the substrate in 2,6 di-chloro-hydroquinone(2,6 Dcq), which under reductive conditions will convert into 6-chloro-hydroquinol (6 Chq-ol).

1.9 4-Hydroxyphenylacetate 3-Monooxygenase (HpaB)

The structure of HpaB was used for modeling studies and comparison with the protein structures of PhzO and TcpA, as it will be shown in chapter 4.6. The 4-hydroxyphenylacetate 3-monooxygenase is involved in the initial step of the degradation pathway of 4-hydroxyphenylacetate (4HPA). The enzyme catalyzes the hydroxylation of 4HPA to 3,4-dihydroxyphenylacetate (DHPA)^[43]. HpaB is the oxygenase component of the 4-hydroxyphenylacetate 3-Monooxygenase from *Thermus thermophilus* HB8 and a member of the two-component flavin-diffusible monooxygenases. Kim *et al*^[43] describe the crystal structure of the monooxygenase HpaB in three states: ligand-free form, in complex with FAD and in a ternary complex with FAD and the substrate 4HPA. In addition to the structural determination, the conformational changes that occur during ligand and substrate binding were also analyzed in detail. The crystal structures of all three states of HpaB are homotetramers, arranged as dimer of dimers. When FAD complexes the enzyme, conformational differences are observed at the loops between the sheets $\beta 5$ and $\beta 6$, and the loop between $\beta 8$ and $\beta 9$ (**Figure 18** left marked in cyan).

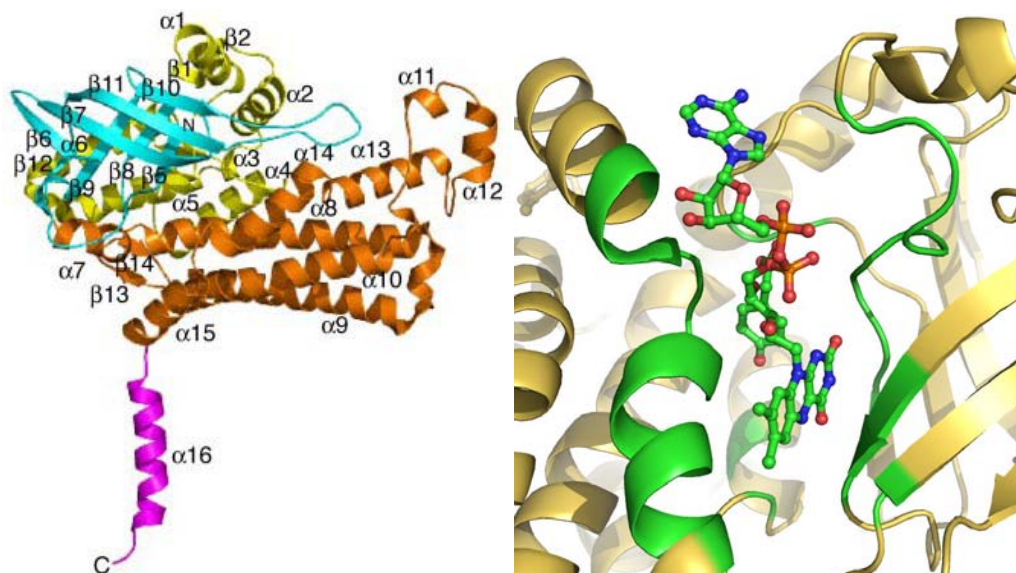


Figure 18 Left: stereo view of the structure of HpaB monomer with the N-terminal domain (yellow), the middle domain (cyan), the C-terminal domain (orange), and the α -helical tail (magenta). Right: Residues involved in forming the FAD binding pocket are highlighted in green. FAD and 4HPA are colored by element (C-green, N-blue, O-red, P-orange)

Figure 18 depicts the FAD-binding site which is shaped by residues marked in green: H142—R151, T183—T185, D247 and R433—R447. In addition, residues from the neighboring monomer, A312—V318 and Q378—S382 also contribute to the binding of the AMP moiety (data not shown). FAD is stabilized in the active site by the amino acids T183, L144, Q148, R151, H182 (**Figure 19**) and residues from the neighboring monomer S382, Q378, H317 and Y315. After FAD binding, the entrance of the groove is still wide enough to allow substrate and molecular oxygen to access the active site. The substrate 4HPA forms hydrogen bonds with the side chain of S197 and its main chain nitrogen atom and the side chains of the amino acids R100, Y104, H142 and T198 (**Figure 19**).

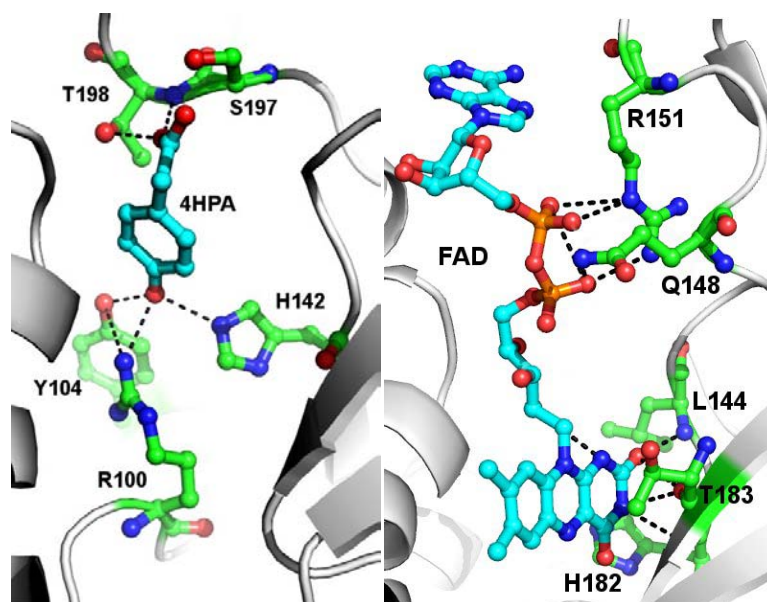


Figure 19 Left: 4HPA(cyan) is bound by the amino acids R100, Y104, H142, S197 and T198 (green). Right: The cofactor FAD (cyan) is stabilized in the active site via hydrogen bonds with residues L144, Q148, R151, H182, T183 (green) and S382, Q378, H317, Y315 from the neighboring chain (not shown here). Hydrogen bonds are marked with black dashes.

These residues R100, Y104, and H142 are likely to select the substrate and define its orientation. All these residues are conserved in the *E. coli* type oxygenase components of the TC-FDMs family^[43]. However amino acids involved in FAD binding are not conserved in enzymes that belong to the TC-FDM protein family.

2. AIMS OF THIS WORK

Oxygen-dependent enzymes are of great interest because they catalyze reactions that are difficult to achieve by chemical synthetic methods, characterized by high stereospecificity and regioselectivity. As aforementioned the large class of oxygen-dependent enzymes is classified into oxidases, dioxygenases and monooxygenases. The later contains the protein super family of two-component flavin-diffusible monooxygenases (TC-FDM). PhzO from *Pseudomonas aureofaciens* and TcpA from *Cupriavidus necator* are members of the TC-FDM protein family. While PhzO is involved in production of compounds with antibiotic properties, TcpA was shown to decompose xenobiotics and various environmental pollutants via dechlorination.

The main aim of this work is to determine the structures of two two-component flavin-diffusible monooxygenases PhzO and TcpA, and to investigate their substrate specificity using X-ray crystallography and a variety of different biochemical and biophysical techniques.

Biochemical studies on these enzymes could open up plethora of opportunities in biotechnology. A better understanding of the biocatalysis of hydroxylation and dechlorination processes could lead to better applications of polychlorophenol-degrading organisms in the bioremediation of polychlorophenols. Based on the structure/activity relationships, new methods concerning site-specific hydroxylation could be developed. On the other hand, by changing the substrate specificity, PhzO and TcpA could become more interesting for biotechnology.

3. MATERIALS AND METHODS

3.1 Materials

3.1.1 Chemicals

Chemicals	Supplier
Acetic acid	Merck (Darmstadt, DE)
Acetonitrile	JT Baker (Deventer, NL)
Acetone	JT Baker (Deventer, NL)
Acrylamid/ Bisacrylamid (30% w/v)	Applichem (Darmstadt, DE)
Adenosine diphosphate (ADP)	Pharma Wadorf (Düsseldorf, DE)
Adenosine triphosphate (ATP)	Pharma Wadorf (Düsseldorf, DE)
Ammonium carbonate	Riedel de Haen (Seelze, DE)
Ammonium sulfate	Applichem (Darmstadt, DE)
Ammonium persulfate (APS)	Merck (Darmstadt, DE)
Ampicillin (Amp)	Serva (Heidelberg, DE)
Bradford reagent	Bio-Rad (München, DE)
Bromphenol blue	Serva (Heidelberg, DE)
Bovine serum albumin (BSA)	Sigma
Chloroform	JT Baker (Deventer, NL)
Chloramphenicol (Cam)	Merck (Darmstadt, DE)
Coomassie Brilliant Blue G250+R250	Serva (Heidelberg, DE)
Dichlormethane	JT Baker (Deventer, NL)
Dimethylsulfoxide (DMSO)	Fluka
Disodium hydrogenphosphate	JT Baker (Deventer, NL)

Dithioerythritol (DTE)	Gerbu (Gaiberg, DE)
Dithiothreitol (DTT)	Gerbu (Gaiberg, DE)
Ethylenediaminetetraacetic acid (EDTA)	Gerbu (Gaiberg, DE)
Ethanol	JT Baker (Deventer, NL)
Ethidium bromide	Sigma
Guanidinium hydrochloride (GdmHCl)	Applichem (Darmstadt, DE)
Glycerol	Gerbu (Gaiberg, DE)
Glycine	Roth (Karlsruhe, DE)
4-(2-Hydroxyethyl)piperazine-1-ethanesulfonic acid (HEPES)	Gerbu (Gaiberg, DE)
Hydrochloric acid	JT Baker (Deventer, NL)
Imidazole	JT Baker (Deventer, NL)
Isopropyl- β -D-thiogalactopyranoside (IPTG)	Gerbu (Gaiberg, DE)
Kanamycin	Boehringer (Mannheim, DE)
Methanol	Applichem (Darmstadt, DE)
B-Mercaptoethanol	Serva (Heidelberg, DE)
Phenylmethylsulfonylfluoride (PMSF)	Sigma
Potassium dihydrogenphosphate	JT Baker (Deventer, NL)
Potassium hydroxide	JT Baker (Deventer, NL)
2-Propanol	JT Baker (Deventer, NL)
Sodium chloride	Fluka
Sodium dihydrogenphosphate	JT Baker (Deventer, NL)
Sodium dodecylsulphate (SDS)	Gerbu (Gaiberg, DE)
Sodium hydroxide	JT Baker (Deventer, NL)
N,N,N',N'-tetramethylethylenediamin (TEMED)	Roth (Karlsruhe, DE)

Trifluoroacetic acid (TFA)	Fluka
Trihydroxymethylaminomethane (TRIS)	Roth (Karlsruhe, DE)

3.1.2 Other materials

Amicon Ultra-4, 15 (30K) Concentrator	Milipore (IE)
BioSep-SEC-2000 gel filtration	Phenomenex (Aschaffenburg, DE)
Dialysis membrane tubing (MWCO:12-14kDa)	Spectrum Lab Inc. (Racho Dominguez, USA)
Electroporation cuvettes	Bio-Rad (München, DE)
Eppendorf Tube (0.5 ml, 1.5 ml, 2.5 ml)	Eppendorf (Hamburg, DE)
Falcon Tube (50 ml, 15 ml)	Falcon GmbH (Gräfeling-Locham, DE)
HiTrap Ni-NTA column	Pharmacia Biotech (Uppsala, SE)
Jupiter 5µm C4 reverse phase column	Phenomenex (Aschaffenburg, DE)
Low molecular weight marker	Amersham Biosciences (Uppsala, SE)
NAP-5 desalting column	Amersham Biosciences (Uppsala, SE)
PD-10 desalting column	Amersham Biosciences (Uppsala, SE)
PRONTOSIL 120-5-C18-AQ 5 µm reverse phase column	Bischoff-Chrom (Leor, DE)
Superdex 75/200 Gel filtration column	Pharmacia Biotech (Uppsala, SE)
ZapCap filter	Sigma-Aldrich (DE)

3.1.3 Instruments

Äkta Prime system with REC112 recorder	Pharmacia Biotech (Uppsala, SE)
Biorad PE 9700 thermocycler	Applied Biosystems (Weiterstadt, DE)
Centrifuge Allegra X-22R	Beckman Coulter (Palo Alto, CA, USA)
Centrifuge Avanti J20-Xp	Beckman Coulter (Palo Alto, CA, USA)
Centrifuge Optima L-70K Ultracentrifuge	Beckman Coulter (Palo Alto, CA, USA)
Centrifuge Eppendorf 5415C/D benchtop	Eppendorf (Hamburg, DE)
Electroporation device <i>E.coli</i> Pulser	Bio-Rad (München, DE)
Deionized water apparatus	Millipore (Eschborn, DE)
Gel-electrophoresis system	Bio-Rad (München, DE)
High pressure liquid chromatography (HPLC)	Waters (Eschborn, DE)
HPLC-ESI-MS	Agilent , Finnigan
HPLC-APCI-MS	Agilent , Finnigan
Isothermal titration calorimeter	MicroCal (Northampton, USA)
Microfluidizer	Microfluidics (Newton, USA)
pH-Meter 761	Calimatic Knick (Berlin, DE)
SDS-PAGE Mini-Protean II system	Bio-Rad (München, DE)
Shaker	Infors (Bottmingen, CH)
Thermomixer 5436 (1.5 ml)	Eppendorf (Hamburg, DE)
Ultrasonic cell disruptor (SONIFIER)	Branson (Danbury, USA)
UV/Visible Spectrometer DU 640	Beckman Coulter (Palo Alto, CA, USA)

3.1.4 Buffers and growth media

LB medium

5 g/l	yeast extract
10 g/l	Tryptone
10 g/l	NaCl

LB agar plate

15 g/l	Bacto agar
50 mg/l	Ampicillin

Antibiotics

125 mg/l	Ampicillin
34 mg/l	Chloramphenicol
50 mg/l	Kanamycin

SDS-PAGE running buffer (10x)

0.25 M	Tris-HCl
2 M	Glycine
1% (w/v)	SDS

SDS-PAGE stacking gel buffer (4x)

0.5 M	Tris-HCl, pH 6.8
0.4%(w/v)	

SDS-PAGE resolving gel buffer (4x)

1.5 M	Tris-HCl, pH 8.8
0.4%(w/v)	SDS

SDS-PAGE loading buffer (2x)

62.3 mM	Tris-HCl, pH 6.8
2% (w/v)	SDS
10% (v/v)	Glycerol
5% (v/v)	β – Mercaptoethanol
0.001%(w/v)	Bromophenol blue

Coomassie staining solution

10% (v/v)	Acetic acid
40% (v/v)	Ethanol
0.1% (w/v)	Coomassie brilliant blue R250

Destaining solution

10% (v/v) Acetic acid

TAE buffer

40 mM Tris acetate, pH 8.5

2 mM EDTA

20 mM Glacial acetic acid

PBS (10x)

80 g/L NaCl

2 g/L KCl

14.4 g/L $\text{Na}_2\text{HPO}_4 \cdot 2\text{H}_2\text{O}$ 2.4 g/L KH_2PO_4 **DNA loading buffer (5x)**

30% (w/v) Sucrose

20% (w/v) Glycerol

0.2% (w/v) Orange G

Bug Buffer50 mM Na_2HPO_4 , pH 8.0

0.3 M NaCl

Buffer A for Ni-affinity chromatography50 mM Na_2HPO_4 , pH 8.0

0.3 M NaCl

2 mM β – Mercaptoethanol**Buffer B for Ni-affinity chromatography**50 mM Na_2HPO_4 , pH 8.0

0.3 M NaCl

2 mM β – Mercaptoethanol

0.5 M Imidazole

Breaking/ lysis Buffer25 mM Na_2HPO_4 , pH 8.0

0.5 M NaCl

2 mM β – Mercaptoethanol

3.2 Molecular cloning methods

3.2.1 General aspects

The complete gene of *phzO* was extracted from *P. aureofaciens* genomic DNA by PCR amplification using a proofreading DNA polymerase (Phusion polymerase). The cloning into the expression vector pOpinE was performed by the Dortmund Protein Facility (DPF). The following oligonucleotide primers were used for polymerase chain reactions: 5'-ATGCTAGATTTTCAAACAAGCGTAAATATCTGAAAAGTG -3' (PhzO-up strand) and 5'-TTTGCGTTGAGCCCCACTAGGCG -3' (complementary PhzO-low strand), whereby a 1476 bp DNA fragment encoding PhzO was amplified using a PTC-200 thermocycler (MJ Research). The obtained PCR product was inserted into the pOpinE vector using the In-Fusion™ cloning approach. DNA sequencing and analysis confirmed the accuracy of the resultant fusion product.

3.2.2 Plasmids and bacterial strains

3.2.2.1 Expression vector

The expression vector used is from the plasmid depicted in **Figure 20**. The gene that encodes PhzO was cloned in the pOPINE-vector of Oxford Protein Production Facility using the In-Fusion PCR cloning system. This vector contains the gene for the enzyme β -lactamase, so that the bacteria that possess this plasmid have an ampicillin resistance. The *phzO* gene is preceded by a nucleotide sequence that encodes the His-tag of six histidines. This way, the expressed PhzO will have an N-terminal His-6-tag which is important in the protein purification steps.

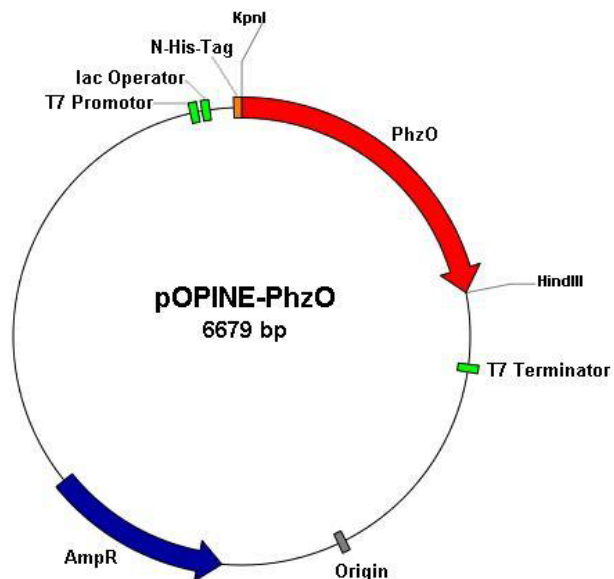


Figure 20: Physical map of the plasmid pOPINE-PhzO

3.2.2.2 Bacterial strains

Bacterial strains

Genotypes

XL1 Blue (Stratagene)	<i>recA1, endA1, gyrA96, thi-1, hsdR17, supE44, relA1, lac[F',proAB, lacI'ZΔM15, Tn10(Tet^r)]</i>
BL21(DE3) (Novagen)	<i>F⁻, ompT, lon, hsdS (r_B⁻, m_B⁻), dcm, gal, λ(DE3)</i>
BL21 (DE3) Codon Plus RIL (Stratagene)	<i>F⁻, ompT, lon, hsdS (r_B⁻, m_B⁻), dcm, gal, λ(DE3), endA, Hte [argU ileY leuW Cam^R]</i>
BL21(DE3) Rosetta (Novagen)	<i>F⁻, ompT, lon, hsdS (r_B⁻, m_B⁻), dcm, gal, λ(DE3), pRARE2 (Cam^R)</i>

3.2.3 Polymerase chain reaction (PCR)

DNA constructs used in this work were created with polymerase chain reaction. This reaction consists of a three-part cycle: denaturation in which a DNA template is denatured at high temperature into single strands, followed by hybridization where the reaction is supplemented by the addition of complementary oligonucleotides and finishing with the elongation at moderate temperatures using DNA polymerase with free nucleotides to form double strands. In subsequent cycles, a new synthesized strand serves as a template. Remains of the reaction can be removed by PCR purification kits, but for a clean and pure product an agarose gel electrophoresis is required.

3.2.4 Preparative PCR

The reaction mixtures including the appropriate 5'- and 3'- primers were prepared as shown in **table 3-1**.

Table 3-1 Protocol for preparation of PCR reaction mixture

Step	Material	Volume (µl)
1	Sterile water	30-34
2	Template DNA (10-100 ng)	2-6
3	Buffer (Phusion High Fidelity 5x)	10
4	DMSO	1
5	Primers (final conc. 1 µM)	1
6	dNTPs (10 mM, final conc. 100 µM)	1
7	Enzyme: 3-5 units of Phusion Polymerase	1
Total		50

The mixture was transferred into a PCR tube and incubated in the thermocycler using the PCR program described in **table 3-2**.

Table 3-2 PCR program

Temp (C)	Time	Step description
1. 98	1-2 min	Initial denaturation: melting of DNA template and primers
2. 98	30 s/cycle	Denaturation: the first cycling event causes melting of DNA template and primers
3. 50-68	30 s/cycle	Annealing: the annealing temperature is dependent on melting temperature (T_m) of the primers, and usually is 2-5C bellow T_m .
4. 72	40 s/kb/cycle	Extension: the time is dependent upon the length of amplifying fragment.
5. 72	10-12 min	Final elongation: after the last PCR cycle to ensure that any remaining single-stranded DNA is fully extended.
6. 4	indefinite	Final Hold: short-term storage of the reaction.

Steps 2,3 and 4 are repeated 30-35 by times

3.3 Subcloning

3.3.1 Restriction

For ligation of the DNA fragment with the vector, both components must be treated with the proper restriction enzymes to ensure a specific insertion. In this case the enzymes recognize individual palindrome DNA sequences and cleave double-stranded DNA at this specific point. The restriction digestion can be used for analysis of manufactured DNA or used in generating new plasmids. To perform a proper restriction digestion, the conditions are adjusted to those indicated by the manufacturer. **(table3-3)** The mixture is incubated for at least one hour at 37 °C.

Table 3-3 Restriction enzyme digestion

Step	Material	Volume (µl) Vector/Insert
1	Sterile water	34 / 60
2	Buffer (Fast digest 10X)	5 / 10
3	Vector (0.2 µg/µl) or PCR product (0.1 µg/µl)	5 / 20
4	Enzyme: NdeI (20 U/µl)	3 / 5
5	Enzyme: XhoI (20 U/µl)	3 / 5
Total		50 / 100

3.3.2 Ligation of DNA fragments into a vector

After the production and digestion of a PCR fragment, this was ligated with the desired vector to a plasmid. Both components had been previously digested with the same restriction enzymes, allowing in this way the T4 ligase to connect the protruding 3' and 5' ends of the PCR fragments with those of the vector. The ligation mixture was made according to the protocol described in **table 3-4** and incubated at 20 °C for 2-3 hours.

Table 3-4 Preparation of ligation reaction mixture

Step	Material	Volume (µl)
1	Vector (10 ng/µl)	5
2	Insert (15 ng/µl)	5
3	Ligation buffer Rapid Ligase (5x)	4
4	T4 rapid ligase (2U/µl)	2
5	Sterile water	4
Total		20

3.3.3 Transformation

For propagation of plasmids or for expression of proteins, the plasmids or ligation mixture must be transformed into certain bacterial *E. coli* strains. The transformation process is done with the electric shock method or the chemical-heat shock method. As follows bellow, the electric shock method will be described. 2 μ l to 10 μ l of ligation mixture or plasmid (up to 100 ng) were mixed with 70 μ l *E. coli* competent cell suspension and incubated for 20 minutes on ice. After being transferred into an electroporation cuvet, the cells were exposed to a voltage of 2.4 volts for a couple of seconds. After the addition of 1 ml LB medium, the mixture was incubated at 37 °C for 45 minutes. The cells were plated on LB plates with appropriate selection marker and incubated overnight at 37 °C.

3.3.4 Colony PCR screen

After overnight incubation at 37 °C, single growing colonies were picked randomly and analyzed whether they contain the desired DNA construct. The reaction mixture was prepared with respect to the protocol described in **table 3-5**. The mixture was then transferred into a PCR tube and incubated in the thermo cycler according to the PCR program described in **table 3-2**.

Table 3-5 Protocol for colony PCR screening

Step	Material	Volume (μl)
1	Template DNA (single colony mixed with sterile water)	5
2	Buffer (RedTaq 10X)	1
3	Primers A+B (final conc. 1 μ M)	1+1
4	dNTPs (10mM, final conc. 200 μ M)	1
5	Enzyme: 1u Red Taq polymerase	1
Total		10

3.3.5 Isolation of plasmid DNA

Plasmid DNA was purified in the required quantity from small to medium bacterial cultures per Miniprep kits from Qiagen. In this case the appropriate manufacturer's protocols were used. The isolation and purification are based on the principle of the alkaline lysis, subsequent precipitation of proteins with potassium dodecyl sulfate and separation by ion exchange chromatography. The DNA was finally eluted in H₂O or TE buffer and stored at -20 °C.

3.3.6 DNA sequencing

The DNA sequencing was carried out with the chain termination method by cycle sequencing in the presence of fluorescently labeled dideoxynucleotides.^[98] The different lengths of DNA fragments were separated by capillary gel electrophoresis combined with fluorescence detection. The DNA sequence can be read off from the resulting chromatogram since each dideoxynucleotide has a different fluorescent label. For the sequencing PCR, a Big-Dye Terminator mix was used, which consists of the AmpliTaq DNA polymerase and the four fluorescence-labeled ddNTPs (**table 3-6**).

Table 3-6 Sequencing mixture

Step	Material	Volume (µl)
1	Plasmid (0.2-1 µg)	5
2	Primers (3 pmol)	1
3	BigDye mix	4
Total		10

The protocol used for cycle sequencing is shown in **table 3-7**.

Table 3-7 The cycle sequencing program for DNA sequencing

Temp (C)	Time	Step
94	2 min	Initial denaturation
94	20 s /cycle	Denaturation
50	30 s /cycle	Annealing
60	3 min /cycle	Extension
4	indefinite	Hold

PCR for 25-35 cycles

After the incubation period in thermocycler, the mixture was precipitated with ethanol and the pellet dried after a washing step with 70% ethanol. The capillary gel electrophoresis and recording of the chromatogram was carried out in the biotechnological facility at the MPI-Dortmund.

3.3.7 Glycerol stock

For storage of transformed bacteria, the bacteria culture were grown to an $OD_{600} = 0.4$ and then, 1 ml of bacterial culture is mixed with 1 ml 50% glycerol. After shock freezing in liquid nitrogen, the aliquots can be stored at -80 °C.

3.4 Protein Chemical Methods

3.4.1 Protein expression strategies

Using the homologous expression of a protein the yield of expression is mostly very low and the protein purification inefficient. In order to overcome these problems, the heterologous expression is used. Here, other easy- to- grow organisms, such as *E. coli*, are used to biosynthesize the protein in large amounts. The process of expressing proteins in large quantities is called over-expression. A special affinity tag, such as for example the His-6-tag which was used in this work, allows easier purification of the protein by affinity chromatography. The affinity tag can sometimes be eliminated by appropriate proteases after purification. The transcription of the target gene is controlled by the T7 RNA polymerase, which it comes from the T7 phage and was incorporated into the bacterial genome. The plasmid containing the gene for the desired protein has a T7 promoter and a T7 terminator recognition site. However, the transcription of the target gene is first induced when lac repressor is inhibited. The lac repressor binds to the operator, which is behind the T7 promoter, so that the T7 polymerase cannot bind the promoter. By adding a suitable induction agent that binds to the lac repressor will lead to the dissociation of the lac repressor from the operator. The lac repressor becoming free, the T7 polymerase will bind to the promoter region and reading of the target gene will start. The T7 polymerase has such a high affinity to the promoter that gene expression is directed to the target gene. A commonly used induction agent is IPTG. This is not metabolized, so that its concentration remains constant and the repressor inactive.^[99] Another way of induction is described by Studier auto-induction by lactose,^[100] which was also applied here. Lactose can be converted by the enzyme β -galactosidase into the isomer allolactose, which then binds to the lac repressor and thus induces gene expression. However, the induction takes place only when the glucose is consumed in the medium, as this would otherwise inhibit the absorption of lactose into the cells by the lactose permease. One advantage of the auto-induction with lactose in comparison with induction with IPTG is that cell cultures reach a higher optical density and therefore the protein yield achieved is much higher. Furthermore, the ratio of

glucose and lactose can be adjusted, which determines the time of induction such that the optical density of the culture has not to be monitored.^[100-101]

3.4.2 Expression of PhzO and TcpA

3.4.2.1 Expression of native proteins

The proteins PhzO and TcpA were expressed in *Escherichia coli* BL21-CodonPlus(DE3)-RIL by inoculating Terrific Broth (TB) medium supplemented with 100 mg l⁻¹ ampicillin and 34 mg l⁻¹ chloramphenicol with an overnight culture that was grown from a single colony. The inoculated culture was grown at 310 K with continuous shaking at 250 rpm until OD₆₀₀=0.4. Induction of gene expression via isopropyl β-D-thiogalactoside (IPTG) proved to be unsuccessful, and so another induction reagent was chosen. Inducing with 0.2% α-Lactose for 22-24 h at 298 K the protein over expression was achieved. By the end of the expression the optical density of the culture showed OD₆₀₀ = 1.2. The cells were harvested by centrifugation for 20 minutes at 4000 g and washed in 50 mM Na₂HPO₄ pH 7.5, 300 mM NaCl, 2 mM PMSF supplemented with a protease inhibitor cocktail.

3.4.2.2 Expression of selenium-L-methionine labeled proteins

The selenium-L-methionine labeled proteins were overexpressed in *Escherichia coli* BL21-CodonPlus(DE3)-RIL cells carrying pOpinE with His₆-tagged PhzO or His₆-tagged pET27-TcpA, respectively. The overnight culture was grown in Luria-Bertani medium supplemented by ampicillin and chloramphenicol, then harvested and resuspended in Minimal M9 medium. The culture was grown at 310 K until OD₆₀₀=0.4, when amino acids lysine, threonine and phenylalanine to 100 mg l⁻¹; valine, leucine and isoleucine to 50 mg ml⁻¹ and selenium-L-methionine to 60 mg l⁻¹ were added. Protein expression was induced with 0.2% of α-Lactose for 30 hours at 298 K under rigorous shaking.

3.4.3 Cell disruption

Depending on the amount of the harvested bacterial cells, these were disrupted either using a microfluidizer or by ultrasound. For this, the cells were resuspended in a lysis buffer which had an individual composition depending on the protein of interest. Using the microfluidizer the bacterial suspension was repeatedly placed in a narrow capillary under high pressure (800 bar) destroying the cell membranes. To check the complete lyses, the suspension was examined under the microscope. Subsequently, the lysate was centrifuged at 120,000 g for 45 minutes at 4 °C after which the insoluble components were separated from the aqueous fraction.

To check the expression level and the protein solubility, samples were taken before and after induction, before lysis and after the centrifugation step from the supernatant as well from the inclusion bodies. Samples were loaded on a 15% SDS gel (see **table3-8**).

Table 3-8 Recipes for preparing SDS-PAGE gels.

	1	2	3	4	5	6
Type of gel (%)	Acrylamide/ bisacrylamide (29:1, 30%)	Mili-Q H₂O	Resolving gel buffer (4X)	Stacking gel buffer (4X)	10% APS	TEMED
Resolving gel (60 ml)						
10%	20 ml	25 ml	15 ml	-	300 µl	30 µl
15%	30 ml	15 ml	15 ml	-	300 µl	30 µl
Stacking gel (30 ml)						
5%	5 ml	17.5 ml	-	7.5 ml	240 µl	30 µl

3.4.4 Nickel Affinity Chromatography

For purification of the proteins described in this work, the method of Nickel Affinity Chromatography was used. This method is based on the properties of a matrix formed by Ni-NTA (nickel-nitrilo-tri-acetic acid) and a well known property of the macromolecule of interest. The Ni^{2+} ions are complexing the NTA-material in such a way that two more ligand binding sites are freely accessible for positively charged molecules, such as histidines. The macromolecule of interest must have a special recognition sequence that will trap them on the solid phase Ni-NTA. A series of six histidines, called His-6-Tag, will specifically bind to these binding sites in the nanomolar range, while other proteins will not bind at all or just very weakly. During the washing steps, all the non-specifically bound protein can be washed away so that the matrix will contain the pure protein of interest. This is eluted by imidazole, which competes with the His-6-Tag for the free ligand binding sites on the nickel.

After cell disruption, the cytosolic fraction was loaded on a nickel column and washed until absorption at 280 nm was no longer detected. In order to remove non-specifically bound proteins, the running buffer contained 20 mM imidazole. Subsequently, the desired protein was eluted with 100-250 mM imidazole and fractionated. The fractions were tested for purity using SDS gel electrophoresis and the correct mass was confirmed by ESI-MS measurements. Finally, fractions containing the desired and pure protein were combined. The imidazole was removed by dialysis or buffer exchange chromatography.

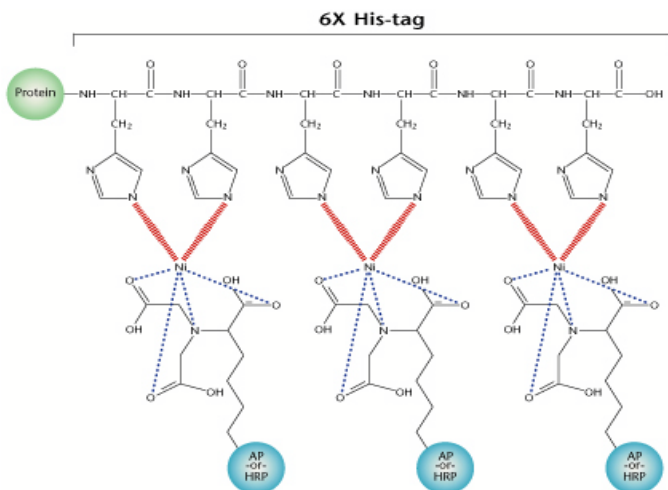


Figure 21: Ni-NTA affinity chromatography. Binding of a protein with His-6-tag (figure adopted from [103])

3.4.5 Preparative gel filtration

Unlike the affinity chromatography, in the gel filtration proteins are not separated by binding to the matrix but because of their size and shape. The matrix consists of porous beads which have a defined size. These limit the permeation of large molecules in the beads and they have a shorter path through the matrix as the molecules that are smaller than the beads. The larger the molecule is, the faster it will be eluted.

Size exclusion chromatography was used here for further purification of the protein of interest and for getting rid of pollutants originating from the affinity chromatography, but also for separation of aggregates from the rest of the protein. The separation was better, the smaller the volume of protein solution that was loaded on-to the column was. Depending on the size of the macromolecules, Superdex 75 16/60 or Superdex 200 16/60 gel filtration columns (GE Healthcare) can be used. The flow rate here was not more than 2 ml / min. The collected fractions were analyzed by SDS gel electrophoresis and the desired fractions were then combined, concentrated, shock frozen in liquid nitrogen and stored at -80 °C.

3.4.6 Analytical size exclusion chromatography

In the analytical size exclusion chromatography, a method similar to the one described for the preparative gel filtration in **3.4.5**, proteins are separated according to their stoichiometrical gradient. The difference between the analytical and preparative size exclusion chromatography lies in the smaller scale of the column, so that a considerably smaller volume of sample is needed. The column has a volume of 30 ml as compared to the preparative column that varies between 120 to 330 ml. For injection of samples, detection and sample analysis a computer-controlled HPLC system was used that was connected to a two-channel absorbance detector. To detect the mass of a protein, a gelfiltration standard (BioRad) is injected initially in the column and the elution volumes of the standard proteins are correlated with the elution volumes of the protein to be analyzed. Knowing the elution volumes for the standard proteins and for the protein of interest as well as the total and the exclusion volumes, the distribution coefficient for the column can be calculated as shown in the **formula 3-1**.

$$K_{av} = \frac{V_e - V_t}{V_t - V_0}$$

Formula 3-1 Calculation of the K_{av} -distribution coefficient, V_e : elution volume, V_0 : exclusion volume, V_t : total volume

Plotting the K_{av} values versus the logarithm of the molecular mass of the standard proteins results in a linear relationship. From this relationship, the mass of an unknown globular protein can be calculated from its running/elution performance.

In order to characterize the protein solution obtained in the two step purification of PhzO and TcpA regarding their purity, size and the number of subunits, the analytical gel filtration method described above was used. The first gel filtration run was performed with 20 μ l of standard marker proteins (Bio-Rad) for determining the elution times of these proteins with known molecular weight. Then 10 μ l of PhzO and TcpA solutions with a concentration of 200 μ M were investigated and their elution profile was compared to the standard in order to determine their degree of polymerization in aqueous solution *in vitro*. The flow rate was 0.5 ml / min.

3.4.7 Concentration of the proteins

To increase the protein concentration, protein solutions were concentrated with Amicon ultra filtration units, whose membranes have pores with a defined size. By centrifugation at a maximum of 3500 g the protein solution is pressed by centrifugal force through the membrane. Molecules of smaller size than the pores of the membrane are passing easily, while larger molecules remain in the centrifuge cup. Decreasing the volume of the protein solution will increase the content concentration. The protein solution is centrifuged until the desired concentration is reached.

3.4.8 Determination of protein concentration

Protein concentrations were determined by the method of Bradford^[102] as well as UV-absorption at 280 nm.

The first method is based on the acid dye that binds Coomassie brilliant blue to the side chains of the amino acids arginine, histidine, tryptophan, tyrosine and phenylalanine, and thus the anionic form of the dye is stabilized. Compared to the unbound cationic form, the absorption maximum is shifted from 465 nm to 595 nm. In this study, the Bradford reagent used was produced by BioRad and the measurements of protein concentration were carried out according to the manufacturer.

The second method for determining the protein concentration utilizes the properties of the aromatic amino acids to absorb at 280 nm. For a proper determination, this method requires a complete denaturation of the macromolecules with 6 M guanidinium. For calculating the concentration, any of the equations depicted in **formula 3-2 and 3-3** may be used.

$$C = \frac{A_{280} * 100 * MW}{\epsilon}$$

Formula 3-2 UV-Abs. at 280 nm. c : concentration in $g L^{-1}$, ϵ : extinction coefficient of the protein in $mol^{-1}cm^{-1}$, MW : molecular weight in $g mol^{-1}L^{-1}$.

$$A_{280}(1 \frac{mg}{ml}) = \frac{5690 * N_w + 1280 * N_y + 120 * N_c}{MW}$$

Formula 3-3 N_w , N_y , and N_c are the numbers of Trp, Tyr, and Cys residues in the protein with molecular weight MW and 5690, 1280 and 120 are the respective extinction coefficients for these residues.

The extinction coefficient of the protein was determined by entering its sequence into the online server ProtParam (<https://us.expasy.org>).

3.5 Biophysical methods

3.5.1 Isothermal Titration Calorimetry (ITC)

Isothermal titration calorimetry (ITC) is a very sensitive method to measure the thermodynamic parameters of interaction between two molecules ^[105]. In the binding process between two molecules, energy is released or consumed depending on the type of reaction. This heat energy can be recorded and measured. The measurement principle is in keeping the temperature between the measuring cell and the reference cell constant by an electrical control circuit. Depending on the type of reaction, less or more power is necessary to keep the temperature of the measuring cell the same as the temperature of the reference cell. The two cells are contained by an insulating coat to prevent the exchange of heat with the environment.

In the calorimetric experiments of this study, the ligand was titrated stepwise with a syringe into the measuring cell that contained a protein solution of the binding partner. The heat exchange involved in keeping the temperature of the measuring cell equal to that of reference cell, when ligand and protein interact is detected and measured. The integral of the measured thermal effect is plotted versus the molar ratio of ligand (syringe) / protein (cell). A titration follows a sigmoidal curve from which the thermodynamic parameters for a binding, ΔG , ΔH , ΔS , the stoichiometry and the dissociation constant K_d can be determined.

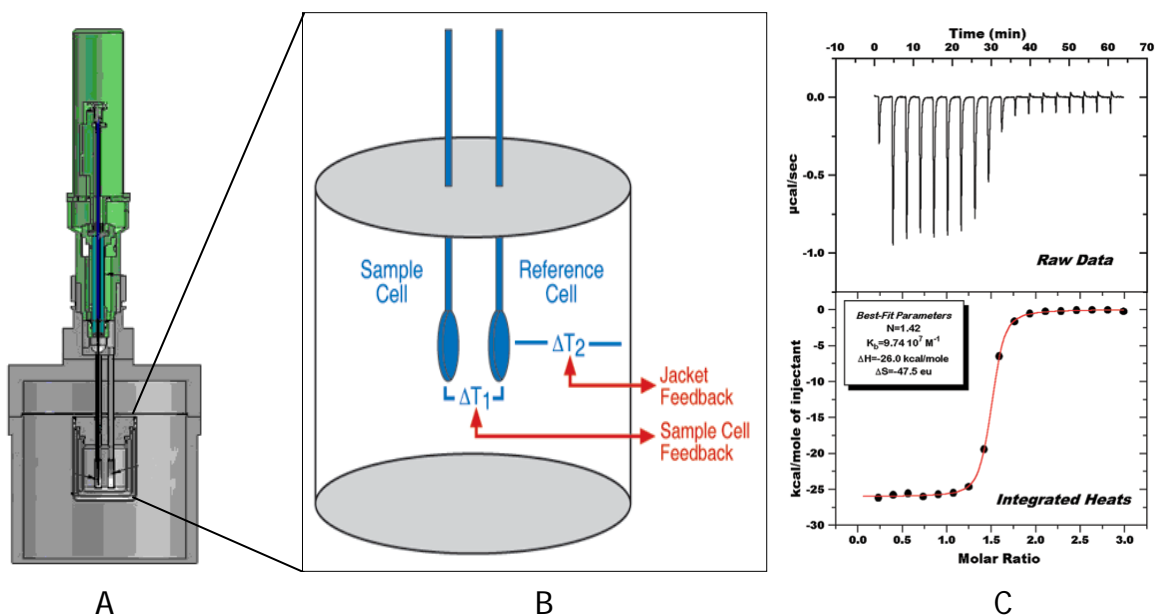


Figure 22 (A) syringe (green) and cells (gray), (B) measuring unit, (C) representative ITC data (figure adopted from [107])

The free enthalpy can be described by the Gibbs function:

$$\Delta G = \Delta H - T * \Delta S$$

Formula 3-4 Gibbs function: ΔG : free enthalpy, ΔH : enthalpy, ΔS : entropy, T :Temperature

The enthalpy ΔH and the entropy ΔS may have a different effect on the free enthalpy ΔG . The observed temperature change is caused by the non-covalent interactions between protein, ligand and solvent. Non-covalent interactions are formed by hydrogen bonds, hydrophobic interactions, ionic interactions, Van der Waals forces between ligand and protein, but also by structural changes in the solvation shell of the protein or ligand.^[106] However, the factors which determine the size of and can vary. For example, by destroying the hydration shell of a protein around the binding pocket the entropy will increase. By complex formation, free particles are removed from the system and this will reduce the freedom for translational rotation. The amino acid side chains and / or entire domains are restricted in their mobility, which may result in a negative

entropy change.^[107] The entropy measured while protein complex formation is also called solvation entropy or conformational entropy.

The measurements were performed in a MicroCal VP-ITC apparatus, at 25 °C in 50mM Tris buffer (pH 7.5) and 150 mM NaCl. The apoenzyme placed in the sample cell was titrated consecutively with the following ligands: FAD, FMN, ADP, AMP, PCA, DCP and TCP. The syringe containing the ligand was set to stir with 180 rpm, at 25 °C in 50mM Tris buffer (pH 7.5). The ligand molecules were dissolved exactly in the same buffer as the protein. To perform the measurements, different concentrations of the enzyme, from 50 μM to 400 μM, were prepared and the ligand concentration was adjusted to the tenfold of the enzyme concentration. After 30 minutes of equilibration the measurement started with an initial 0.2 μl injection, followed by 18 injections of each 2 μl at 4-minute intervals.

The raw data of the enthalpy changes corresponding to the measurements performed in this work, were analyzed and computed with Origin version 7 (OriginLab Corporation). The equation used for the plotting the curve is shown below in **formula 3-5**. The association constant K for the binding of the ligand L and the protein P can be described as:

$$K = \frac{\nu}{(1 - \nu) * L}$$

Formula 3-5 K : association constant in M^{-1} , ν : binding ratio (proportion of occupied ligand binding sites), $[L]$: concentration of free ligand in M

The mass balance for the ligand is:

$$[L]_0 = [L] * n * \nu * [P]_0$$

Formula 3-6 $[L]_0$: initial total concentration of ligand in M , $[L]$: free ligand concentration in M , $[P]_0$: total concentration of the protein in M , n : number of binding sites, ν : binding ratio (number of the ligand-occupied binding sites)

Combining equation 3-5 with equation 3-6 will give:

$$\nu^2 - \nu * \left(1 + \frac{[L]_0}{n * [P]_0} + \frac{1}{n * K * [P]_0} \right) + \frac{[L]_0}{n * [P]_0} = 0$$

Formula 3-7

The measured heat Q for a certain bonding ration ν is:

$$Q = n * \nu * [P]_0 * \Delta H * V_0$$

Formula 3-8

Q : heat quantity in J, ΔH binding enthalpy in J mol⁻¹, V_0 : volume of the measuring cell

Inserting the calculated bond ratio from formula 3-7 into formula 3-8, the measured heat becomes:

$$Q = \frac{n * [P]_0 * \Delta H * V_0}{2} \left(1 + \frac{[L]_0}{n * [P]_0} + \frac{1}{n * K * [P]_0} \right) - \sqrt{\left(1 + \frac{[L]_0}{n * [P]_0} + \frac{1}{n * K * [P]_0} \right)^2 - 4 * \frac{[L]_0}{n * [P]_0}}$$

Formula 3-9

Q is the heat measured in J, $[P]_0$: total concentration of the protein in M $[L]_0$: total concentration of ligand in M, v_0 : volume in the cell in l, ΔH : molar enthalpy of ligand binding in J mol⁻¹, n : number of binding sites of the protein, K : equilibrium association constant in M⁻¹

The stoichiometry of binding n , the association constant K and the molar enthalpy ΔH can be determined in a single experiment. From the value of ΔH and ΔS , and the

relationship $\Delta G = -RT \ln K = \Delta H - T * \Delta S$ the Gibbs free energy ΔG and the entropy ΔS can be calculated.

3.5.2 Mass Spectrometry

3.5.2.1 ESI-MS

The mass of micro and macromolecules can be determined by matrix-assisted laser desorption/ionization mass spectrometry (MALDI-MS) or electrospray ionization mass spectrometry (ESI-MS). The process for ESI-MS is sensitive and far gentler than MALDI-MS but also more easily upset by salt contained in the protein solutions. The sample is therefore injected in a C4 desalting column before the analysis in the ionization chamber with a high electrical potential is started. The resulting dispersion is charged electrically, and proteins and micro molecules contained in the gaseous phase are getting protonated. In an ion trap the protonated micro and macromolecule fragments are analyzed and raw data are collected. The processing and evaluation of the raw data is made with the help of software MagTrans, which calculates the molecular mass of the molecules under consideration with high exactness.

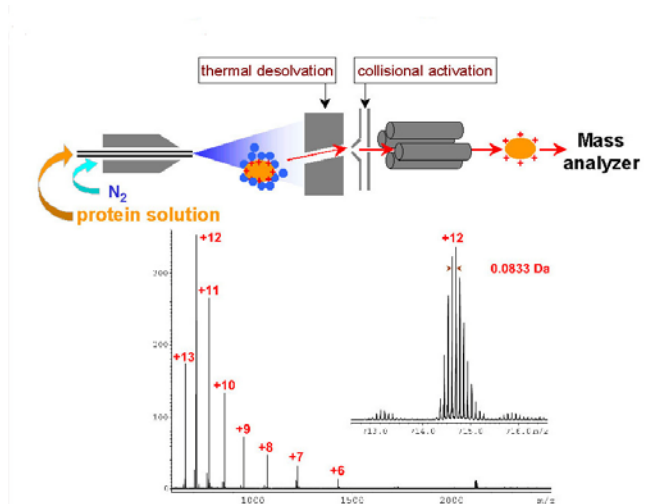


Figure 23 Electrospray ionization mass spectrometry ESI-MS (figure adopted from [117])

In this work, ESI-MS was used to verify successful labeling of the proteins with selenium-L-methionine during the protein overexpression, by measuring the molecular weight. The programs used for ESI-MS measurements are listed in **table 3-9**.

Table 3-9 Gradient program for LC-ESI-MS measurement of protein using a C4 column

Time (min)	Buffer A (0.1%FA, H ₂ O)%	Buffer B (0.1%FA, ACN)%
5	20	80
15	70	30
17	90	10
19	90	10
20	20	80
22	20	80

3.5.2.2 HPLC - APCI - MS Measurements

In the HPLC-APCI-MS analysis, the liquid chromatography process is coupled to mass spectrometry. First, the sample of interest is separated by HPLC into its individual components. These are evaporated and ionized during the ionization process (APCI) and then passed to the detector, which will analyze the components based on the mass / charge (m/z) ratio.

In the HPLC process, components are separated based on their polarity. The stationary phase is formed by silanes with long, non-polar hydrocarbon chains. The interaction of the substances with the stationary phase is thus via hydrophobic interaction. Samples are usually located in a polar solvent and are eluted with non-polar organic solvents like acetonitrile, methanol or isopropanol. The organic solvent competes with the analyte for the binding sites of the stationary phase so that it is washed away from the column and detected by a UV detector.^[103]

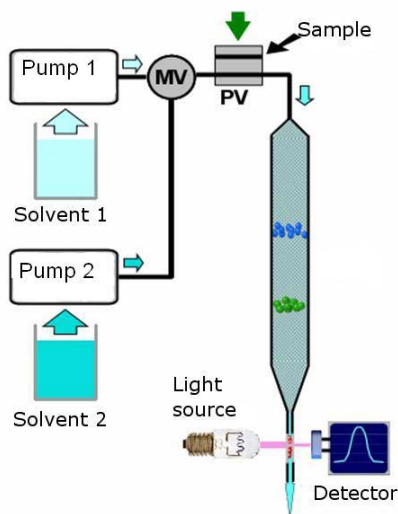


Figure 24 HPLC apparatus (solvent 1: H₂O, solvent 2: ACN, MV: mixing valve, PV: sample valve) (figure adopted from [110])

The separation of the compounds via HPLC is followed by their mass determination with the method of atmospheric pressure chemical ionization mass spectroscopy (APCI-MS). For this, the analyte is directed into a nitrogen steam through a capillary, atomized into a spray and heated up to the temperature of 300 to 400 °C. Then, the ionization takes place by means of a needle-shaped electrode, called the corona needle to which a voltage of 4 to 5 kV is applied. By corona discharge, the solvent molecules will be ionized in the first step with consecutive protonation by the corona. These primary ions in turn ionize in a second step, the analyte molecules.^[112]

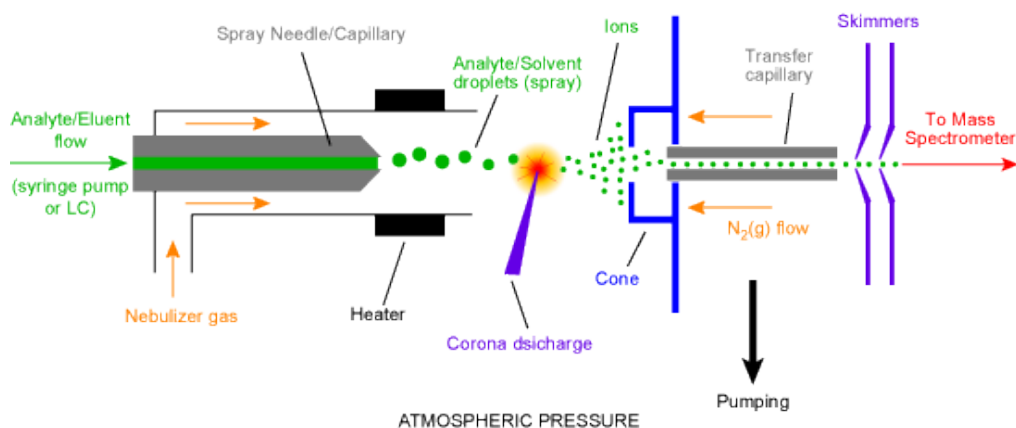


Figure 25 APCI apparatus (figure adopted from [109])

After ionization, mass analysis of the ions takes place under high vacuum conditions using a quadrupole. Here, four rod-shaped metal electrodes are arranged in parallel, with adjacent electrodes which are polarized in the opposite manner. (**Figure 26**) By applying a combined AC/DC field, only ions having a defined mass / charge ratio will have a stable oscillation and reach the detector. The remaining ions collide due to their unstable trajectory with the metal electrodes and do not reach the detector. By changing the voltage of the field applied it can be achieved that each type of ion is detected individually in order to analyze the entire mass spectrum.^[103]

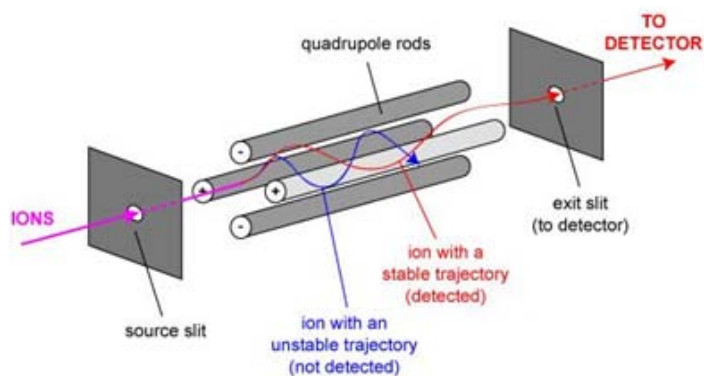


Figure 26 Quadrupole mass analyzer (figure adopted from [108])

The method described above was used to monitor the hydroxylation activity of PhzO. The reaction was carried out in the presence of FADH₂ delivered from the NADH/FAD oxido-reduction reaction and catalyzed by the flavin reductase Fre from *Escherichia coli*. Substrate concentration decrease and product concentration increase were monitored. Separation of the substrate from the product was achieved with an Atlantis C18 column and the eluted compounds were then analyzed in real time by APCI-MS. Assays were performed under aerobic condition at 20 °C and under rigorous shaking in the thermomixer at 300 rpm in 20 mM Tris-HCl (pH 7.5) containing 1 mM FAD, 200 μM PCA, 1 μM Fre, 5 mM Na₂S₂O₄ as reducing agent and 10 μM caffeine. To initiate the reaction 5 mM NADH and 20 μM PhzO were added to the reaction mixture. Immediately after the reaction started, a sample of 20 μl was taken and mixed with 20 μl of

acetonitrile supplemented by 0.1% acetic acid to quench the reaction. This sample was considered to be at 0 min after reaction initiation. Other samples were taken at different time intervals: 2, 5, 10, 15, and 20 minutes. Assays were repeated varying cofactor, substrate, and enzyme concentration. A cross check was performed by repeating the same assay in absence of PhzO. Caffeine was added to the reaction as an inert component to scale the results of various measurements, thus permitting the raw data computation. The results were processed by the Xcalibur software for the integration of the peaks and determination of the compounds based on mass charge ratio Microsoft Office and Origin7 were used to plot the results on graphs.

3.6 Protein crystallography

3.6.1 Introduction

For the biochemical study of enzymes with yet unclear or undefined activity it is very helpful to know their spatial structure. The structural characterization of proteins can predict to some extent or explain the reaction mechanism catalyzed by the enzyme and its substrate specificity. The most common methods used for determining protein structure are X-ray crystallography, NMR and electron microscopy. Images obtained with electron microscopy show the quaternary structure of a protein or enzyme complex, in contrast to X-ray crystallography, which delivers information at atomic level. In case of optical microscopes the maximum achievable resolution of a lens d is proportional to the wavelength λ of the light and inversely proportional to the refractive index n :

$$d = \frac{\lambda}{2 * n}$$

The refractive index for most materials is approximately 1 and a carbon-carbon single bond is about 1.5 Å. In order to obtain a resolution at atomic level, the wavelength employed must be at least 0.3 nm. The visible light (VIS) and ultra violet (UV) have wavelengths in the range of micrometer (μm) and nanometer (nm), respectively. X-rays coming e. g. from a Cu rotating anode have a wavelength of 0.154 nm, while the synchrotron light is about 0.01 nm.

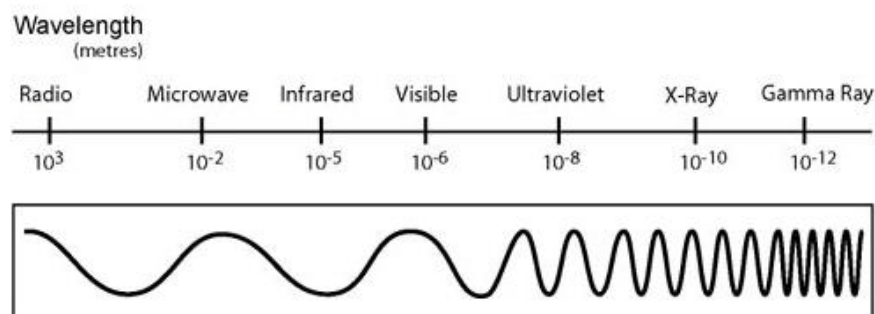


Figure 27 The electromagnetic spectrum (figure adopted from [116])

3.6.2 Crystallization

If one wants to study a protein structure by X-ray analysis, this must be first crystallized. A so-called "single crystal" contains many protein molecules arranged in a perfect and uniform crystal lattice so that radiation coming from any region of the protein molecule will add up to a strong signal. The crystal serves as a kind of amplifier for diffracted X-rays. The most commonly used method to crystallize proteins from a solution is vapor diffusion. This method requires very pure proteins and also a high concentration of about 10 mg/ml. In a crystallization plate, a drop of 0.1 μl to 2 μl of the protein solution is mixed with an equal volume of reservoir solution. The 500 μl of reservoir solution and the drop mixture are in a sealed cavity of the plate. The reservoir solution contains a water attracting precipitant as well as salt and a buffer maintaining the pH level. Precipitants like polyethylene glycol (PEG) will induce the movement of the water molecules from the drop containing the protein solution through the gaseous phase into the reservoir solution. In this way, the protein is concentrated slowly, until its solubility limit is exceeded and it eventually forms crystals. Temperature plays also an important role in the crystallization processes. By higher temperatures of up to 25 °C the vapor diffusion is faster, leading to rapid crystallization in case of very stable proteins. Other options would be crystallization at 4 °C and 12 °C, which stabilizes the protein in the crystallization plates for longer time and lowers the chances for protein precipitation.

If the protein and precipitant concentrations are further increased in the supersaturated region, this can lead to precipitation of the protein (**Figure 28**). The crystallization phase diagram is a function of the protein and precipitant concentration. Crystal growth is possible only in the supersaturated region.

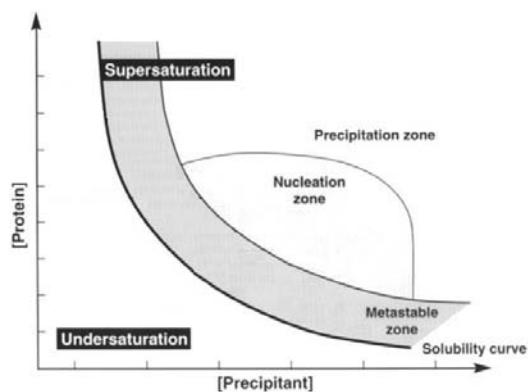


Figure 28 A schematic drawing of a protein crystallization phase diagram based on the protein and precipitant concentrations (figure adopted from [117])

In order to determine the appropriate crystallization conditions for each protein, initial screening experiments are carried out in which a variety of conditions are tested. To this end, the sitting drop method was used in a 96 well format in the scale of 200 nl. The drops were pipetted here by a robot (Mosquito, TTP Labtech, UK). The conditions under which crystals were growing are then further optimized in order to obtain large and well-shaped crystals. The fine tuning of the initial conditions was performed manually with the hanging drop method in a 24 well format and in a 2 μ l drop-scale. (Figure. 29)

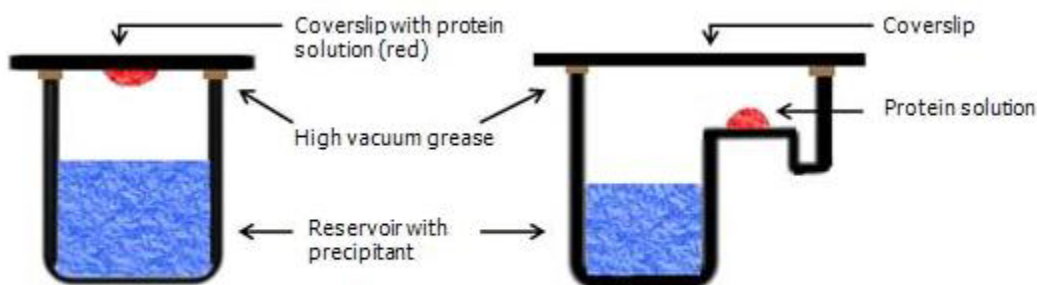


Figure 29 Crystallization by vapor diffusion method in hanging (left) and sitting drop (right)

3.6.3 Cryo-protection

For minimizing the radiation damage in the crystals during data collection at higher temperatures, the method of cryo-protection at 100 K in nitrogen flow was used. The crystals were transferred from their crystallization solution into a cryo-solution and cooled in liquid nitrogen. The most commonly used cryo-solutions are characterized by low water content in order to prevent the formation of ice crystals, which scatter the X-ray as well. In this work, the cryo-solutions were obtained by adding 15% glycerol or 10% PEG400 to the crystallization conditions.

3.6.4 Data collection and processing

After suitable preparation of the crystals with cryo protectant (3.6.3), they were analyzed with monochromatic X-rays. In this work a Cu-K α radiation at about 1.54 Å at 100 K was used. Dataset collection was performed at beamline X10SA of the Swiss Light Source (SLS) at the Paul Scherrer Institut (Villigen, Switzerland) using a MAR 225 detector. A diffraction pattern with regularly spaced reflections of different intensities is shown in **Figure 30**.

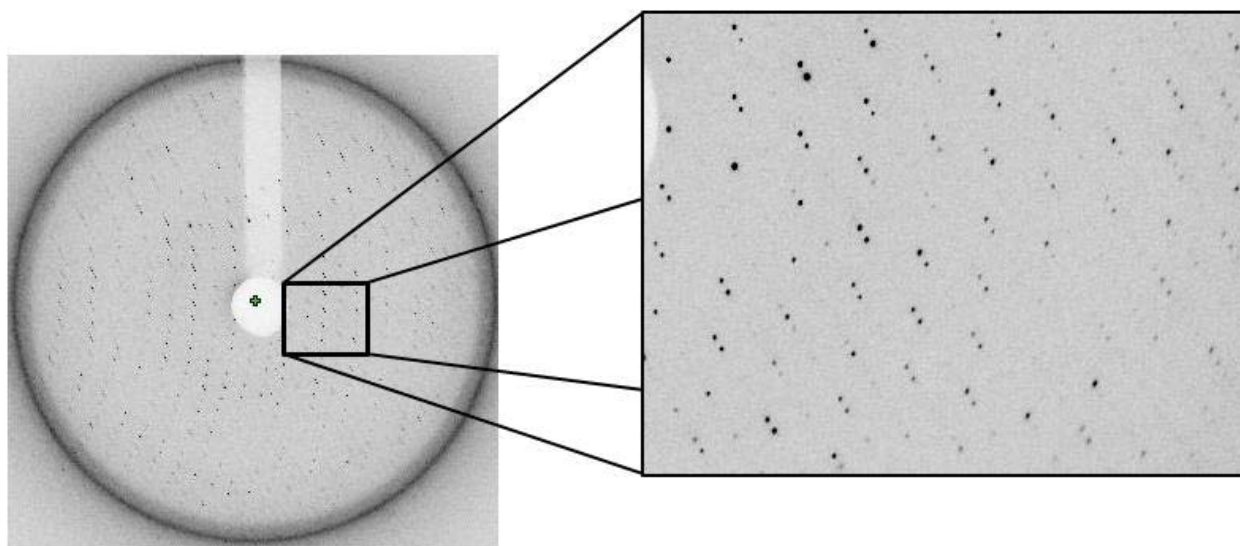


Figure 30 Diffraction pattern of a protein crystal (TcPA)

The diffraction patterns of the scattered X-rays include almost the complete information excluding the phase, about the three-dimensional arrangement of the atoms in the crystal. The position of the atoms can be calculated by knowing the following parameters: wavelength and amplitude of the electromagnetic wave of the X-ray beam and by determining the phase of the wavelength with special methods.

From the intensities of the reflections and the distances and angles between them, the cell parameters lengths and angles of the unit cell of the crystal lattice can be calculated using a computer program package such as XDS/XSCALE^[119]. Based on the values of the reciprocal unit cell parameters, the Bravais lattice type of the unit cell are determined. During the indexing procedure, the correct crystallographic coordinates h, k, l (Miller indices) are assigned for each detected reflection. The quality of the data was evaluated by calculating the value of R_{sym} :

$$R_{sym} = \frac{\sum_{hkl} \sum_i |I_{i,hkl} - [I_{hkl}]|}{\sum_{hkl} \sum_i [I_{hkl}]}$$

Formula 3-10 $I_{i,hkl}$ = observed intensity of the i-th related reflection with Miller indices hkl, $[I_{hkl}]$ = average intensity of the reflections I_{hkl}

The wavelength of the X-ray beam diffracted by the crystal is identical with the wavelength of the initial beam. To calculate the electron density map of the protein structure, the value of the structure factor $\vec{F}(hkl)$ must be determined. This is obtained from the structure factor amplitudes $|F(hkl)|$ and of the phase angle α :

$$\vec{F}(hkl) = |F(hkl)| e^{2\pi i \alpha(hkl)}$$

Formula 3-11 hkl = position of the lattice point in reciprocal lattice, $F(hkl)$ = structure factor of the hkl reflection, $|F(hkl)|$ = structure factor amplitude, $\alpha(hkl)$ = phase information

The relative intensity of the beam can be determined by the degree of blackening of an X-ray film or digitally by measuring the intensity of a reference spot on the detector. The relative intensities $I(hkl)$ are proportional to the square of the structure factor amplitudes $|F(hkl)|$:

$$I(hkl) \propto |F(hkl)|^2$$

The electron density at any point in the Cartesian coordinate system can be derived from the structure factor amplitude and the phase angles calculated as follows:

$$\rho(xyz) = \frac{1}{V} \sum_{hkl} |F(hkl)| e^{2\pi i \alpha(hkl)} e^{-2\pi i (hx+ky+lz)}$$

Formula 3-12 $\rho(xyz)$ = density of the Cartesian coordinates x , y and z ; V = the volume of the unit cell; F = structure factor amplitude defined as a function of the crystallographic coordinates h , k and l .

The Fourier transformation gives a preliminary structure model of the protein based on the diffraction data, but is still lacking information concerning the phase, which cannot be measured directly by experiment, but must be determined by special methods (see sections **3.6.5**).

3.6.5 Solving the phase problem

As mentioned earlier, it is not possible to determine the phases directly from the resulting X-ray diffraction peaks. To solve the phase problem, four approaches are available: molecular replacement, singular or multiple anomalous dispersion (MAD), singular or multiple isomorphous replacement (SIR / MIR) and the direct method of phase determination for small molecules.

3.6.5.1 Molecular replacement (MR)

The method of molecular replacement (MR) can be used when the crystal structure of a structurally similar protein is already known and can be used as a model. For this, databases like NCBI and PDB are browsed for proteins with high sequence identity to the protein of interest, as they often have a very similar structure. Through molecular replacement, the structure factor amplitudes and phases are calculated backwards from the coordinates of the model. Combining the phase of the model α_{calc} and the measured structure amplitudes $|F_{\text{obs}}|$ of the crystal, an electron density map for the new crystal structure is generated. The space group and the orientation of the model can differ from the new crystal structures and therefore the model must first be optimally fitted in the new crystal cell. This is done via rotation functions by adjusting the three rotational and three translational variables using the Patterson map of the model and the observed structure factor amplitude $|F_{\text{hkl}}|$. The better they match, the better is the resulting rotational and translational function. After the model is applied to the crystal unit cell, the new electron density can be calculated based on its structure.

3.6.5.2 Singular or multiple anomalous dispersion (SAD/MAD)

Proteins labeled with heavy atoms are used in order to determine the phase of their structure. There are two principle methods of labeling with heavy atoms: incorporating selenium-L-methionine recombinantly instead of methionine or site specific and non-covalent incorporation of heavy metals. In the last, heavy atoms are incorporated in the protein structure by soaking experiments, where the solution containing the crystals is supplemented by different concentrations of various heavy metals. These will diffuse in time into the crystals.

The reflections (hkl) and (-hkl) are defined as Friedel pairs. In non-derivatized protein crystals, the structure amplitudes of the Friedel pairs are identical. For heavy metal atoms, this is no longer valid if they absorb X-rays of a certain wavelength and emit it

again as anomalous diffraction. The resulting differences in intensity are called anomalous dispersion, which becomes significant especially when the excitation of the metal is near the wavelength of the X-ray beam. From the intensity differences, one can determine the exact position of the heavy metals and also the phase of the heavy metals from which the phase of the whole protein can be assessed (**Figure 31**).

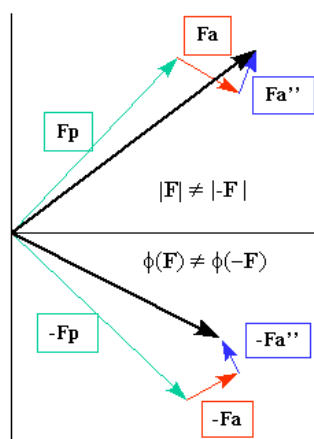


Figure 31 Correlation of native and derivative scattering factors: $|F_a|$ and $|F_{a''}|$ (anomalous scattering contributions) and $|F_p|$ (protein)

During data set collection, mostly three sets at different wavelengths are collected from the same crystal. Another popular method used in determining protein structures is the SAD phasing. Essential for this method is to break the phase ambiguity by density-modification techniques.

3.6.6 Model building and refinement

Based on the initial structure model and using the method of molecular replacement, an electron density could be determined. The model and the electron density were then used to build in detail the correct protein structure and to insert the water molecules which are forming approximately 50% of the solvent content. For this purpose, the computer programs COOT and ONO were used ^[124, 125]. After the complete construction

of the desired protein structure model, the computer program Refmac5^[121] was used to refine the structure by minimizing against the diffraction data. During refmac refinement the energy function E which consists of a geometric and a crystallographic part is minimized. The result of the refinement is a new structure model. This is obtained by recalculating the structure factor amplitude and phase angle. The quality of the new structure model is given by the value of R_{cryst} which compares the observed structure factor amplitude ($|F_{obs}|$) with the calculated one ($|F_{obs}| - |F_{calc}|$):

$$R_{cryst} = \frac{\sum (|F_{obs}| - |F_{calc}|)}{\sum |F_{obs}|}$$

In addition to the R_{cryst} there is another R value, called R_{cryst} . The calculation of the new phases based on the building and refinement can be defective because computer programs will try to fit the model under all circumstances, causing over-fitting of the model in the electron density. As a cross check, 5% to 10% of the measured reflections are excluded from the refinement process and the R value so obtained will be named as R_{cryst} ^[122]. If the structure building and refinement are correct, the R_{free} value must be very close to the value of R_{cryst} and decrease with each run of refinement.

4. RESULTS AND DISCUSSION

4.1 Expression of the proteins

4.1.1 Preliminary tests for the expression

The plasmids resulting from the molecular cloning procedure were transformed for expression in the *E. coli* strain BL21 (*DE3*) RIL. Cell cultures at the scale of 10 ml were prepared for the test expression and induced with 1 mM IPTG or 0.2% α -lactose at a cell density of $OD_{600} = 0.6$. Before induction and after 4 hours, samples were taken from the cultures and lysed in SDS buffer, than loaded on an SDS-PAGE and checked for the protein expression level. The induction procedure which resulted in higher levels of protein expression was used later in large scale cell cultures. In the work presented here, cell cultures induced with 0.2% α -lactose resulted in a higher yield of the protein expression in comparison with the cell cultures induced with IPTG. In case of PhzO, this was not expressed at all via IPTG induction. The reason for this may be different cellular mechanisms that inhibit the protein overexpression by induction with IPTG. Another reason could be that the expressed protein is toxic for the host cell so that the entire expression machinery is switched off by the cell itself. The expression of the proteins used in this work was induced with 0.2% α -lactose at 20 °C under continuous shaking for at least 24 hours.

4.1.2 Expression and purification of PhzO.

4.1.2.1 Wildtype PhzO

The expression was induced under conditions described in section **3.4.2.1**. After harvesting and disrupting the cells, fractionation of the cytoplasmatic and membrane proteins was achieved by centrifugation. The soluble fraction of the desired protein was purified by Ni-NTA chromatography (**3.4.4**). As it is depicted in **Figure 32**, bands 1 to

RESULTS AND DISCUSSION

12, almost pure protein was eluted after contaminations were removed in the “flow through” or during the washing steps (not shown in the figure) with up to 40 mM imidazole. The binding of the His-Tag to the Ni-beads was already inhibited with 100 mM imidazole, which caused the elution of the PhzO. Fractions containing PhzO were collected and dialyzed over night against dialysis buffer to remove imidazole from the protein solution.

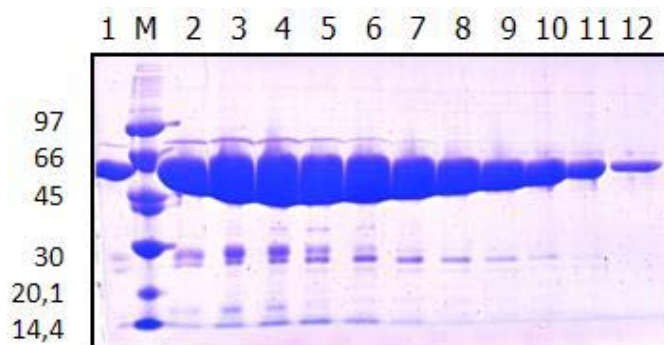


Figure 32 SDS-PAGE of the Ni-IMAC for the native PhzO

For the second purification step, PhzO was concentrated to the desired volume and applied on the gel filtration column as described in section **3.4.5**.

In the preparative gel filtration, fractions were collected by measuring the absorbance at 280 nm and investigated for the presence of proteins. The chromatogram and the corresponding gel electrophoresis are shown in **Figure 33**. The chromatogram shows a large product peak corresponding to an elution time between 60 min and 111 min (fractions 21-37). This matches with the elution time from the calibration curves of the gel filtration column (16/60 HiLoad™ Superdex™ prepgrade 200) for proteins with a molecular weight of about 220 kDa. The native PhzO is eluted as a tetramer and clearly separated from a small fraction of aggregated protein (data not shown here). In the same figure, the bands 1 to 12 in the gel electrophoresis depict the elution of the protein with a molecular weight of 55 kDa, which follows a Gaussian curve typical for gel filtration chromatographies. Fractions containing the pure protein were collected and concentrated up to the required concentration for protein crystallography, shock

RESULTS AND DISCUSSION

frozen in liquid nitrogen and stored at $-80\text{ }^{\circ}\text{C}$ until next crystallographic and biochemical applications. The overall yield of the expression and two step purification of the native PhzO is about 20 mg protein per liter of cell culture (20 mg/l).

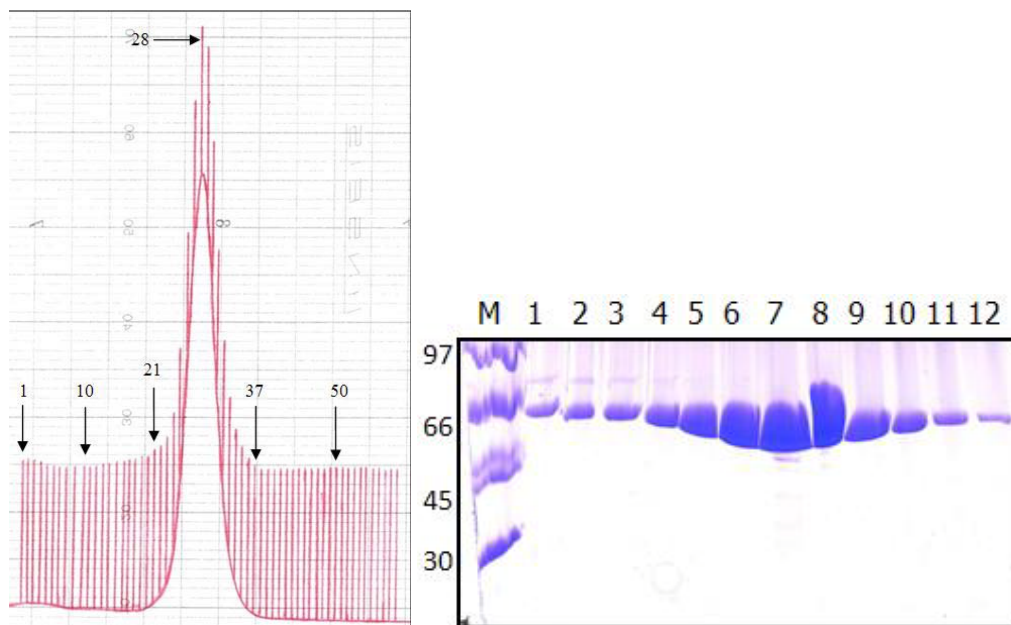


Figure 33 Preparative gel filtration chromatogram (left) and the associated SDS-PAGE for native PhzO (right)

4.1.2.2 Selenium-L-methionine labeled PhzO

To solve the phase problem involved in the process of structural determination of PhzO, a heterologous expression of a selenium methionine derivative of the protein was performed. The bacteria were cultured in a minimal growing medium and the required amino acids for the suppression of methionine biosynthesis were added to the culture right before induction of the protein expression was started with 0.2% α -lactose. At this step, 7 amino acids were added into the culture and selenium-L-methionine was added instead of methionine. The successful incorporation of the selenium-L-methionine amino acid during the protein biosynthesis offers the opportunity to locate selenium atoms by their anomalous scattering. The purification of the PhzO selenium-L-methionine derivative was similar to the purification of the native PhzO protein, using

the two step purification method: Ni-IMAC and size exclusion chromatography. PhzO SeMet was expressed and eluted with a high purity of up to 95%, while impurities were washed away in the “flow through” fraction and in the washing steps with up to 40 mM imidazole. The yield of the PhzO SeMet was about 12 mg/l cell culture.

Eluted proteins were collected and dialyzed over night against dialysis buffer, in order to get rid of the imidazole which was mixed with the protein solution during the elution procedure. Proteins were concentrated up to a required degree and volume needed for the size exclusion chromatography but with regard to the protein stability. The size exclusion chromatography was performed as described in section **3.4.5**. Selenium-L-methionine derivative of PhzO forms a tetramer in the solution.

After separation of the aggregated protein from the tetramer, fractions containing pure protein were collected, concentrated up to three different concentrations and immediately used for crystallographic screening.

4.1.3 Expression and purification of TcpA.

4.1.3.1 Wildtype TcpA

As described in material and methods, section **3.4.**, an expression plasmid that contained the gene encoding TcpA was transformed in the *E. coli* strain BL21 (DE3) RIL. An isolated colony was pre-cultured over night for inoculating the main culture used on the next day for expression. After induction with 0.2% α -lactose, reduction of the division rate was observed. During the protein expression for 24 h, only a fourfold increase of the cell density could be observed while control cultures reached densities equivalent to OD >6. From one liter of culture, 9-10 g cell pellet were obtained. The sediment was stored for further processing at -80 °C. Before cell disruption with the microfluidizer, the cell pellet was resuspended in buffer A and an EDTA-free protease inhibitor cocktail was added to prevent proteolytic degradation. The purification was similar to that described for native PhzO in section **3.4.4**.

Fractions containing pure TcpA were collected and concentrated with regard to the protein stability. It was observed that TcpA had a slightly different behavior compared to PhzO and addition of reducing agents like β -mercapto-ethanol and up to 10% glycerin was required to stabilize the protein during the concentration process.

As compared to PhzO, TcpA had a lower expression yield, and after the two step purification procedure, the total amount of protein obtained was about 14 mg/l culture. The protein solution was immediately used for crystallographic screening or stored at -80 °C for longer time, until biochemical assays were developed and biophysical measurements performed.

4.1.3.2 Selenium-L-methionine labeled TcpA

Cell harvesting, disruption and protein purification were done following the protocols used to purify the wildtype TcpA. **Figure 34** depicts the SDS-gel electrophoreses with the samples taken after induction (column 1), before induction (column 2), “flow through” (column 3), the washing step with 40 mM imidazole (column 4) and the fractions containing the wanted protein (column 5 to 12), which were eluted from the Ni-beads with up to 250 mM imidazole. The protein band at the level of 57 kDa in column 3 indicates that probably not all expressed TcpA was bound to the Ni-beads and a part of it is still in the “flow through”. A reason for not binding could be an unfavorable folding of the macromolecule which could hide the His-Tag and so making it inaccessible for Ni-beads. An overloading of the Ni column is excluded as explanation since the yield of the protein expression is the lowest from all expressions described in this work, up to 8 mg per liter culture, but the methods for the two step purification as well the instruments used were the same.

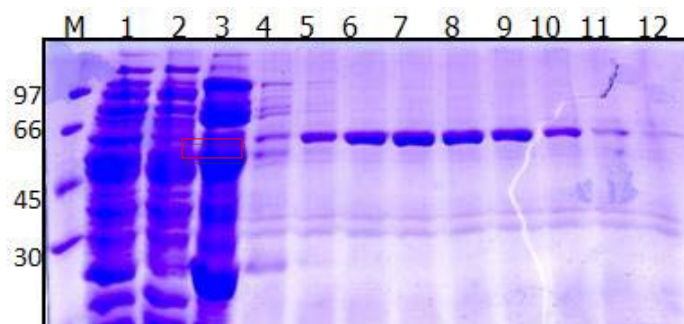


Figure 34 SDS-PAGE of the Ni-IMAC for TcpA_Se-Met_Ni-IMAC.

Fractions containing the desired protein solution were dialyzed over night against dialyses buffer as described in section 3.4 to get rid of imidazole which could perturb the protein stability during concentration and sample preparation for the preparative gel filtration. Knowing about the difficulties involved in stabilizing the native form of TcpA during the concentration procedure, the protein solution was supplemented by 2 mM β -mercapto-ethanol and up to 10% glycerin. The SDS-gel-chromatography shown in **Figure 35** reveals the high purity of the SeMet labeled TcpA (columns 1 to 10) and its clear separation from degradation products as well contaminants with a different molecular weight (column 11 and 12).

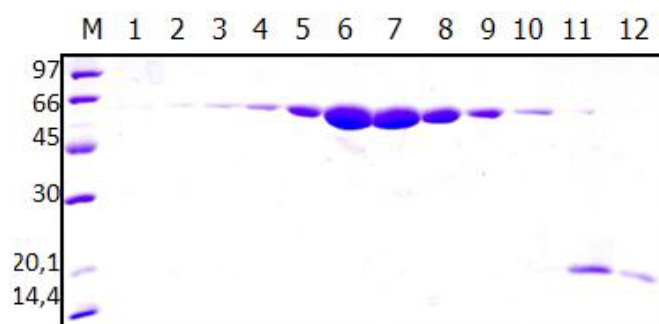


Figure 35 SDS-PAGE with the fractions collected during the size exclusion chromatography for SeMet labeled TcpA.

Although SeMet labeled TcpA was purified in smaller amounts compared with the other proteins presented in this work, its purity reached at least 95%. The protein was concentrated to various concentrations needed for crystallographic screening

experiments and stored and -80 °C. It was observed that best crystallographic results were obtained with fresh purified protein and before storage at -80 °C.

4.1.4 Expression and purification of Fre.

The monooxygenases described in this study are delivered with reduced FAD by a second enzyme, which is the flavin reductase. Until now, no flavin reductase from *Pseudomonas aureofaciens* has been reported, but a previous publication describes a successful way of determining TcpA activity with the contribution of the flavin reductase from *E.coli* [97]. For this reason, in all the biochemical assays described in section 4.6, the flavin reductase (Fre) is the one belonging to the bacterial genera *E.coli* and not to *P. aureofaciens* or *R. eutropha*. The pET7 plasmid encoding the gene of flavin reductase (Fre) was obtained from D. Mavrodi from Washington State University, Pullman, USA. Fre was expressed in *E.coli* with overnight induction at 20 °C with 0.5 mM IPTG. After cell harvesting and cell disruption, the protein solution was loaded on a nickel column, washed with 40 mM imidazole and finally eluted with up to 250 mM imidazole, as described in section 3.4.4.

After overnight dialyses of the collected fractions which were containing the desired and eluted protein, size exclusion chromatography was performed to separate the aggregates from the rest of the protein. The purified Fre was at least 90% pure and showed a high activity when used in cross check assays with NAD(P)H (data not shown). Fre was concentrated to the required concentration needed for the biochemical assays, aliquoted in 50 µl aliquots, deep frozen in liquid nitrogen and stored and -80 °C.

4.2 Characterization by ESI mass spectrometry

In order to check whether the labeling of the proteins with selenium-L-methionine was successful, the mass of the obtained proteins were analyzed by ESI-MS and compared with the mass of the native proteins. The molecular weight of PhzO is 56262 Da and contains 14 methionines. Exchanging methionine with selenium-L-methionine yields a mass difference of 46,9 Da for each aminoacid which should be measured and in case of a complete exchange, the mass of the protein derivative should increase by 662 Da. Thus, the expected molecular weight of the PhzO derivative is 56924 Da. The measurements shown in **Figure 36** depict the mass differences between native and labeled PhzO and prove a successful labeling of the enzyme.

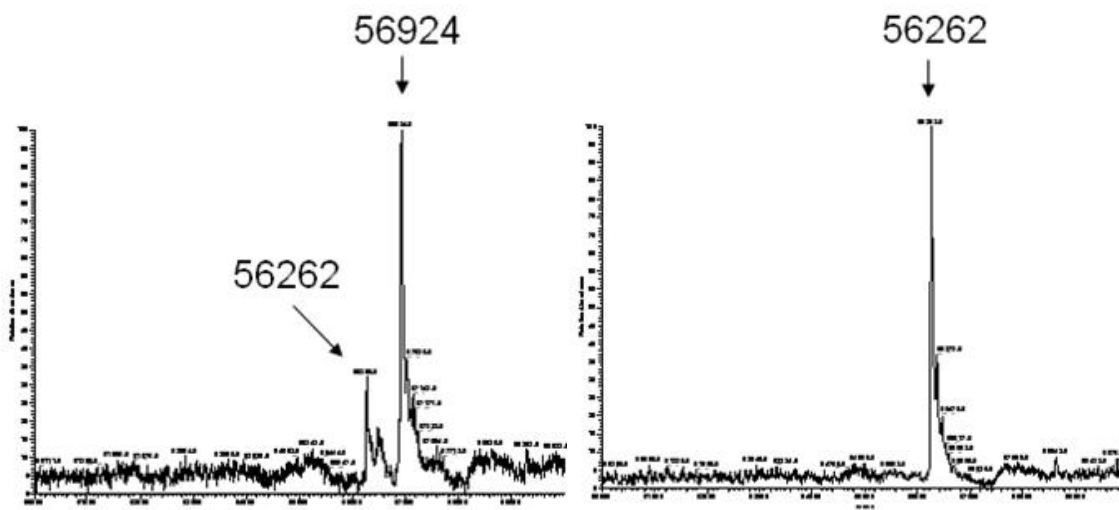


Figure 36 ESI-MS measurements for native PhzO (left) with a molecular weight of 56262 Da and selenium-L-methionine labeled PhzO (right) with the mass of 56924 Da.

The same measurements were performed for the selenium-L-methionine labeled TcpA. The molecular weight of the native enzyme is 58470 Da and the expected mass of its derivative is 59132 Da.

4.3 Crystallization

4.3.1 Crystallization of native and selenium labeled PhzO

In order to determine the suitable crystallization conditions for PhzO, screening experiments were performed in 96-well plates at 20 °C, as it was described in section 3.6.2. Native PhzO with various concentrations for up to 22 mg/ml was used to determine the initial crystallization conditions. Crystallization screens “PEGs Suite”, “PACT Suite” and “Classics” from Qiagen performed best, giving 6 consistent crystallization conditions. Some of these conditions were then optimized at a larger scale in 24-well plates by varying the concentration of the precipitant, salt and the buffer pH. Crystals were grown over a two-week period. The ligand free, native PhzO was crystallized in 0.2 M NaBr, 18-20% (*w/v*) PEG 3350 and 0.1 M bis-Tris pH 7.4-7.7. Crystals have a needle like shape with a length of about 120 μm , are colorless and mostly single crystals. The crystals are surrounded by protein precipitation, which suggests high concentrations of precipitant and protein. By lowering the concentrations to prevent protein precipitation, crystals failed to grow. **Figure 37** depicts the native PhzO crystal.

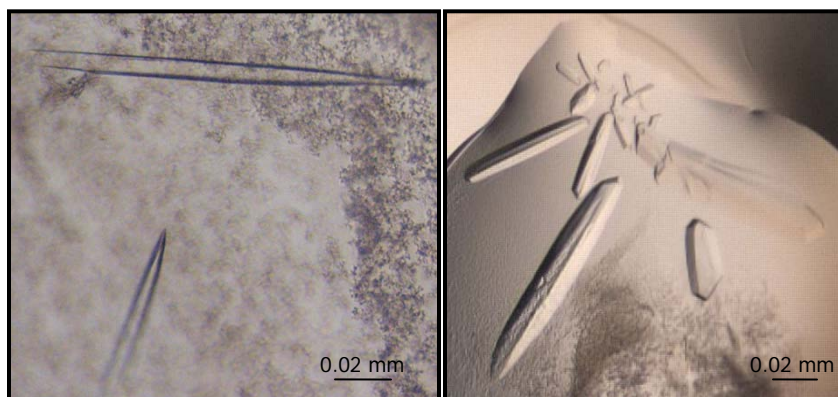


Figure 37 PhzO native crystals produced in 200 mM NaBr, 18-20% PEG 3350 and 100 mM bis-Tris pH 7.4-7.7 (left) and the selenium-L-labeled PhzO crystallized in 1 M LiCl, 0.1 M Bicine pH 8.9–pH 9.2, and 8-10%(*w/v*) PEG 6000 (right)

Selenium-L-methionine labeled PhzO was crystallized in conditions different from the native enzyme. In order to define the conditions, a new screening experiment was

performed. The best conditions under which SeMet derivative of PhzO was crystallized were: 1 M LiCl, 0.1 M Bicine pH 8.9–9.2, and 8-10% (*w/v*) PEG 6000. These crystals grew over night and had a rood like shape as it can be seen in **Figure 37**.

4.3.2 Crystallization of TcpA and selenium-L-methionine labeled TcpA

Just as in the case of PhzO, in order to define the initial crystallization conditions, screening of the enzyme was made under several different conditions. The native TcpA crystallized in 0.3 M NaNO₃, 19-21% PEG 3350 and 0.1 M Tris pH 7.1-7.5. Conditions had to be optimized several times to obtain single crystals. X-ray diffraction analyses showed that crystals lumped together, resulting in double diffraction patterns at certain rotation angles, or they tended to reorganize the unit cell so that data processing did not gave useful results. A TcpA single crystal is depicted in **Figure 38**. It has a pyramidal shape, is colorless and about 100 μm long.

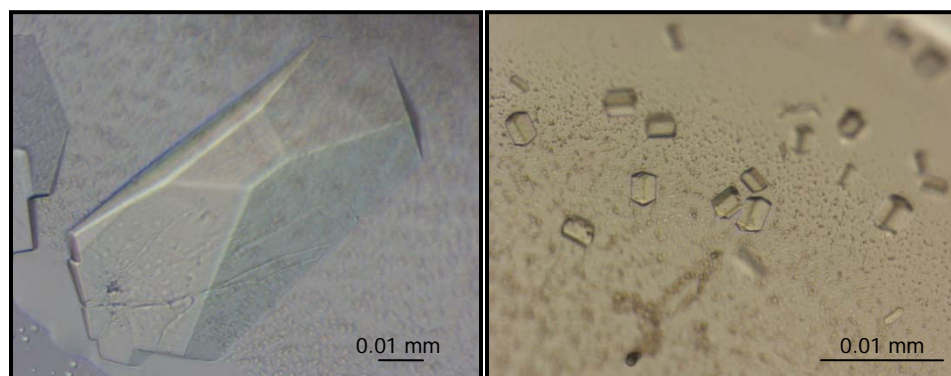


Figure 38 TcpA native single crystals produced in 0.3 M NaNO₃, 19-21% PEG 3350 and 0.1 M Tris pH 7.1-7.5(left) and the selenium-L-labeled TcpA crystallized in 0.2 M NaNO₃, 19% PEG 3350 and 0.1 M Tris pH 7.2-7.4(right)

Based on the data set collected for the native and ligand free TcpA crystals and the known structure of similar monooxygenases, the structure of the TcpA could not be solved by molecular replacement. Therefore selenium-L-methionine labeled TcpA was crystallized in similar conditions to that of native protein. Crystals were mostly single

crystals, colorless and about 40 μm long. **Figure 38** shows the native TcpA crystals (left) and selenium-L-methionine labeled TcpA (right).

4.3.3 Substrate and cofactor soaks and co-crystallization of PhzO

To gain insight into the binding of cofactors of PhzO, several soaking and co-crystallization experiments were performed. All the co-crystallization experiments described in this section were performed under similar conditions in which the native and ligand free PhzO was crystallized at 20 °C. Native crystals were soaked for a time span between 5 minutes and 24 h under different conditions with precipitant solution containing 0.1-10 mM FAD or 0.1-10 mM PCA.

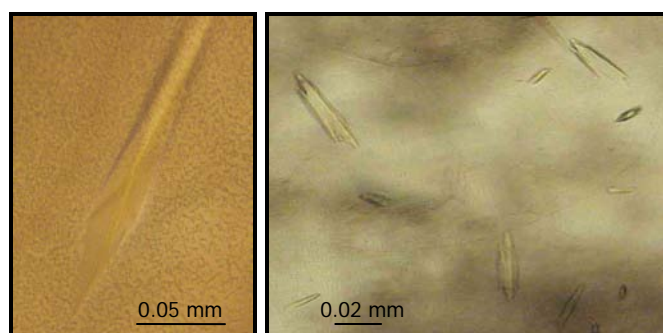


Figure 39 PhzO crystals soaked in a solution containing up to 10 mM FAD(left) and co-crystallization with 0.1 mM FAD(right).

For co-crystallization, the native enzyme was mixed with FAD, PCA in different concentrations ranging from 100 μM to 5 mM. After a short incubation at 4 °C to allow complex formation, screening protocols were developed and crystallization conditions were optimized. The crystallization conditions of the co-crystallization are identical with the conditions used to crystallize the native PhzO. The crystals obtained by the co-crystallization with FAD show irregular shape which points to an increased mosaicity of the crystal packing. **Figure 39** illustrate the PhzO crystal soaked in an FAD solution (left) and the crystals of the assumed PhzO-FAD complex (right) obtained by co-crystallization.

Crystals obtained in the co-crystallization with PCA were very small (up to 15 μm) and not diffracting x-rays. Soaking of the native PhzO crystals in PCA solution led to crystal

RESULTS AND DISCUSSION

cracking which provides clear evidence that major conformational changes are taking place while the substrate forces its way into the catalytically active site of the protein. Previous publications show that substrate binding leads to additional conformational change in the structure of 4-hydroxyphenylacetate 3-monooxygenase, which is a two component flavin diffusible monooxygenase similar to PhzO^[128-129]. Crystals obtained via co-crystallization with PCA are depicted in **Figure 40**.

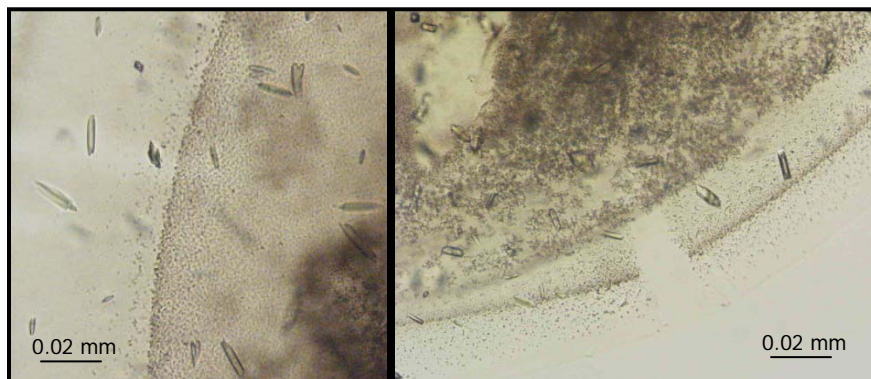


Figure 40 Co-crystallization of the native PhzO with PCA

FAD as chemical compound can be divided into 3 parts: the adenosyl moiety, ribityl and the isoalloxazine ring. In order to be able to analyse in detail the binding of FAD to PhzO, soaking and co-crystallization experiments were carried out with ADP and FMN.

Because x-ray analysis of the crystals treated with a solution containing up to 10 mM FMN were not showing the expected complex formation, co-crystallization was chosen as an alternative method. The protein crystals complexed with FMN appear in small number after 7 to 10 days growth, have a regular shape and are yellow in color indicating that these crystals absorbed FMN (see **Figure 41**). The same figure shows the crystals of the assumed PhzO-ADP complex.

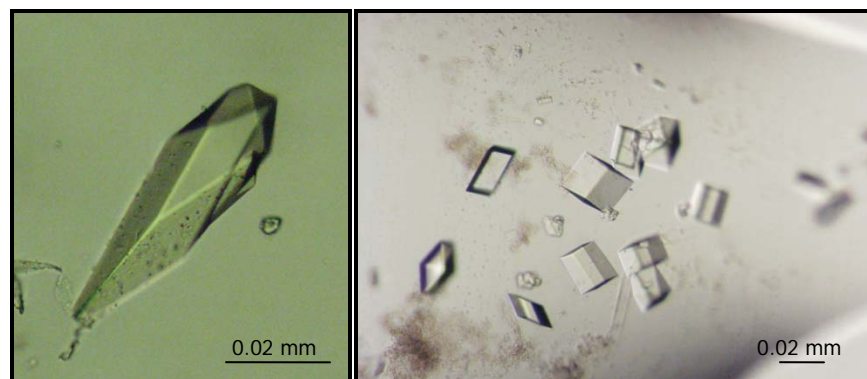


Figure 41 Co-crystallization of the native PhzO with 5 mM FMN (left) and with 5 mM ADP (right)

In both of the cases, crystals grew under similar conditions as the native PhzO, but show different morphology and size. Crystals presented in this section were treated with a cryo-protectant that was supplemented with 5 mM of FAD and 5 mM of ADP respectively to prevent the complex dissociation while undergoing cryo-protection. Then, crystals were shock flash frozen using liquid nitrogen and analyzed by x-ray diffraction (chapter 4.5.2).

4.3.4 Substrate and cofactor soaks and co-crystallization of TcpA

All experiments described in section 4.3.3 were carried out for TcpA as well. TcpA crystals are very unstable during the soaking experiments with any kind of ligand, be that a cofactor FAD, FMN, ADP or the substrate TCP or the substrate analog DCP. **Figure 42** shows that crystals treated with an FAD solution of a low concentration (0.5 mM) cracked. No crystals of the complexed TcpA could be provided for x-ray analysis.

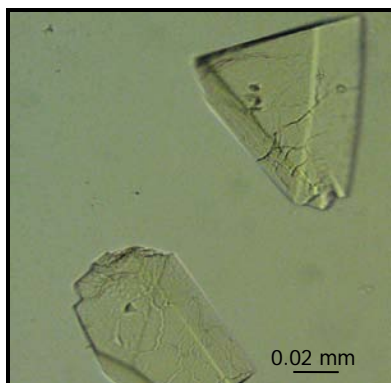


Figure 42 Soaking of native TcpA with 0.5 mM FAD.

4.4 Structure determinations

4.4.1 Sequence alignment of PhzO, TcpA and HpaB

For functional analysis and biochemical characterization of the enzymes, information about their 3D structure and a well described catalytically active site are highly desirable. Sometimes, hints about the structure and conserved amino acid sequences can be obtained just by simple amino acid sequence alignment. In this work, the amino acid sequences of PhzO and TcpA were submitted to the data bases of NCBI and PDB to search for similar proteins which may have similar structures. Both of the enzymes show similarities to the HpaB protein superfamily (**Figure 43**). The complete sequence alignment of PhzO and TcpA with HpaB is attached to the appendix. HpaB is about 25% identical and 40% similar to PhzO and TcpA.

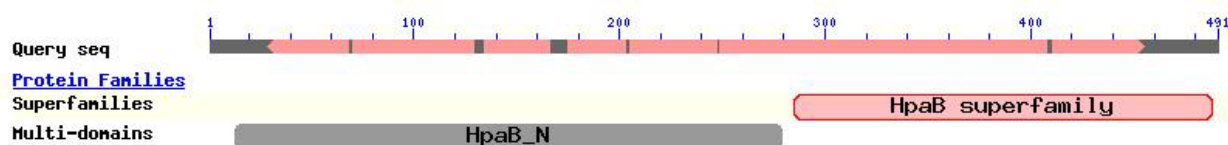


Figure 43 Blast search result. The C-termini of PhzO and TcpA are related to the HpaB superfamily, while their N-termini are related to the HpaB_N superfamily.

4.4.2 Data collection, solving and refinement of PhzO

PhzO native and soaked crystals, as well those coming from co-crystallization, were tested using a RIGAKU rotating anode X-ray generator equipped with a MAR Research imaging plate detector. The best diffracting crystals were sent to the Swiss Light Source (SLS) for X-ray analysis. A data set for the native and the labeled crystals each was collected at 100 K as non-overlapping 360° images of 1° oscillation. For native PhzO, a dataset with a maximum resolution of 1.7 Å and for the SeMet derivative of PhzO, a complete SAD dataset with 2.3 Å at the Selenium-K-edge were collected. Data processing revealed that native crystals belong to space group C222₁, with unit-cell parameters of $a = 104$, $b = 159$, $c = 114$ Å, $\alpha = \beta = \gamma = 90^\circ$, while the selenium-L-methionine labeled PhzO crystals belong to space group P2₁, with unit-cell parameters of $a = 103.8$, $b = 109.7$, $c = 104.4$ Å, $\alpha = \gamma = 90^\circ$, $\beta = 99.1^\circ$. The data set of a multiple anomalous diffraction contains information about the structure factor of the

RESULTS AND DISCUSSION

selenium-L-labeled protein, which combined with the integration results of the native data set, allows the phase determination of the native protein. Based on the anomalous signal, the Patterson map was calculated and the position of all selenium atoms was determined. The structure of PhzO was determined with AutoSharp, manually built in COOT to introduce minor adjustments and refined in REFMAC5. At the end of the refinement, the TLS option in REFMAC5 was employed as this produced lower R_{free} values^[125]. The statistics of data collection and refinement are summarized in table 4-1.

Table 4-1 Data collection statistics for PhzO and PhzO_SeMet

	NATIVE - PhzO	Se-SAD – PhzO
Data collection		
Space group	C222 ₁	P2 ₁
Cell dimensions		
<i>A</i> , <i>b</i> , <i>c</i> (Å)	104, 159, 114;	104, 110, 104
α , β , γ (°)	90, 90, 90	90, 99, 90
Wavelength	0.97886	0.97915
Resolution Å	50 - 1.75 (1.85 – 1.75)	20-2.3 (2.4-2.3)
$R_{\text{sym}}(I)$	10.9	9.7
$R_{\text{merge}}(F)$	8.4 (43.1)	10.7 (37)
$I / \sigma(I)$	22.2 (4.1)	12.0 (4.5)
Completeness (%)	100 (100)	100 (99.9)
Redundancy	7.5 (7.5)	3.9 (3.9)
Refinement		
Resolution (Å)	50 - 1.75 (1.80 – 1.75)	
(Highest Shell)	(1.80 – 1.75)	
No. reflections	90276 (7007)	
R_{work}	14.8 (17.9)	
R_{free}	19.1 (24.8)	
No. atoms		
Protein	7688	
Ligand/ion	88	
Water	773	
<i>B</i> -factors		
Protein	19.37	
Ligand/ion	-	
Water	31.55	
R.m.s deviations		
Bond lengths (Å)	0.024	
Bond angles (°)	1.946	

Values in parentheses refer to the highest resolution shell.

$R_{\text{sym}}(I) = \sum \sum I(h)_j - \langle I(h) \rangle / \sum \sum I(h)_j$, where $I(h)_j$ is the measured diffraction intensity, and the summation includes all observations.

$R_{\text{merge}}(F)$ is a redundancy-independent merging R-factor of structure factor amplitudes

RESULTS AND DISCUSSION

The Ramachandran plot (see appendix) obtained after complete building and refinement shows 96.65% of the total amino acids in the preferred region, 1.89% in the allowed region and 1.47% in the outliers.

4.4.3 Data collection, solving and refinement for PhzO complexed with FAD

The native PhzO crystals soaked with FAD possess a lower symmetry of $P2_1$ compared to the space group of the native PhzO which is $C222_1$. In contrast, data taken from the latter crystals were anisotropic. This indicates that their crystal packing was disturbed by the incorporation of FAD, while the native crystals on their own showed a good diffraction up to 1.7 Å.

Stable crystals were obtained when crystals grown via co-crystallization with ADP were soaked with FAD. In these crystals as depicted in **Figure 41** protein was packed in the orthorhombic space group $C222_1$. The crystals were diffracting up to 3.2 Å. The corresponding data collection record is summarized in Table 4-2.

Table 4-2 Data collection statistics for PhzO complexed with FAD

PhzO - FAD	
Data collection	
Space group	$C222_1$
Cell dimensions	
<i>A, b, c</i> (Å)	103.61, 174.56, 110.97
α, β, γ (°)	90, 90, 90
Wavelength	1.036763
Resolution Å	50 – 3.2 (3.3 - 3.2)
$R_{\text{sym}}(I)$	7.1 (23.7)
$R_{\text{merge}}(F)$	10.5 (46.7)
$I / \sigma(I)$	20.4 (4.4)
Completeness (%)	99.9
Redundancy	7.4 (7.5)
Refinement	
Resolution (Å)	50 – 3.2
(Highest Shell)	(3.28 – 3.2)
No. reflections	16122 (1253)
R_{work}	19.4 (31.0)
R_{free}	25.4 (37.6)

No. atoms	
Protein	15399
Ligand/ion	106
Water	0
<i>B</i> -factors	
Protein	55.19
Ligand/ion	81.14
Water	-
R.m.s deviations	
Bond lengths (Å)	0.011
Bond angles (°)	1.339

Values in parentheses refer to the highest resolution shell.

$R_{\text{sym}}(I) = \frac{\sum \sum I(h)_j - \langle I(h) \rangle}{\sum \sum I(h)_j}$, where $I(h)_j$ is the measured diffraction intensity and the summation includes all observations.

$R_{\text{merge}}(F)$ is a redundancy-independent merging R-factor of structure factor amplitudes

4.4.4 Data collection, structure determination and refinement of TcpA

Single crystals of the native TcpA were chosen for in-house diffraction tests and the best diffracting crystals were sent to the Swiss Light Source for data collection. A data set with a maximum resolution of 2.9 Å was collected. Data processing revealed that native TcpA crystals belong to space group C222₁, with unit-cell parameters of $a = 126$, $b = 150$, $c = 231$ Å, $\alpha = \beta = \gamma = 90^\circ$. However, the structure of TcpA could not be determined by molecular replacement.

In order to determine the structure of TcpA by the method of single/multiple anomalous diffraction, crystals of the selenium-L-methionine labeled TcpA were crystallized and analyzed by x-ray diffraction. These crystals diffracted up to 3 Å and belong to space group P2₁, with unit-cell parameters of $a = 99$, $b = 228$, $c = 98$ Å, $\alpha = \gamma = 90^\circ$, $\beta = 100^\circ$. Based on the anomalous signal, the Patterson map was calculated and the position of all selenium atoms was determined. The program SHARP was then used to calculate the initial protein phase, using the f' and f'' values determined experimentally. The resulting electron density was of poor connectivity, making tracing of the structure impossible. However, the data collected from the selenium-L-methionine labeled crystal was consistent enough to determine the protein structure by molecular replacement, a procedure that failed with the native TcpA dataset. REFMAC5 was used for automatic rigid body refinement and for several iterations of TLS (translation, libration, screw-rotation displacement) refinement. The statistics are summarized in table 4-3.

Table 4-3 Data collection statistics for TcpA and TcpA_SeMet

	NATIVE - TcpA	Se-SAD - TcpA
Data collection		
Space group	C222 ₁	P2 ₁
Cell dimensions		
<i>A, b, c</i> (Å)	126, 150, 231	96.3, 230.9, 98.0
<i>α, β, γ</i> (°)	90, 90, 90	90, 99.7, 90
Wavelength	0.978	0.9791
Resolution Å	20-2.9 (2.9)	20-2.8 (2.8)
<i>R</i> _{sym} (<i>I</i>)	6.3 (55.8)	27.6 (46.9)
<i>R</i> _{merge} (<i>F</i>)	10.8 (51.8)	8.9 (43.3)
<i>I</i> / <i>σ</i> (<i>I</i>)	13.99 (2.51)	13.6 (3.7)
Completeness (%)	99.9	99.5 (99.9)
Redundancy	2.6	3.8 (3.9)
Refinement		
Resolution (Å)	20-2.8	
(Highest Shell)	(2.8)	
No. reflections	245301 (39848)	
<i>R</i> _{work}	0.25	
<i>R</i> _{free}	0.18	
No. atoms		
Protein	30432	
Ligand/ion	-	
Water	-	
<i>B</i> -factors		
Protein	55.37	
Ligand/ion	-	
Water	-	
R.m.s deviations		
Bond lengths (Å)	0.014	
Bond angles (°)	1.510	

Values in parentheses refer to the highest resolution shell.

$R_{\text{sym}}(I) = \frac{\sum \sum I(h)_j - \langle I(h) \rangle}{\sum \sum I(h)_j}$, where $I(h)_j$ is the measured diffraction intensity, and the summation includes all observations.

$R_{\text{merge}}(F)$ is a redundancy-independent merging R-factor of structure factor amplitudes

The accuracy of the final model of TcpA is represented by the Ramachandran plot (see appendix) obtained after complete building and refinement. This shows 92.89% of the total amino acids in the preferred region, 4.96% in the allowed region and 2.16% in the outliers.

4.5 Structural and functional analysis of the monooxygenases

4.5.1 Structure of PhzO

PhzO is composed of four identical subunits and thus has an overall molecular weight of about 220 kDa. The structure of the PhzO is a dimer of dimers and is shown in **Figure 44**.

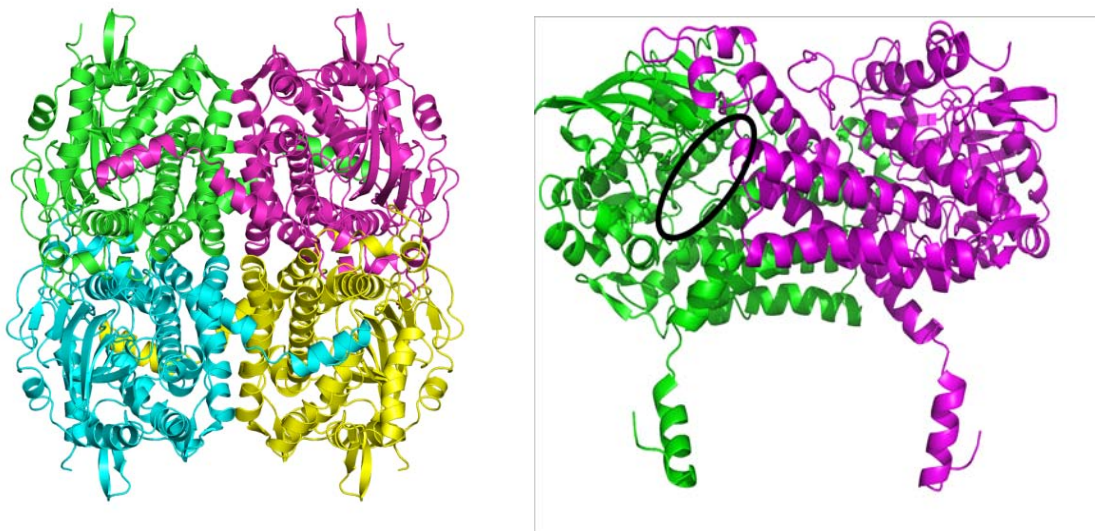


Figure 44 Crystal structure of PhzO as tetramer (left) and the crystal structure of the dimeric subunit of PhzO with the active site marked (right)

One monomer consists of 14 α -helices placed in the N-terminal and C-terminal domains and 14 β -sheets in the middle domain. In addition, each monomer has a C-terminal α -helical tail, which protrudes from the monomers of a dimer and extends over the other dimer. Between the C-terminal and the middle domain, which is comparable to a barrel formed by β -sheets, a major groove can be seen, which serves as binding site for FADH_2 and the substrate PCA.

The monomers, depicted in **Figure 45** have three main domains: the N-terminal (aa 10-149 red), middle (aa 150-283 green), and C-terminal (aa 284-472 blue), which ends with the α -helical tail (aa 473-491 orange).

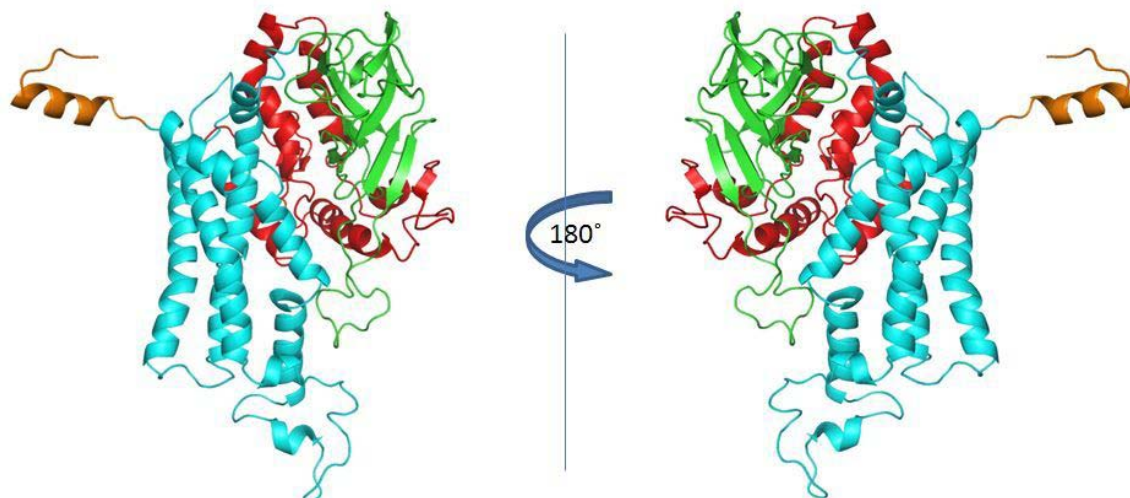


Figure 45 The monomer PhzO, subdivided in 3 domains marked with red (aa 1-149), green (aa 150-283), blue (aa 284-472) and in orange the α -helical tail (aa 473-491).

4.5.2 Structure of PhzO in complex with FAD

The crystal packing allows 4 monomers in the asymmetric unit arranged as two dimers. The evaluation of the x-ray diffraction showed additional electron density in the active site of PhzO, which can not be rationalized as that of the protein backbone. This is probably due to the fact that FAD is not stable upon irradiation by X-rays, which is supported by the fact that the crystals turned black during data collection. As a consequence FAD, which is responsible for the additional electron density, is depleted in quantity, and this may in turn contribute to the resulting decreased electron density.

Initial electron density maps showed FAD bound to the protein, but not in an accurate conformation. Clear electron density maps were calculated for the AMP and ribityl moieties but not for the isoalloxazine ring (see **Figure 46**). In order to reduce FAD, the isoalloxazine ring is solvent exposed and therefore flexible. The flexibility of the ring scales up the difficulty in determining its electron density.

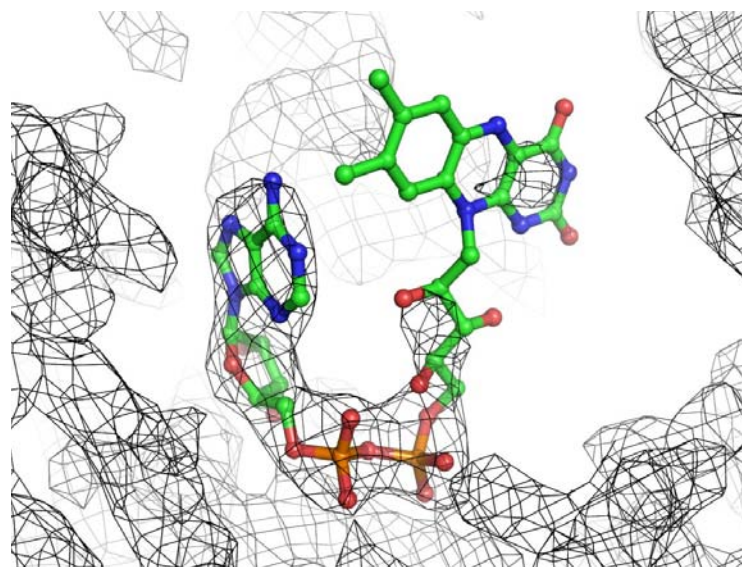


Figure 46 F_o-F_c electron density map of the PhzO-FAD crystal structure. The map is shown in black and FAD is colored differently depending on the element (C green, N blue, S orange, O red).

The space group of PhzO crystals in complex with FAD is $C222_1$, the same as determined for the native PhzO crystals. The overall structure of the PhzO-FAD complex is similar to that of the ligand free form, with r.m.s.d. of 0.709 Å for 491 C_α atoms. Except for a few minor details, these two protein structures are identical, and the binding sites show no significant differences. This suggests that binding of FAD to PhzO did not lead to any conformational changes, as was originally speculated based on the findings on the related HpaB protein structure (see chapter 1.9).

When FAD binds to the active site of native HpaB, the loop Q148 - Y162 closes the entrance of the active site and contributes to ligand fixation. The residue Q148 rotates and thereby makes more space for the isoalloxazine ring moiety of FAD. On the other side of the pocket, R447 comes in proximity to the AMP moiety of FAD and forms hydrogen bonds with it (**Figure 47**).



Figure 47 Comparison of the native monomer HpaB structure (magenta) with the structure of HpaB-FAD complex (green). The FAD molecule is highlighted in green.

Overlaying the structure of a similar monooxygenase in complex with FAD (HpaB) with the structure of PhzO-FAD confirmed the approximate position for the AMP and ribityl in the PhzO protein, but the position of the isoalloxazine ring still remained unclear. FAD was not found in the elongated phase orientated deeper towards the catalytic site, but instead coiled on the surface of the protein (see **Figures 48** and **49**). A possible explanation for the same could be, experiments were performed with the oxidized form of FAD, since the reduced form is highly unstable and thus the isoalloxazine moiety was not able to bind the active site of the protein.

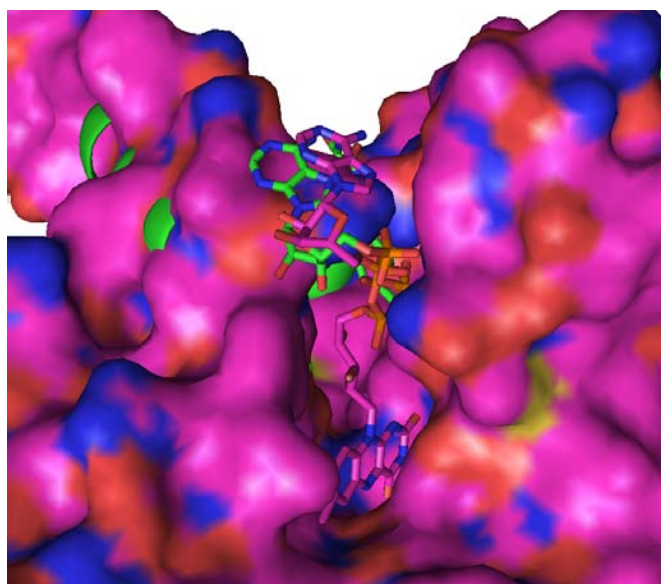


Figure 48 The structure of HpaB-FAD overlapped with the structure of PhzO-FAD. The active site of HpaB in complex with FAD (magenta). The FAD depicted in green is bound to PhzO.

RESULTS AND DISCUSSION

Based on the refined protein complex structure, the location of FAD in the active site and its interactions with the aminoacid residues were analyzed in detail. The results are depicted in **Figure 49**. Only a few hydrogen bonds are formed between the residues and the ligand. FAD binds to Q161 and R166 of the chain A and to Q397 and E393 of the neighboring chain B. All these interactions are exclusively with the ADP moiety. The question still remains whether these few interactions are enough to facilitate the binding of FAD to the active site of the enzyme.

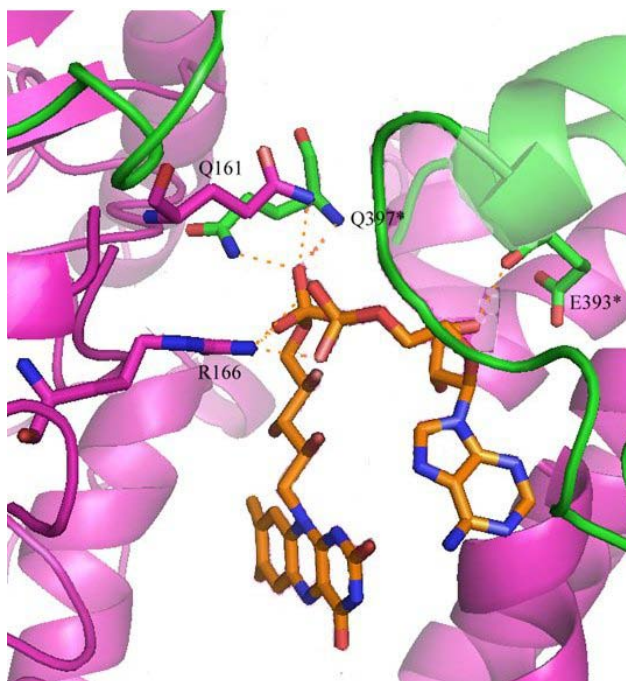


Figure 49 The aminoacids which interact binding FAD (orange) to the active site of PhzO (chain A magenta, chain B green).

Findings from the structural determination of the protein complex are in contradiction with some results from the ITC measurements, which led to the conclusion that the isoalloxazine moiety, and not ADP, is responsible for the binding of FAD to the protein. Because this protein complex structure did not yield decisive clues about the position of FAD in the active site of PhzO, modeling experiments were carried out comparing the active sites of PhzO and HpaB (chapter 4.6).

4.5.3 Structure of TcpA

The output of the refinement with the software REFMAC5 is shown in **Figure 50**. Compared to PhzO, which crystallized as one dimer of dimers, the asymmetric unit of the TcpA crystals contains 8 monomers arranged as two dimer of dimers.

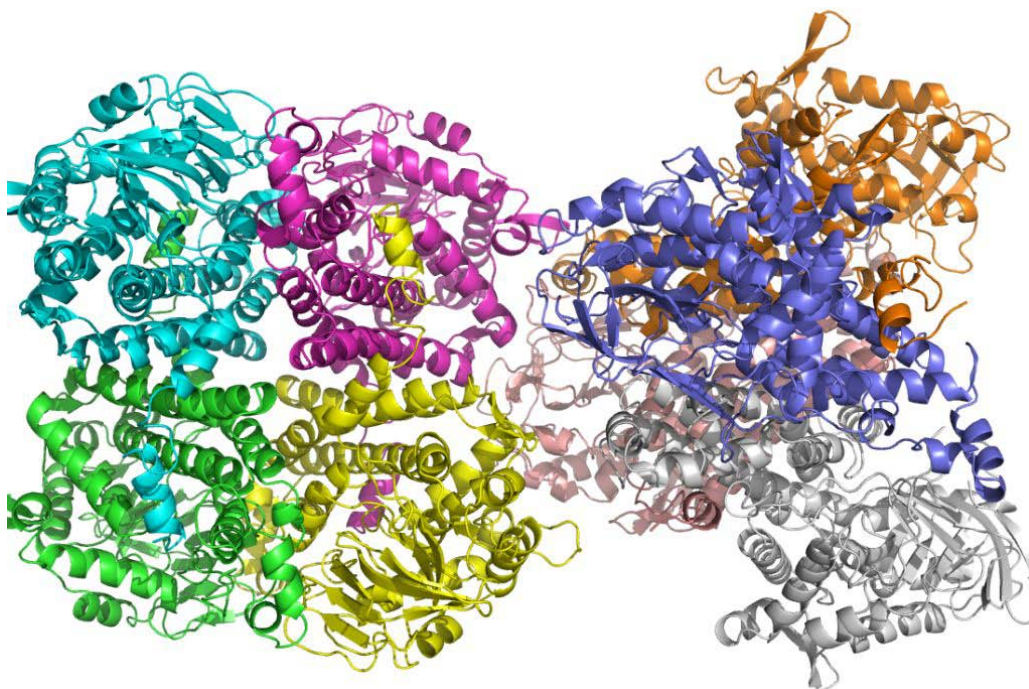


figure 50 Crystal structure of TcpA. A total of 8 monomers are occupying the unit cell. The monomers marked in yellow, green, cyan and magenta are forming the first dimer of dimers (left). The second dimer of dimers contains the chains highlighted in orange, rose, blue and gray (right)

The tertiary structure of TcpA is very similar to the structure of other monooxygenases from the same protein superfamily, such as PhzO and HpaB. Structural analysis revealed that TcpA has the same three domain composition as PhzO: the N-terminal (aa 1-146 red), middle (aa 147-274 green), and C-terminal (aa 275-472 blue), which ends with the α -helical tail (aa 473-480 orange), see **Figure 51**.

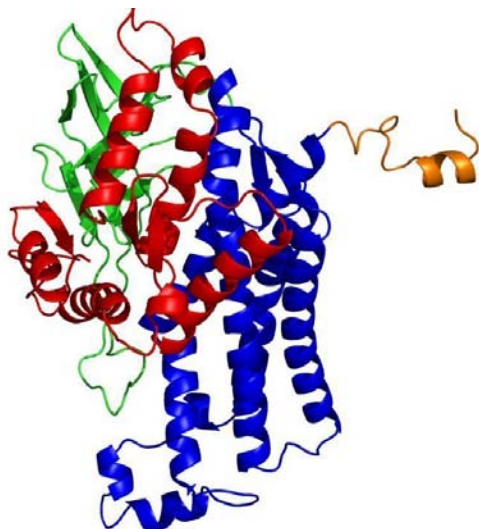


Figure 51 The monomer of TcpA with its four domains highlighted in red, green, blue and orange.

Unfortunately, the resolution of 3.0 Å is not sufficient enough in order to determine the exact position of some of the loops. Although the individual refinement of all eight chains and the superimposition of the monomers were of great help in determining the structure of flexible loops, some amino acids are still missing. Thus, amino acid residues S157-S169 forming the loop in the green middle domain (see **Figure 52**) could not be associated with any electron density and so they could not be defined in the structure model. These residues are not directly involved in the catalytically active site of the protein, but the loop is more or less like a lid that closes the binding pocket, as was shown in **Figure 47** for HpaB.

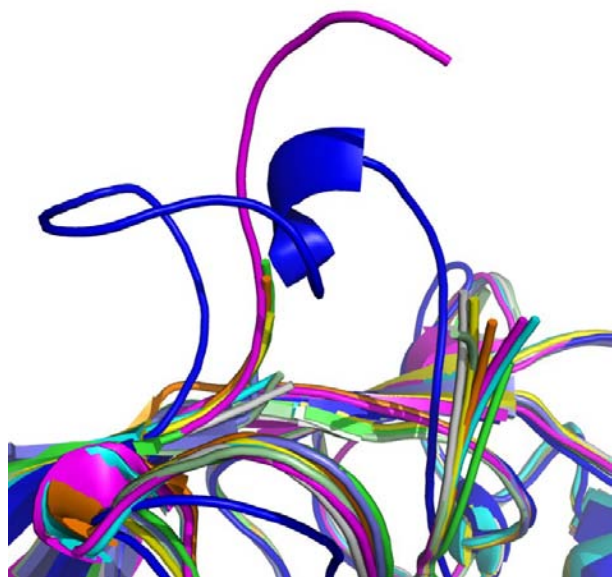


Figure 52 Superimposition of the TcpA chains (various colors) and PhzO (blue) are showing the interruption in the very flexible loop. PhzO suggests what the loop in the case of TcpA might look like.

4.6 Modeling

In order to get insights into the binding of potential ligands of PhzO and TcpA, their resulting structures were compared to that of the related protein from *T. thermophilus* HBB HpaB^[124]. For this purpose, the software PyMOL and MAESTRO were used to overlay both protein structures and analyze the structural differences. The structure of HpaB in complex with the cofactor FAD is shown in **Figure 53**. As it can be recognized from the figure, the active site is widely open and thus the cofactor FAD can bind into it. First it was analyzed in detail how the FAD binds into the active site of HpaB by determining the hydrogen bonds which are formed between the amino acid residues and the cofactors.

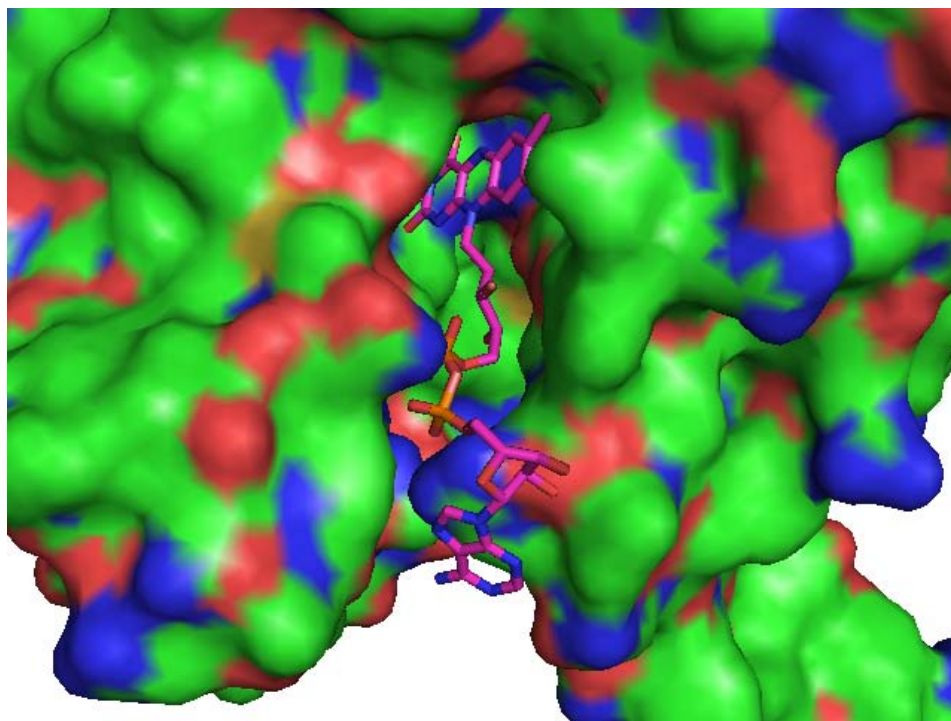


Figure 53 Structure of the active site of HpaB (green) in complex with FAD (magenta)

FAD binds to HpaB by eight hydrogen bonds with the amino acid backbone, seven with the amino acid side chains and eight with water molecules. FAD has an elongated shape and lies within the binding pocket, which is formed by the following amino acids: R100,

RESULTS AND DISCUSSION

Y104, H142 to R151, T183 to T185, D247 and R433 to R447 (see **Figure 54**). The pocket gains additional stability by some of the amino acid residues of the adjacent monomer: A312 to V318 and Q378 to S382 (data not shown). These amino acids form hydrogen bonds with the ADP moiety of FAD.

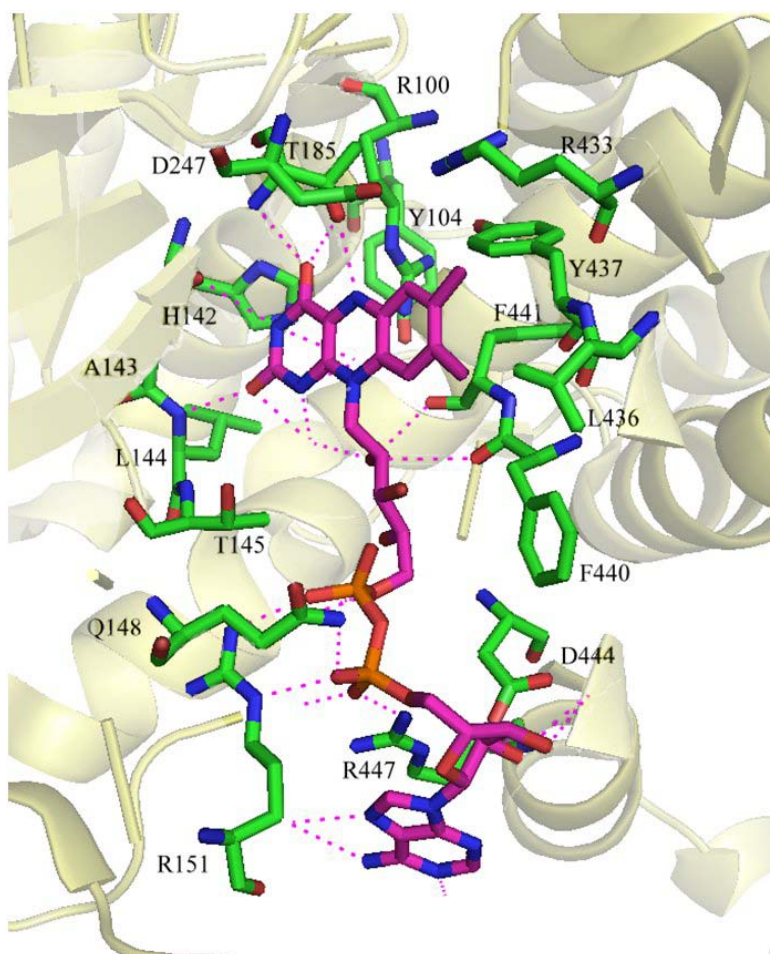


Figure.54 Interaction between the amino acid residues of HpaB (green) and FAD (magenta)

The comparison of the TcpA and PhzO with HpaB of *T. thermophilus* HB8 in complex with FAD (PDB ID: 2YYI) was expected to show which amino acids could be responsible for the binding of FAD in the active site of PhzO and TcpA, respectively.

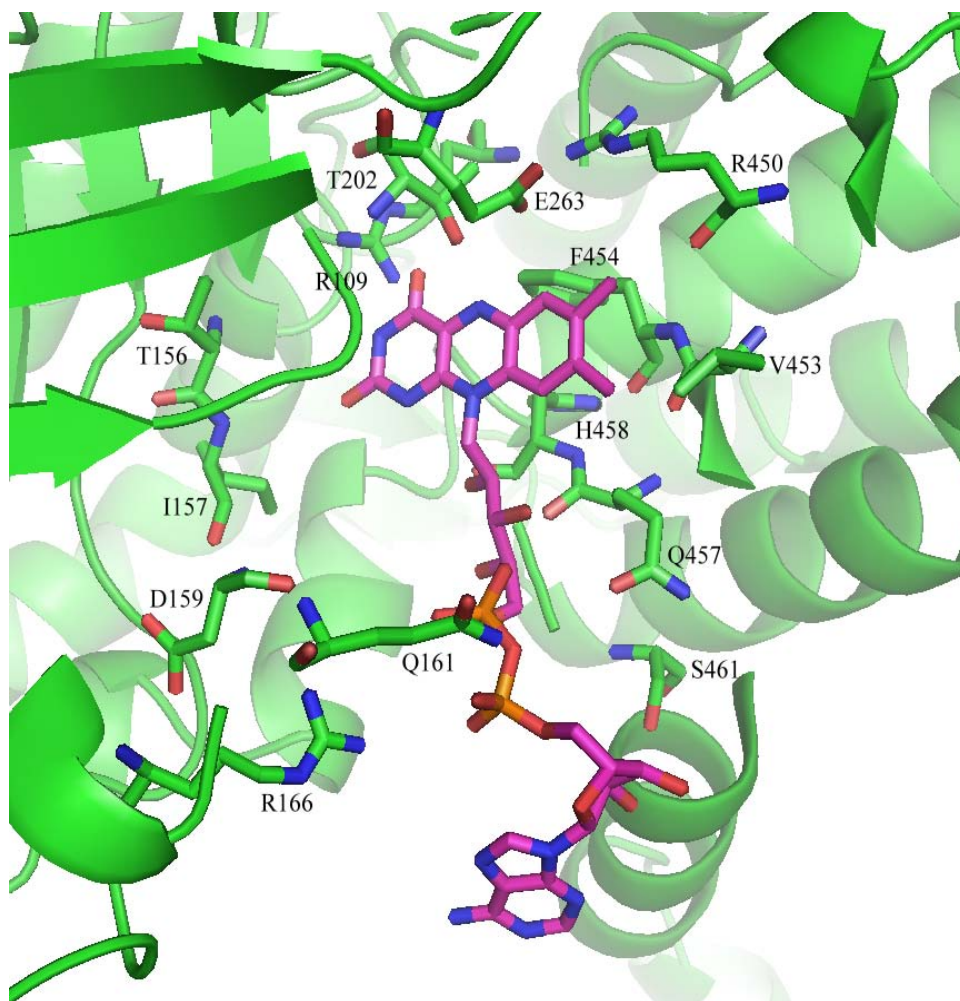


Figure 55: Amino acid residues assumed to interact with FAD (magenta) in the active site of PhzO (green)

By assuming that the position of FAD in PhzO is similar to that in HpaB, the following amino acids are likely to be involved in the formation of the binding site for FAD: R109, T156 to R166, T202, E263 and R450 to S461.

The structure of HpaB in complex with FAD and its substrate 4-hydroxyphenylacetate (4-HyPhAc) was used as a model for docking experiments with PCA and PhzO. These suggest that PCA occupies a similar position in the catalytically active site of PhzO as in the case of 4-hydroxyphenylacetate in HpaB. **Figure 56** shows the position of FAD and PCA complexing PhzO. In addition, the amino acids involved in binding the ligands are highlighted, and black dashes represent the polar contacts formed between atoms.

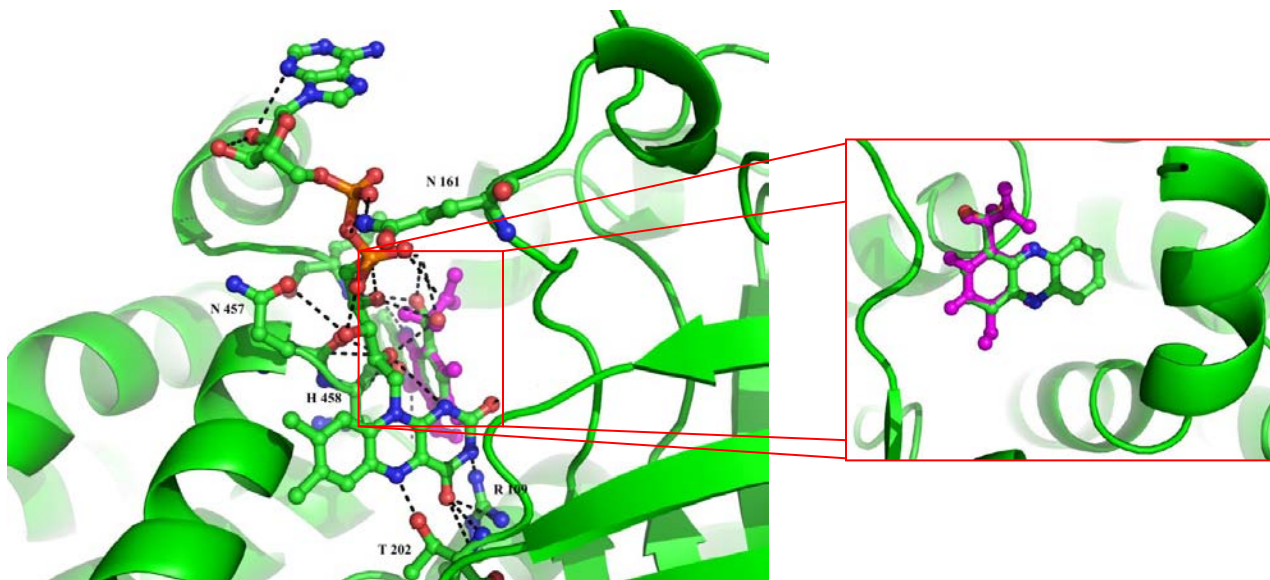


Figure 56: Docking of FAD (green) and PCA (green) in the PhzO molecule (green). The polar contacts between amino acids, FAD and PCA are marked with black dashes. The highlighted picture is showing a superposition of PCA over the substrate of HpaB, 4-HyPhAc (magenta).

Even though PCA is a three ring system compared with 4HPA which has just one ring, their positions match accordingly to the docking experiments. In order to transfer a hydroxyl group on the C2 atom of the substrate, PCA must be in the proximity of the C4a atom of the isoalloxazine ring. The docking revealed that C2 atom of PCA and C4a of the FAD are in opposite directions which would prevent a successful transfer of the hydroxyl group. Further docking experiments were carried with PCA and FAD in order to find a better position for PCA, which would allow the hydroxylation taking place.

An additional position of PCA was found (**Figure 57**) between the last α -helix of the C-terminal domain (blue) and the loop E240-R263 (red) of the middle domain. It seems that the active site of the enzyme is closed at its ends by two loops. Similar to HpaB, in PhzO the loop P160-M182 (red) should be responsible for the FAD stabilization in the binding pocket. While P160-M182 acts like a lid for the FAD binding site, the loop E240-R263 it may be involved in the substrate fixation and product release. The actual position of PCA is in the immediate proximity of the isoalloxazine ring and such orientated that the C2 atom of PCA is 6.47 Å apart from the C4a atom of the

RESULTS AND DISCUSSION

isoalloxazine ring. Soaking experiments of native PhzO crystals with the substrate PCA were unsuccessful because of crystal cracking, which is mainly induced by conformational changes. If the loop E240-R263 plays a role in substrate-product exchange, this would probably lead to conformational changes and explain crystal cracking while soaking experiments.

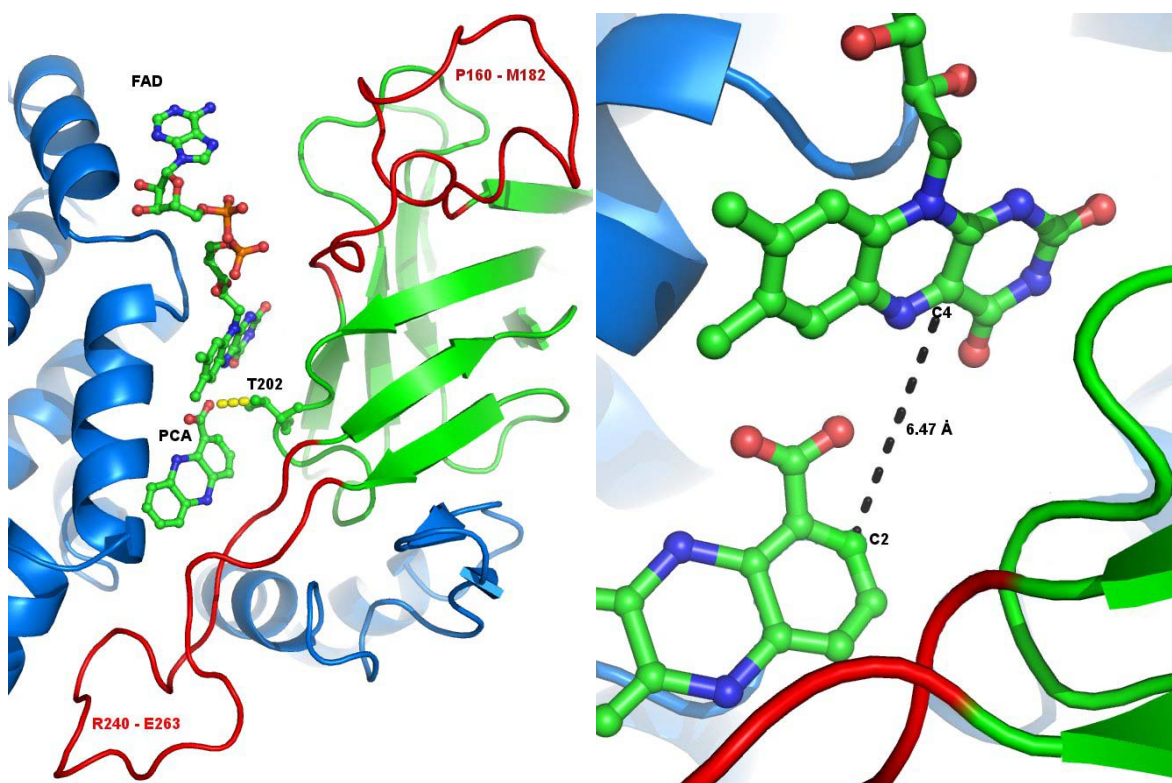


Figure 57: Docking of FAD and PCA in PhzO. Left: the loops P160-M182 and R240-E263 (red) probably stabilize the cofactor FAD and substrate PCA, respectively. Both loops are a part of the middle domain (green). The binding pocket is between the middle domain (green) and C-terminal domain (blue) and closed by two loops. Right: The measured distance between C2 atom of PCA and C4a of FAD is 6.47 Å.

Furthermore, the second docking experiment described here shows that PCA forms a hydrogen bond with the amino acid residue T202, in contrast to the first docking experiment, where PCA was not forming any hydrogen bond with the residues of the main chain.

HpaB in complex with FAD and 4-HyPhAc were used as model for docking FAD and TCP in the active site of TcpA. The resulting TcpA structure in complex with both ligands is depicted in **Figure 58**.

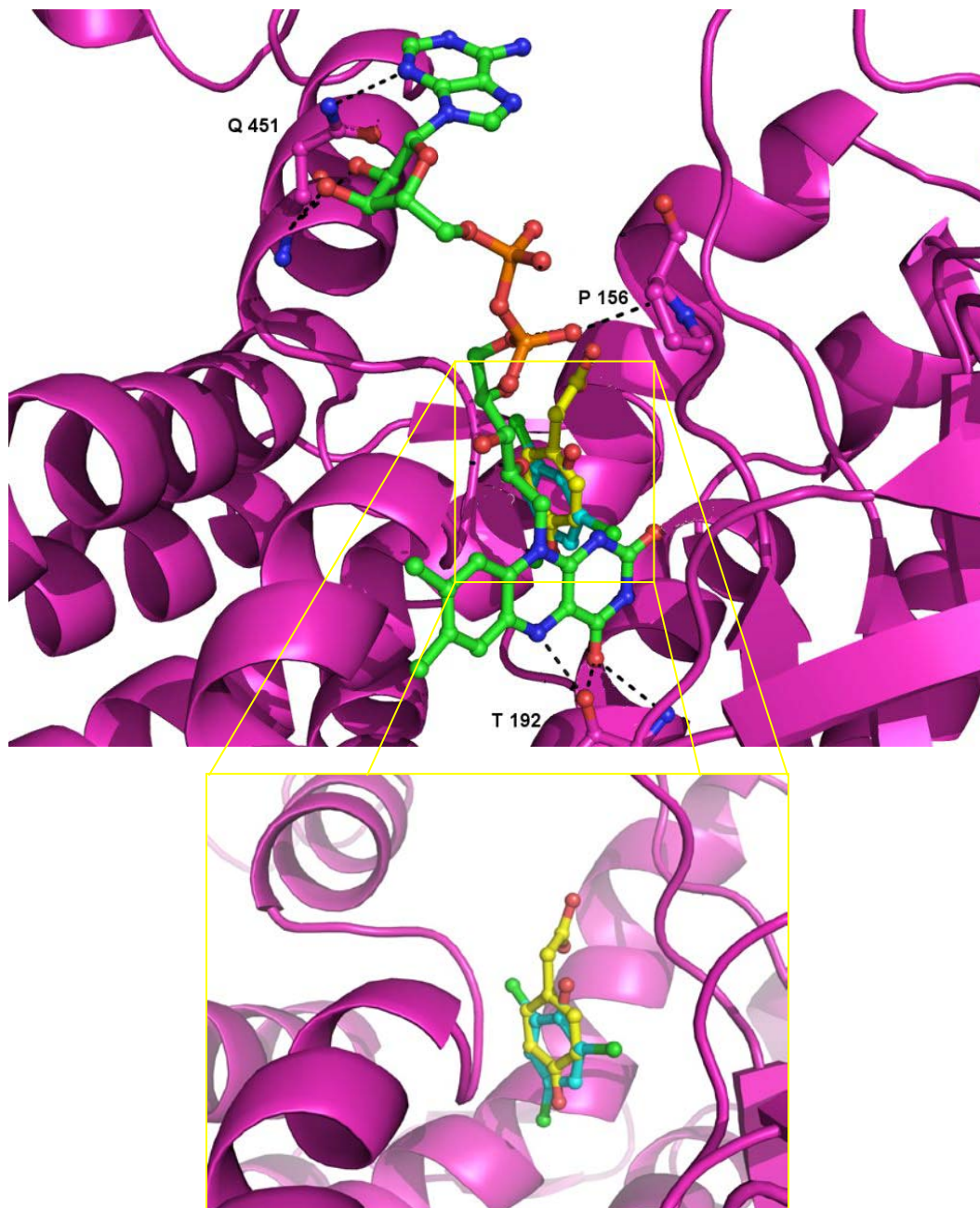


Figure 58: Docking of FAD (green) and TCP (cyan) in the TcpA molecule (magenta). The polar contacts between amino acids and FAD are marked with black dashes. The highlighted picture is showing a superposition of TCP over the substrate of HpaB, the 4-hydroxyphenylacetate (yellow).

RESULTS AND DISCUSSION

Measurements were influenced by the lack of the S157-S169 loop, which in case of PhzO is involved in the binding of FAD. Unfortunately just three hydrogen bonds were determined for binding FAD using the docking procedure. As already mentioned before, the hydrophobicity of TCP should induce large hydrophobic interactions with the enzyme. Although FAD and TCP are positioned in TcxA similar to FAD and 4-HyPhAc in HpaB, their real location in the catalytically active site of TcxA remains uncertain. The only chance to obtain a clearer view of the active site occupancy for both of the enzymes is to crystallize them in complex with the ligands and analyze them using x-ray diffraction. As it was reported in the section dedicated to crystallization, soaking and co-crystallization experiments were unsuccessful. However, docking and modeling the ligands in the active site of the enzymes made it possible to determine their approximate position and gave a hint about the number and type of aminoacids that could interact with them. In order to determine the exact type of aminoacids which are involved in substrate and cofactor binding, mutant proteins which include modifications in the structure of the active site must be biosynthesized and used in biochemical assays to monitor the reaction turnover.

4.7 Ligand affinity measurements

The following describes the results of measurements concerning the affinity of the enzymes PhzO and TcpA for different ligands. For isothermal calorimetric titration, the ligands FAD, FMN, ADP, AMP, PCA, 2OHPCA, TCP and DCP were used.

4.7.1 Preliminary test for buffer contribution

The preliminary tests must reflect whether the substrate samples can be transferred into comparable buffer conditions like in the ITC experiment without allowing the release of dilution heat. While PCA is very well soluble in water, this is not the case for the 2OHPCA, TCP and DCP without the addition of 20% DMSO. In the ITC measurements in general, the reactants are used in a concentration ratio of about 10:1. In a test run, 20% DMSO substrate-buffer solution and protein-buffer solution (in which the proteins are eluted) were titrated to each other. In the syringe was the buffer solution, supplemented with 20% DMSO, and in the template the buffer solution only. The measurement showed strong dilution effects caused by the release of dilution heat and associated entropy changes. Due to this result, difficulties were to be expected in the later measurements when ligand is titrated to the protein solution.

4.7.2 Preliminary tests for determining the titration parameters

Another parameter that affects the signal amplitude and the quality of the measurement is the speed with which the reaction equilibrium is reached after injection occurs. If the reaction is fast, this leads to a rapid heat release and thus to a large signal amplitude. For these preliminary experiments, 50 μM of Protein and 500 μM of ligand were used. The proteins were dialyzed overnight against 150 mM NaCl, and 10 mM Tris at pH 8.00 at 4 °C. After the protein solution out of the measuring cell had reached initial thermal equilibration, the titration started by injecting the ligand in increments of 2 μl within 5 seconds. Because of technical constraints, the first dose is

RESULTS AND DISCUSSION

only 0.2 μl . Between each injection, the waiting time for recording the signal is 60 seconds. In the first experiment performed at 5 $^{\circ}\text{C}$, weak signal amplitudes were observed after injection. Increasing the temperature to 20 $^{\circ}\text{C}$ had the consequence that the signal strength increased significantly after each injection. The integration of the signals shows, however, no plausible value for the heat change detected. The main reason for that was the waiting time, since 60 seconds did not appear to be sufficient, i. e. the detected signal had not enough time to decay to the starting level before the next injection occurred. The waiting time was extended to 4 minutes and the concentration of protein and ligand were increased up to 400 μM and 4 mM respectively, in order to allow an accurate determination of the binding affinity.

4.7.3 Binding affinity measurements with FAD, FMN, ADP, AMP and PCA

The evaluation of the ITC measurements carried out in studying the interaction of PhzO with FAD is shown in Figure 59.

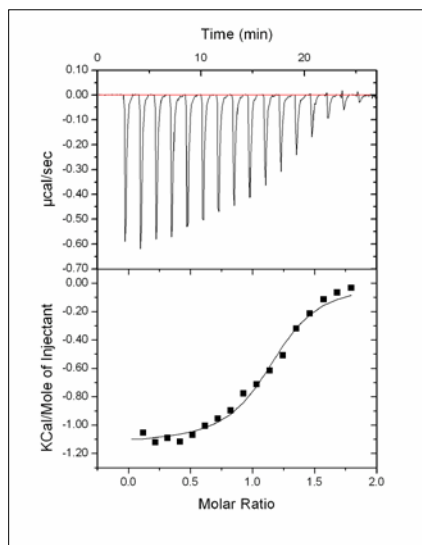


Figure 59 ITC measurement of 400 μM PhzO titrated with 4 mM FAD

In the upper part of the figure, the heating power provided by the calorimeter is plotted versus reaction time. The negative heat output shows that the reaction in which PhzO

RESULTS AND DISCUSSION

binds FAD is an exothermic. As the figure shows, the heat output decreases stepwise until no more free enzyme is available and saturation of the protein solution is achieved. In the lower part of the same figure, the heat required for one mol of ligand was plotted versus the molar ratio of the ligand to enzyme. Here, a sigmoidal curve was obtained. The analysis provided the following data for the binding of FAD to PhzO:

Stoichiometric coefficient $N = 1.14 \pm 0.0174$ sites

Association constant $K = 7.71 \cdot 10^4 \pm 1.45 \cdot 10^4 \text{ M}^{-1} \rightarrow K_D = 1/K = 13 \text{ }\mu\text{M}$

Enthalpy $\Delta H = -1132 \pm 24.13 \text{ cal mol}^{-1}$

Entropy $\Delta S = 18.6 \text{ cal/mol/deg}$

The calculated stoichiometric coefficient of a PhzO-FAD complex is close to 1, as it was to be expected, since each monomer has an active site and thus can bind one molecule of FAD. This result is a positive indication for the accuracy of the fitted curve. The dissociation constant of the complex is $13 \text{ }\mu\text{M}$ and the reaction enthalpy is about -4.7 kJ mol^{-1} , which is in the order of van der Waals bonds. The successful fitting of the data shows that FAD binds to PhzO, even if this bond is relatively weak.

To investigate which part of the FAD is required for the binding to PhzO, additional ITC measurements were carried out with AMP and ADP. Because both of the measurements show similar results, just the one for ADP is shown in **Figure 60** as an example.

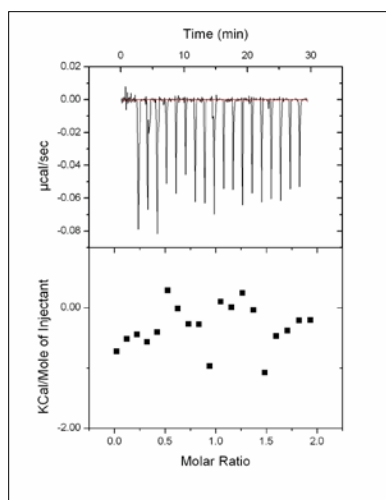


Figure 60 ITC measurement of $115 \text{ }\mu\text{M}$ PhzO titrated with 1.15 mM ADP

RESULTS AND DISCUSSION

In the upper part of the **Figure 60** no trend of the heating power is discernable, and signals are very small on a scale from 0 $\mu\text{cal s}^{-1}$ to $-0.08 \mu\text{cal s}^{-1}$. Even with further experiments at higher enzyme and ligand concentrations, no trend of the exothermic peaks could be detected. This suggests that between ADP and AMP on one hand and PhzO on the other hand no interaction or no detectable binding occurs.

Because ADP and AMP were not binding, further ITC measurements were carried out with FMN, which stays for the isoalloxazine ring and the ribityl moiety of FAD. The results are shown in **Figure 61**.

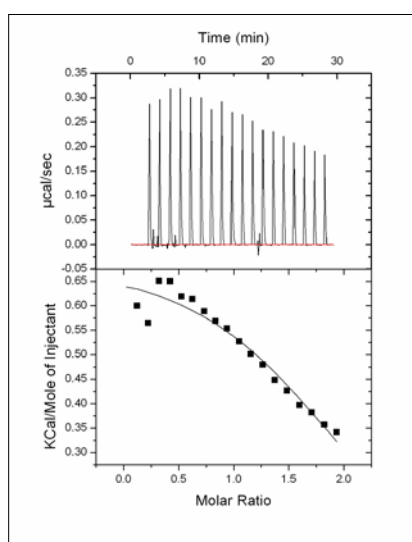


Figure 61 ITC measurement of 270 μM PhzO titrated with 2.7 mM FMN

In contrast to the AMP and ADP measurements, here a clear trend became apparent. The analysis yielded the following results:

Stoichiometric coefficient $N = 2.08 \pm 0.107$ sites

Association constant $K = 1.85 \cdot 10^4 \pm 7.62 \cdot 10^3 \text{ M}^{-1} \rightarrow K_D = 1/K = 54 \mu\text{M}$

Enthalpy $\Delta H = 700.6 \pm 35.05 \text{ cal mol}^{-1}$

Entropy $\Delta S = 21.3 \text{ cal/mol/deg}$

RESULTS AND DISCUSSION

While the binding of FAD is exothermic, here the heating power input is positive, suggesting an endothermic reaction, which is reflected in the positive value of the reaction enthalpy of 2.9 kJ/mol^{-1} . This may suggest that during the binding of FMN conformational changes of the enzymes are taking place and heat must be absorbed. However, this raises the question why this result is different from the one obtained in the experiments performed with FAD. It may be possible that a conformational change of the enzyme is also induced by the binding of FAD, but there are larger exothermic contributions from FAD in contrast to those of FMN. The stoichiometric coefficient of about 2 points out that one ligand molecule binds to two catalytically active sites. A measurement error is unlikely because a repetition yielded similar results. An incorrect fitting of the curve could be possible because the heating power did not decrease to zero, showing that saturation of the enzyme was not yet achieved. Therefore, the ITC measurement was repeated with the twofold FMN concentration and again, a very similar result was obtained (data not shown). From the data obtained from the ITC measurements it can be concluded that an interaction between FMN and PhzO occurred, but led to conformational changes in the enzyme. This assumption is supported by current knowledge about the mechanism in the PhzO related enzyme from *T. thermophilus* HB8 HpaB. Here, mainly the isoalloxazine ring and only to a small extent the ADP portion of FAD are responsible for the binding to the enzyme. Binding of FAD changes the conformation of the HpaB so that the active site becomes accessible for molecular oxygen and the actual substrate^[43, 125].

It is known from previous publications that the reduced form of FAD and FMN has a higher affinity towards the monooxygenases than their oxidized forms^[126,127]. ITC measurements in anaerobic conditions with the reduced form of these compounds were not performed.

To determine the affinity of the substrate PCA to the enzyme PhzO, ITC measurements were carried out with a set of different concentrations and variations of the ligand / enzyme ratio. 2.5 mM of PCA were titrated to 250 μM PhzO and the results are shown in **Figure 62**.

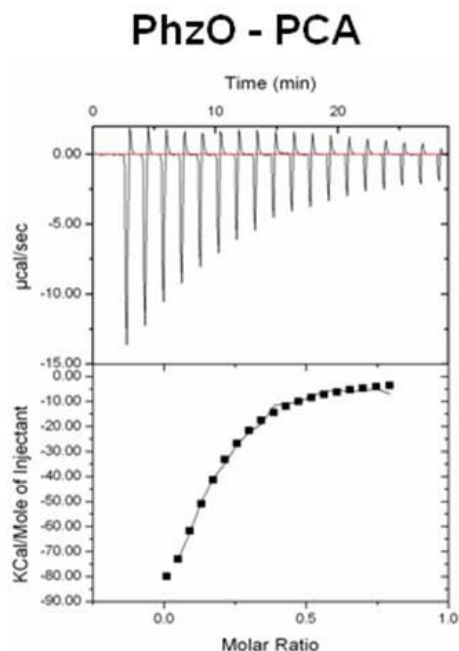


Figure 62 ITC measurement of 250 μM PhzO titrated with 2.5 mM PCA

Stoichiometric coefficient $N = 0.154 \pm 0.07$ sites

Association constant $K = 3.92 \cdot 10^4 \pm 5.28 \cdot 10^3 \text{ M}^{-1} \rightarrow K_D = 1/K = 25.5 \mu\text{M}$

Enthalpy $\Delta H = -3.98 \cdot 10^4 \pm 7.4 \text{ cal mol}^{-1}$

Entropy $\Delta S = 121 \text{ cal/mol/deg}$

The value for K_D is 25.5 μM which indicates that PCA binds to the enzyme but very weakly. The reason for that could be that PCA is produced *in vivo* in the reduced form, and this could show a better affinity to the enzyme. The stoichiometric coefficient of 0.15 indicates that maybe PCA was not stable during the titration. The precipitation of the ligand leads to changes in the molar ratio, which influence the correct calculation of the stoichiometric coefficient. Measurements with reduced PCA were not performed for the simple reason that reducing agents used to reduce PCA_{ox} to PCA_{red} would lead to dilution effects which would overshadow useful data detection. Adding the reducing agent to the protein solution led to slight protein precipitation.

4.8 Enzyme assay and HPLC-APCI-MS measurements

4.8.1 Measurements for PhzO

The turnover of the reaction catalyzed by PhzO was monitored by HPLC-APCI-MS measurements. It was not possible to monitor the reaction by simple photometric approaches because the absorption maxima for PCA is at 248 nm and 371 nm, which are very close to that of 2OHPCA at 257 nm and 369 nm^[33].

Educt and product concentrations were monitored over a time period of up to 20 minutes. A decrease of substrate concentration was recorded, while the concentration of the product was increasing. The characteristic retention time peaks for the substrate PCA and product 2OHPCA were integrated using the software Xcalibur, and the resulting values were divided by the area of the caffeine peak. This served as a reference value in the integration process, because the caffeine concentration does not change during the reaction. For a detailed description of the procedure, see section 3.5.2.2. Due to a possible spontaneous decarboxylation of 2OHPCA to 2OHPHZ, the measurements were scanned for both compounds. Below the results are presented concerning PCA consumption and 2OHPCA formation.

Preliminary experiments were performed to determine which form of PCA and which FAD concentration is most favorable to study the reaction catalyzed by PhzO. **Figure 63** shows that the reduced form of PCA is consumed in bigger amount by PhzO than its oxidized form. Even if the reaction was monitored for 50 minutes, unfortunately the complete substrate consumption was not achieved.

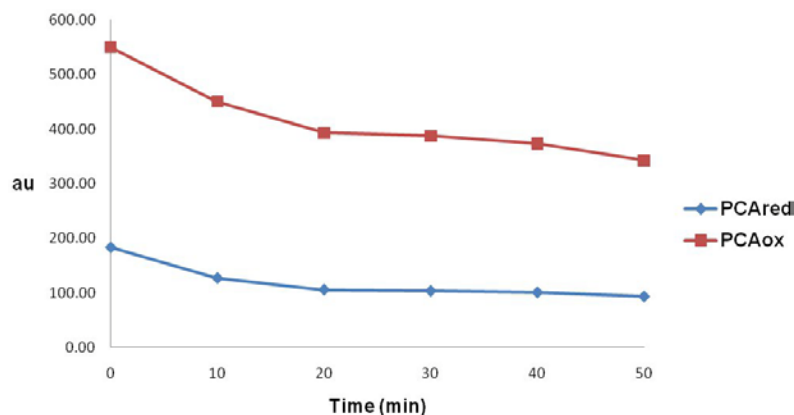


Figure 63 HPLC-APCI-MS measurements with PCA_{red} and PCA_{ox} as substrates. The reduced form of PCA is consumed more than its oxidized form.

RESULTS AND DISCUSSION

Parallel to the substrate consumption, the product formation was also monitored. The chart in **Figure 64** shows the formation of different products, dependent on the substrate type that was used in the assay.

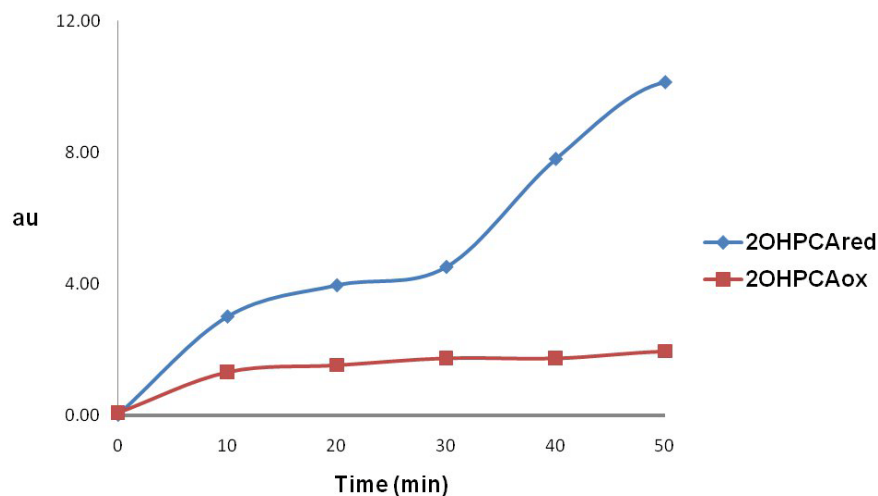


Figure 64 HPLC-APCI-MS measurements showing the product formation, 2OHPCA_{ox} (red) and 2OHPCA_{red} (blue)

The increase in 2OHPCA is not as strong as the decrease in PCA, but still clearly discernable. Due to a decrease in the concentration of PCA and the simultaneous increase in the concentration of 2OHPCA, the reaction of PCA to 2OHPCA is confirmed by PhzO. Trying to optimize the conditions, various FAD concentrations were chosen to perform a new set of measurements. By varying the concentration of FAD in the range from 250 to 1000 μM , measurements did not indicate any significant change in product formation. All the assays performed in this work were done in the presence of 1 mM FAD. Results are presented in **Figure 65**.

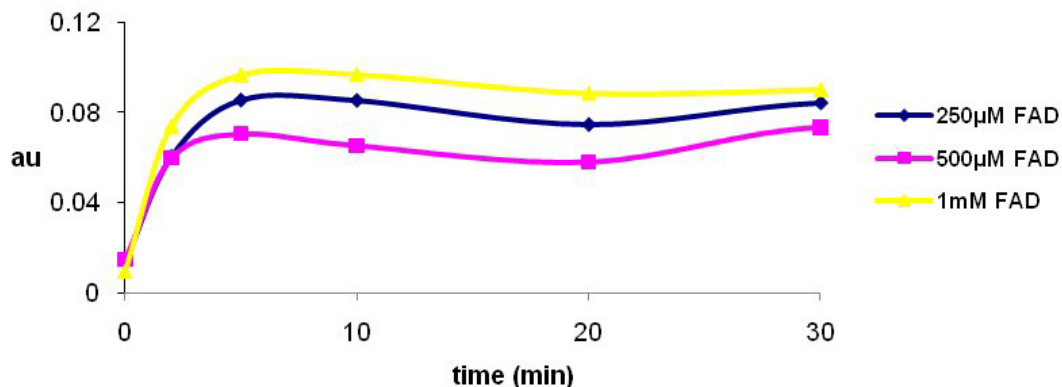


Figure 65 HPLC-APCI-MS measurements with various FAD concentrations. Comparable 2OHPCA is generated independent on the FAD concentration.

This optimization is important because a high concentration of FAD could inhibit the activation of the monooxygenase and decrease the substrate turnover.

Despite much effort, it was not possible to run the reaction until complete substrate consumption. Just about 10 to 20% of the substrate was used up even if a higher concentration of enzyme was added to the reaction mixture (see **Figure 66**).

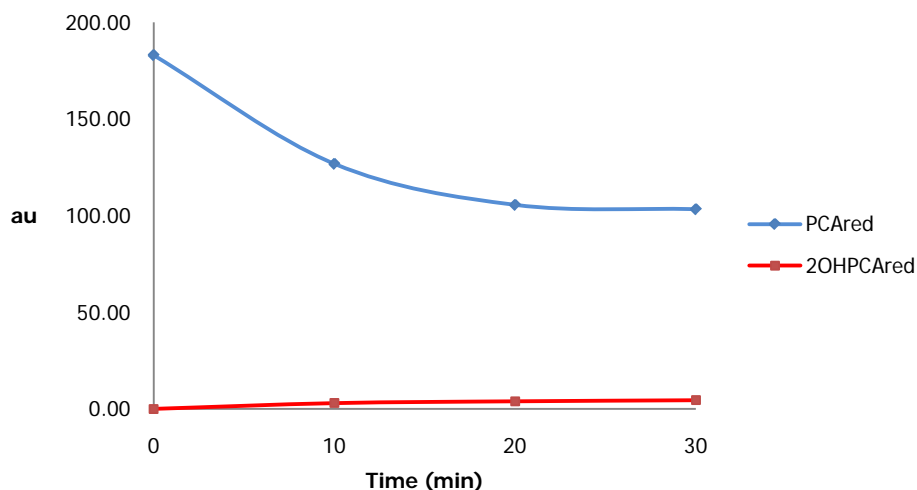


Figure 66 HPLC-APCI-MS measurement showing substrate concentration decrease and simultaneous product formation

PhzO could not only produce 2OHPCA but also other phenazine derivatives and this may explain why more PCA is consumed than 2OHPCA is produced. The measurements

presented in this work could not show any significant formation of other phenazine derivatives.

In order to increase the reaction yield, it was tested whether NADPH or NADH is a better electron donor in the oxido/reduction reaction catalyzed by the flavin reductase Fre. Because Fre is the flavin reductase component of the two-component flavin-diffusible system, its properties to produce and deliver $FADH_2$ may be relevant. Reaction assays supplemented by NADH were performing better than those by NADPH. The overall reaction yield measured on the base of 2OHPCA is shown in **Figure 68**.

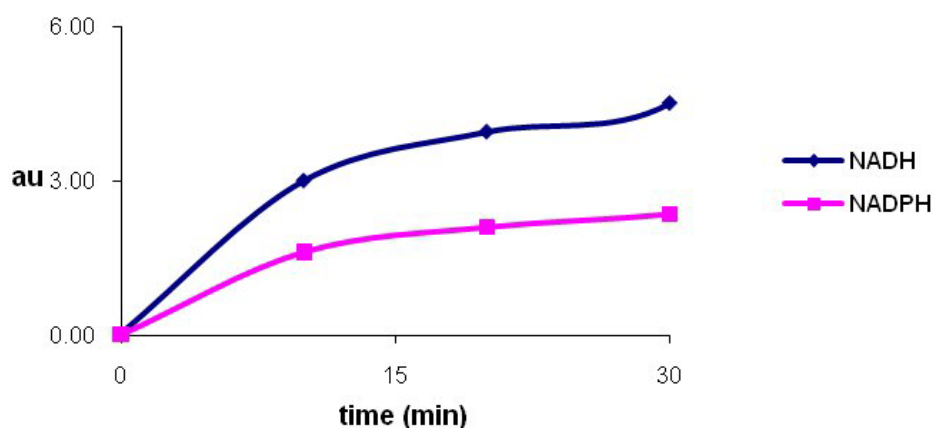


Figure 68 HPLC-APCI-MS measurements showing the increase of 2OHPCA dependent on the cofactors NADH and NADPH. The reaction yield is higher when NADH is used instead of NADPH.

By increasing the concentration of the enzyme, a higher product formation was observed in the first 5 minutes, after which no further product release has been detected. It was concluded that the reaction catalyzed by PhzO ends after approximately 5 minutes, as it can be seen in the chart shown in **Figure 67**.

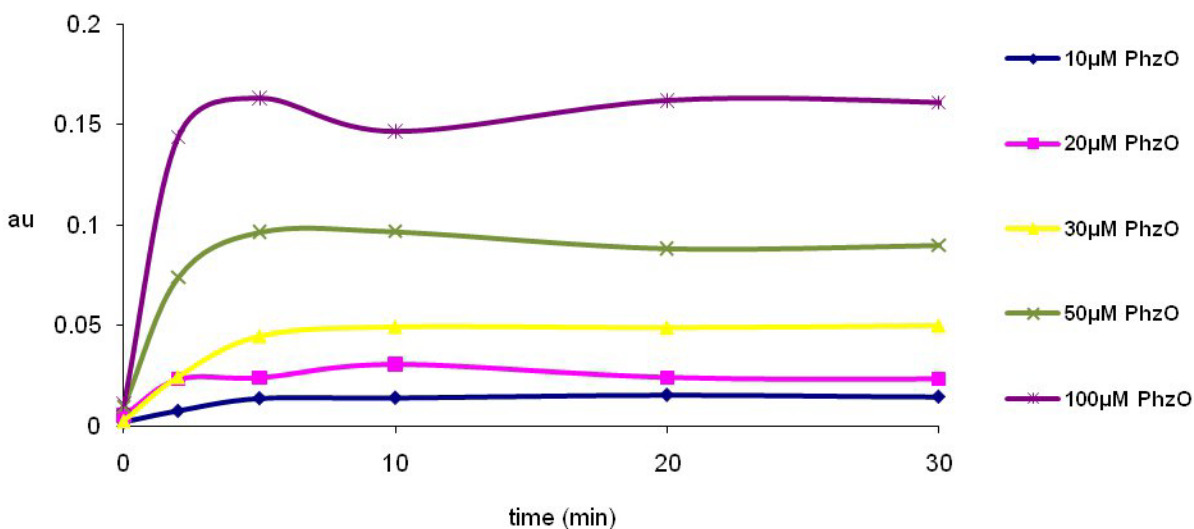


Figure 67 HPLC-APCI-MS measurement with various concentration of PhzO on the base of 2OHPCA. The more enzyme is added, the more 2OHPCA is formed in the first 5 minutes.

It is assumed that reaction stops basically after 5 minutes because of lack of reduced FADH_2 . An explanation for the very low reaction efficiency could be that the transfer of the reduced flavin from the reductase to the monooxygenase is not efficient enough, so that FADH_2 is oxidized to FAD instead of being used up by PhzO.

It is important to note that we used the flavin reductase from *E.coli*, instead of the reductase of *P. aureofaciens*, which is not yet known. Furthermore, reactions were carried out under aerobic conditions since the monooxygenase needs molecular oxygen to be transferred into the substrate molecules. The presence of O_2 is essential for the monooxygenase but it interferes with the stability of FADH_2 which can be easily oxidized to FAD with concomitant release of H_2O_2 .

4.8.2 Measurements for TcpA

Similar enzyme assays were performed and HPLC-APCI-MS measurements were carried out for TcpA, by using the actual substrate TCP but also the substrate analog DCP. In

none of the cases, measurements ended with concluding results. A real substrate concentration decrease concomitant to product formation could not be recorded.

4.9 Photochemical reduction of FAD

The biochemical assays described in the previous chapter could not confirm complete substrate consumption. A reason could be the inefficient transfer of the reduced FAD from the flavin reductase to the monooxygenase. In order to overcome this, anaerobic photochemical reduction of FAD by light and EDTA was carried out.

FAD with 250 mM EDTA was exposed to a light source of at least 100 W under anaerobic conditions. The change in color, from yellow to colorless indicates the successful reduction of FAD. Unfortunately, while supplementing the reduced FAD solution with the monooxygenase and the substrate, the reduced FAD undergoes spontaneous oxidation. Exposing the reaction mixture again to the anaerobic photochemical reduction, results in a colorless solution but the substrate turnover could not be detected. The relatively high concentration of EDTA could be a disturbing parameter in the reaction catalyzed by the monooxygenase, but also the absence of O₂ since the photochemical reduction requires anaerobic conditions.

4.10 Difficulties in dealing with monooxygenases

Monooxygenases are a class of enzymes that are difficult to handle. PhzO and TcpA pose numerous challenges whether it is over-expression, protein purification, protein crystallization or biochemical assays. The heterologous expression and isolation of monooxygenases was shown to be very difficult in some cases, either because they may be toxic for the expression in host cell or because they are multicomponent enzymes which are difficult to stabilize^[21]. The work presented here describes two strategies for induction of protein over expression of which just one was successful.

RESULTS AND DISCUSSION

The biochemical assays and the experiments on the photochemical reduction of FAD could not confirm complete substrate consumption. It is known that monooxygenases have a lower stability compared to other enzymes, which limits the turnover numbers of the biocatalysts using isolated enzymes^[22-25].

Another plausible reason could be the inefficient transfer of the reduced FAD from the flavin reductase to the monooxygenase. Gassner et al.^[130] suggested that two-component monooxygenases would form a transient flavin transfer complex in which the AMP moiety is associated with the monooxygenase, and the isoalloxazine ring is redirected for binding in the catalytically active site of the flavin reductase. Based on this hypothesis, the release and transfer of the isoalloxazine ring would be more efficient and minimize the interaction with molecular oxygen from the solution (**Figure 69**).

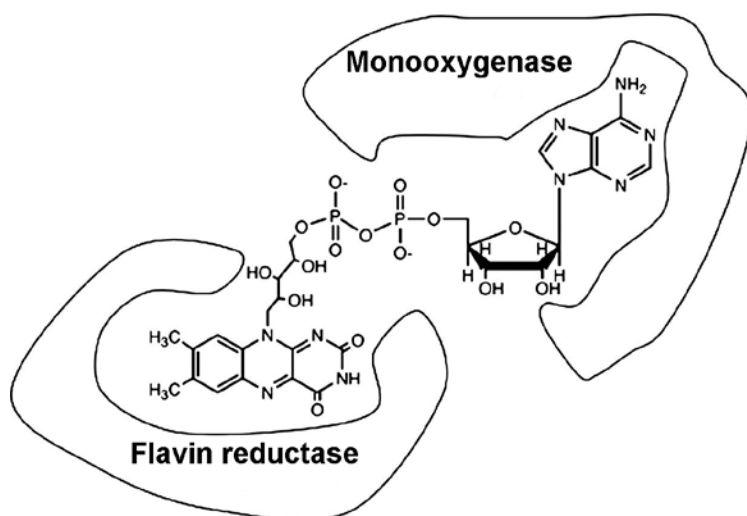


Figure 69 Proposed model for the transient flavin transfer complex (figure adopted from [130])

As was described in chapter 4.7 the affinity of ADP and AMP for the monooxygenase component PhzO could not be detected. In consequence and in contrast, the present results lead to the assumption that FADH₂ transfer from the flavin reductase to the monooxygenase occurs randomly and is more likely to be dependent upon the concentration of the FAD in the solution or inner cell environment than upon the formation of any transient flavin-dependent complex. The concentration of FAD in living cells is uncertain and very much dependent on various physiological conditions. It was

RESULTS AND DISCUSSION

reported that FAD could reach concentrations of about 0.2 mM in the living cell^[132]. Whether the concentration of FAD is high enough in order to explain its low binding affinity to the enzyme PhzO remains unclear.

The biochemical assays were performed with the flavin reductase from *E.coli* and not with the one belonging to each monooxygenase, from *P. aureofaciens* and *C. necator* respectively. This could be another reason why the experiments lacked the efficiency of flavin transfer resulting in incomplete substrate consumption.

In case of PhzO, its substrate PCA is known to be biosynthesized in its reduced form but in the experiments performed in this work, mostly its oxidized form was used. TCP, the substrate of TcpA, has low water solubility. 3 chlorine atoms as substituents decrease the electron charge due to $-I$ effect and hence the aromatic derivate is less susceptible to oxidation.

6. SUMMARY AND OUTLOOK

Biotechnology is understood as the application of living organisms, enzyme complexes or single enzymes in production processes. Common classes of enzymes in the biotechnological processes are monooxygenases. These enzymes are used in biodegradation of xenobiotics e.g. TcpA from *Cupriavidus necator*, as well in generation of various compounds with antibiotic properties e.g. PhzO from *Pseudomonas aureofaciens*. Monooxygenases are able to transfer an atom of oxygen from molecular oxygen into the substrate. The reactions catalyzed by PhzO and TcpA respectively occur in tandem with a flavin reductase which provides monooxygenases with the cofactor FADH₂. Such co-operativity of the enzymes makes the monooxygenases PhzO and TcpA belong to the protein superfamily of two-component flavin-diffusible monooxygenases (TC-FDM).

The focus of work presented here is a structural and biochemical characterization of two two-component flavin-diffusible monooxygenases PhzO and TcpA. In order to describe the molecular structure and function of PhzO and TcpA, these two proteins were cloned, expressed, purified, crystallized and characterized using a variety of different biochemical and biophysical techniques. For detailed structural characterization of both enzymes, X-ray crystallography methods were used and novel biochemical assays were developed for investigating the substrate turnover in the catalyzed reactions via APCI-MS measurements. For an extensive functional characterization, isothermal titration calorimetry measurements were performed.

6.1 PhzO

The crystallization of PhzO was successful both in the native state and in complex with the ligands FAD, ADP and FMN. The native crystals were used for x-ray data set collection and showed diffraction of up to 1.7 Å. Analysis of the crystals with the ligands ADP and FMN resulted in no additional electron density in the active site. PhzO-ADP crystals obtained via co-crystallization were soaked in FAD and used for x-ray diffraction

analysis in order to determine the structure of the PhzO-FAD complex. A crystal structure at 3.2 Å was determined for this protein complex. The position of FAD indicates that the binding occurs mainly through the ADP-part and that isoalloxazine ring is not within the binding pocket. This result is in contradiction with ITC measurements.

The ITC measurements showed that the complex of PhzO with FAD is characterized by a dissociation constant of 13 μM and a reaction enthalpy of -4.7 kJ mol⁻¹. Further ITC measurements have revealed that the isoalloxazine ring of FAD is most probably responsible for the complex formation.

HPLC-APCI-MS measurements demonstrated that PhzO catalyzes the reaction in which the substrate PCA is converted to 2OHPCA. Despite much effort, complete substrate consumption could not be achieved since the reaction stopped after a short time. A quantitative interpretation of the substrate turnover was not possible.

Docking and modeling experiments performed with PhzO and HpaB complexed with FAD showed that in PhzO the amino acids R109, T156 to R166, T202, E263 and R450 to S461 are responsible for the binding of FAD. Based on the findings about the related structure of HpaB complexed with FAD, a model of the complex PhzO-FAD could be designed.

6.2 TcpA

The second enzyme described in this study was crystallized in the native form and as selenium-L-methionine derivative, although crystallization experiments were difficult to perform. Unfortunately, co-crystallization and soaking experiments failed, and it was not possible to study cofactor and ligand binding based on structural analysis. Docking and modeling experiments with the HpaB complexed with FAD and substrate found in scientific literature and with TcpA were performed in order to determine the amino acid residues which could be involved in protein-cofactor and protein-substrate interaction.

6.3 Outlook

Experiments pertaining to reaction catalysis could not show complete substrate consumption. A plausible reason for that could be that PCA as substrate of PhzO is known to be biosynthesized in its reduced form but in the experiments performed in current work, mostly its oxidized form was used. For TcpA, its substrate TCP has low water solubility which makes it hard to work with and its 3 chlorine atoms lowers the electron charge of the phenol derivate making it hard to be oxidized. Another reason could be that biochemical assays were performed with the flavin reductase from *E.coli* and not with the one belonging to each monooxygenase, from *P. aureofaciens* and *C. necator* respectively.

By determining the protein structures of PhzO and TcpA and comparing them with the HpaB model, it would be possible to determine which amino acids are involved in changing substrate specificity, making the enzymes more interesting for biotechnological applications. Based on these findings, one can generate mutants and express them either heterologously in *E. coli* for further biochemical assays or for *in vivo* cell studies in *P. aureofaciens*. In order to determine the substrate specificity, *in vivo* experiments could be performed, where the gene *phzO* is initially knocked out but reintroduced later as a plasmid DNA. It is assumed that monooxygenases treated in this work could accommodate a broad spectrum of substrates. Screening these enzymes against a class of compounds similar to the original substrates could reveal yet unknown, but possibly desirable functions.

To monitor the reactions catalyzed by the monooxygenases described in this work, and also the concentration of O₂ a clark electrode could be used. It is known that the solubility of O₂ in aqueous solutions at atmospheric pressure and 20 °C is about 7,6 mg l⁻¹ [129]. This oxygen can be used either in the hydroxylation of the substrate or in the reduction to H₂O₂ by FADH₂. In order to prevent H₂O₂ accumulation at the expense of dissolved oxygen, catalase can be added to the reaction mixture which should increase the efficiency of the substrate turnover.

6.4 Zusammenfassung

Die Globalisierung und die drohende Erschöpfung der wichtigsten natürlichen Rohstoffe zwingen die Menschheit dazu, die Herstellungsprozesse einer wachsenden Anzahl von Produkten zu überdenken. Anhand von zahlreichen Beispielen aus der Natur gelingt es Biochemikern und Biotechnologen in zunehmendem Maße, moderne Herstellungsverfahren für die benötigten Produkte zu entwickeln. Dadurch ist das Feld der Biotechnologie entstanden, die als die Nutzung von lebenden Organismen, einzelnen Enzymen oder Enzymkomplexe in technischen Prozessen durch den Menschen definiert wird.

Eine Klasse oft genutzter Enzyme in biotechnologischen Prozessen sind die Monooxygenasen. Diese Enzyme sind an biologischen Abbauprozessen von Xenobiotika und Schadstoffe beteiligt, wie z.B. TcpA aus *Cupriavidus necator*, sowie bei der Erzeugung verschiedener Verbindungen mit antibiotischen Eigenschaften wie z.B. PhzO aus *Pseudomonas aureofaciens*. PhzO und TcpA gehören zu der Proteinfamilie der „Two Component Flavine Diffusible Monooxygenases“ (TC-FDM).

Das Ziel dieser Studie war es, die Struktur, den Reaktionsmechanismus und die Substratspezifität der Monooxygenasen PhzO und TcpA zu untersuchen. Zu diesem Zweck wurden beide Proteine kloniert, überexprimiert, aufgereinigt, kristallisiert und mittels verschiedener biochemischer und biophysikalischer Verfahren analysiert. Für eine detaillierte strukturelle Charakterisierung der beiden Enzyme wurde die Methode der Röntgenstrukturanalyse verwendet. Zur Untersuchung des Substratumsatzes in den katalysierten Reaktionen wurden APCI-MS-Messungen durchgeführt und die Bindungsaffinität der Enzyme an Substrat und Kofaktoren wurde über ITC-Messungen bestimmt.

6.4.1 PhzO

Die Kristallisation von PhzO gelang sowohl im nativen Zustand wie im Komplex mit den Liganden FAD, ADP und FMN. Die nativen Kristalle hatten die Raumgruppe C222₁ und zeigten eine Beugung von bis zu 1.7 Å. Das endgültige Modell von nativem PhzO wurde bis zu einer Auflösung von 1.7 Å mit R = 18% und R_{free} = 20% verfeinert.

Die Analyse der Kristalle mit den Liganden ADP und FMN ergab keine zusätzliche Elektronendichte im aktiven Zentrum. PhzO-ADP-Kristalle wurden mittels Co-Kristallisation gezüchtet und anschließend in eine FAD-Lösung eingetaucht, um die Struktur des PhzO-FAD-Komplexes zu bestimmen. Eine Kristallstruktur mit der Raumgruppe C222₁ bei 3.2 Å und mit R = 15.8% und R_{free} = 20% wurde für diesen Protein-Komplex bestimmt. Die Position des FAD weist darauf hin, dass die Bindung hauptsächlich durch den ADP-Teil erfolgt und dass der Isoalloxazinring nicht an dieser Bindung teilnimmt. Dieses Ergebnis steht im Widerspruch zu den ITC-Messungen.

Die ITC-Messungen zeigten, dass der Komplex aus PhzO mit FAD durch eine Dissoziationskonstante von 13 µM und eine Reaktionsenthalpie von -4.7 kJ mol⁻¹ charakterisiert ist. Der Isoalloxazinring von FAD ist höchstwahrscheinlich für die Komplexbildung verantwortlich.

HPLC-APCI-MS-Messungen haben gezeigt, dass PhzO die Reaktion katalysiert, in der das Substrat PCA zu 2OHPCA umgesetzt wird. Trotz vieler Versuche konnte ein vollständiger Verbrauch des Substrats nicht realisiert werden. Es wird angenommen, dass der Grund dafür die ineffiziente Übertragung des reduzierten Flavins (FAD_{red}) aus der Flavin-Reduktase-Komponente (Fre) auf die Monooxygenase (PhzO) ist.

Docking- und Modellierungsexperimente mit PhzO- und HpaB-FAD-Proteinkomplex zeigten, dass in PhzO die Aminosäuren R109, T156 bis R166, T202, E263 und R450 bis S461 für die Bindung von FAD zuständig sind. Basierend auf den Kenntnissen über die Struktur von HpaB könnte die korrekte Bindung von FAD in das PhzO zu Konformationsänderungen führen, die das aktive Zentrum für das Substrat PCA zugänglich machen.

6.4.2 TcpA

Das zweite in dieser Arbeit beschriebene Enzym wurde in der nativen Form und als Selen-L-Methionin-Derivat kristallisiert. Die Proteinstruktur des nativen TcpAs wurde bei 3.0 Å aufgeklärt und bis auf $R = 18\%$ und $R_{\text{free}} = 25\%$ verfeinert. Kokristallisation und soaking-Experimente mit Kofaktor und Substrat scheiterten, sodass eventuelle Komplexbildungen nicht über die Strukturanalyse untersucht werden konnten. Mit den in der wissenschaftlichen Literatur veröffentlichten Strukturen für HpaB, HpaB-FAD und HpaB-FAD-Substrat und mit TcpA wurden Docking- und Modellierungsexperimente durchgeführt, um die Aminosäurereste zu bestimmen, die in TcpA-FAD und TcpA-TCP Komplex-Wechselwirkungen beteiligt sein könnten. So wurde gezeigt, dass die Aminosäuren P156, T192, Q451 an der TCPA-FAD Komplexbildung beteiligt sein könnten.

6.5 Ausblick

Um einen besseren Substratverbrauch zu ermöglichen, könnte man die reduzierte Form von Phenazin-1-Carboxylsäure (PCA) als Substrat benutzen. Aus der Literatur ist es bekannt, dass Zellen PCA in seiner reduzierten und nicht in der oxidierten Form produzieren, welche in den Experimenten dieser Arbeit verwendet wurde. Im Falle von TcpA hat das dreifach chlorierte Phenol (TCP) eine geringe Wasserlöslichkeit, was die Experimente erschwert. Durch Zugabe von kleinen Mengen an organischen Solventen wie DMSO könnte die Löslichkeit von TCP erhöht werden. Der Aromat mit drei Chloratomen ist wahrscheinlich elektronenarm und dadurch schwerer zu oxidieren.

Die biochemischen Experimente wurden mit der Flavin-Reduktase aus *E.coli* durchgeführt. Um eine bessere Flavin-Übertragung zu ermöglichen, könnte man die Experimente mit den Reduktasen, die jeweils zu der Monooxygenase aus *P. aureofaciens* und *C. necator* gehören, wiederholen.

SUMMARY AND OUTLOOK

Durch die Bestimmung der Proteinstrukturen von PhzO und TcpA und deren Vergleich mit dem HpaB-Modell wäre es möglich zu bestimmen, welche Aminosäuren an der Substratspezifität beteiligt sind, wodurch die Enzyme interessanter für die Biotechnologie werden. Aufgrund dieser Kenntnisse könnten Mutanten erzeugt werden und entweder heterolog in *E. coli* überexprimiert werden, um weitere biochemische Assays durchzuführen, oder in *P. aureofaciens*-Zellen eingeführt werden, um dort die 2-Hydroxy-Phenazinesäure (2OHPCA) Biosynthese zu untersuchen. Es wird davon ausgegangen, dass die Monooxygenasen, die in dieser Arbeit behandelt wurden, ein breites Spektrum an Substraten umfassen könnten. Screening dieser Enzyme gegen eine Klasse von Substratanalogs könnte noch unbekannt aber begehrte Funktionen zeigen.

Als eine weitere Methode zur Überwachung der Reaktion könnte man die O₂ Konzentration in der Reaktionslösung mittels einer Clark-Elektrode messen. Es ist bekannt, dass die Löslichkeit von O₂ in wässrigen Lösungen bei normalen Bedingungen etwa 7,6 mg l⁻¹ beträgt^[129]. Dieser Sauerstoff kann entweder bei der Hydroxylierung des Substrats oder bei der Reduktion zu H₂O₂ durch FADH₂ verwendet werden. Um eine H₂O₂-Ansammlung auf Kosten von gelöstem Sauerstoff zu verhindern, könnte man Katalase zu der Reaktionsmischung geben. Dadurch sollte die Effizienz des Substratumsatzes erhöht werden.

7. REFERENCES

- [1] Raitala A., Karjalainen J, Kosunen T., & Hurme M (2007). Helicobacter pylori-induced indoleamine 2,3-dioxygenase activity in vivo is regulated by TGFB1 and CTLA4 polymorphisms. *Molecular Immunology* 44, 1011-1014.
- [2] F.Peter Guengerich (2006). Cytochrome P450s and Other Enzymes in Drug Metabolism and Toxicity. *AAPS Journal* 8, 101-111.
- [3] Wolf D, Rumpold H, Moschen AR, Kaser A, Obrist P, Fuchs D, Brandacher G, Winkler C, Geboes K, Rutgeerts P, & Tilg H (2004). Overexpression of indoleamine 2,3-dioxygenase in human inflammatory bowel disease. *Clinical Immunology* 113, 47-58.
- [4] L.Daniel, R.Purich, & A.Donald (1994). *Handbook of biochemical kinetics*.
- [5] Osamu Hayaishi (2005). Fifty Years of Oxygen Activation. *Journal of Biological Inorganic Chemistry* 10.
- [6] NC-IUBMB (1956). Classification and Nomenclature of Enzymes by the Reactions they Catalyse.
- [7] Zelko IN, Mariani TJ, & Folz RJ. (2002). Superoxide dismutase multigene family: a comparison of the CuZn-SOD (SOD1), Mn-SOD (SOD2), and EC-SOD (SOD3) gene structures, evolution, and expression. *Free Radical Biology and Medicine* 33, 337-349.
- [8] Wackett LP, Kwart LD, & Gibson DT. (1988). Benzylic monooxygenation catalyzed by toluene dioxygenase from *Pseudomonas putida*. *Biochemistry* 27, 1360-1367.
- [9] Zhi Li, Jan B van Beilen, Wouter A Duetz, Andreas Schmid, Anna de Raadt, Herfried Grieng, & Bernard Witholt (2002). Oxidative biotransformations using oxygenases. *Current Opinion in Chemical Biology* 6, 136-144.
- [10] R.Ulrich & M.Hofrichter (2007). Enzymatic hydroxylation of aromatic compounds. *Cellular and Molecular Life Sciences* 64, 271-293.
- [11] S.M.Roberts & N.J.Turner (1992). Some recent developments in the use of enzyme catalysed reactions in organic synthesis. *Journal of Biotechnology* 22, 227-244.

REFERENCES

- [12] C.J.Schofield, J.E.Baldwina, M.F.Byforda, I.Cliftona, J.Hajdub, C.Hensgensa, & P.Roacha (1997). Proteins of the penicillin biosynthesis pathway. *Current Opinion in Structural Biology* 7, 857-864.
- [13] S.W.May (1979). Enzymatic epoxidation reactions. *Enzyme and Microbial Technology* 1, 15-22.
- [14] K.Drauz & H.Waldmann (2002). 2 ed., edited by Wiley-VCH Weinheim.
- [15] U.T.Bornscheuer & K.Buchholz (2007). Biocatalysis for pharmaceutical intermediates: the future is now. *Trends in Biotechnology* 25, 66-73.
- [16] Liese A. & Filho MV. (1999). Production of fine chemicals using biocatalysis. *Curr Opin Biotechnol.* 10, 595-603.
- [17] A.Schmid, J.S.Dordick, B.Hauer, A.Kiener, M.Wubbolts, & B.Witholt (2001). Industrial biocatalysis today and tomorrow. *Nature* 409, 258.
- [18] C.Wandrey, A.Liese, & D.Kihumbu (2000). Industrial biocatalysis: Past, present, and future. *Org. Process Res. Dev.* 4, 286.
- [19] A.J.J.Straathof, S.Panke, & A.Schmid (2002). The production of fine chemicals by biotransformations. *Current Opinion in Biotechnology* 13, 548.
- [20] S.Flitsch, G.Grogan, & D.Ashcroft (2002). III ed., edited by Wiley-VCH.
- [21] J.B.van Beilen, W.A.Duetz, A.Schmid, & B.Witholt (2003). Practical issues in the application of oxygenases. *Trends Biotechnol.* 21, 170-177.
- [22] Paul J.Loida & Stephen G.Sligar (1993). Molecular recognition in cytochrome P-450: Mechanism for the control of uncoupling reactions. *Biochemistry* 32, 11530-11538.
- [23] A.Z.Walton & J.D.Stewart (2004). Understanding and improving NADPH-dependent reactions by nongrowing *Escherichia coli* cells. *Biotechnol. Prog.* 20, 403-411.
- [24] W.A.Duetz, J.B.van Beilen, & B.Witholt (2001). Using proteins in their natural environment: potential and limitations of microbial whole-cell hydroxylations in applied biocatalysis. *Curr. Opin. Biotechnol.* 12, 419-425.
- [25] S.Narasimhulu (2007). Differential Behavior of the Sub-sites of Cytochrome P450 Active Site in Binding of Substrates and products (implications for coupling/uncoupling). *Biochim. Biophys. Acta* 1770, 360-375.

REFERENCES

- [26] V.Guallar, W.H.Miller, S.J.Lippard, & R.A.Friesner (2002). Dynamics of alkane hydroxylation at the non-heme diiron center in methane monooxygenase. *JACS* 124, 3377-3384.
- [27] B.J.Wallar & J.D.Lipscomb (1996). Dioxygen Activation by Enzymes Containing Binuclear Non-Heme Iron Clusters. *Chemical Reviews* 96, 2625-2658.
- [28] S.Chakraborty, M.Ortiz, B.Entsch, & D.P.Ballou (2010). Studies on the mechanism of p-hydroxyphenylacetate 3-hydroxylase from *Pseudomonas aeruginosa*: a system composed of a small flavin reductase and a large flavin-dependent oxygenase. *Biochemistry* 49, 372-385.
- [29] K.M.Meneely, E.W.Barr, J.M.Bollinger, & A.L.Lamb (2009). Kinetic mechanism of ornithine hydroxylase (PvdA) from *Pseudomonas aeruginosa*: substrate triggering of O₂ addition but not flavin reduction. *Biochemistry* 48, 4371-4376.
- [30] Schlegel H. & Zaborosch C. (1992). *Allgemeine Mikrobiologie*.
- [31] W.Blankenfeldt (2011). Strukturgestützte Untersuchungen zur Phenazin-Biochemie.
- [32] Ahuja E., Bayer P., Blankenfeldt W., Janning P., Herde P., Mavrodi D., & Thomashow.L. (2006). Die Biosynthese von Phenazinen.
- [33] Delaney S., Mavrodi D., & Thomashow.L. (2001). *phzO*, a Gene for Biosynthesis of 2-Hydroxylated Phenazine Compounds in *Pseudomonas aureofaciens* 30-84. *Journal of Bacteriology* 183, 318-327.
- [34] Willetts, H. J. & Bullock, S. (1992). Developmental biology and sclerotia. *Mycol. Res.* 96, 801-816.
- [35] Kevin D.Young (2006). The Selective Value of Bacterial Shape. *Microbiology and Molecular Biology Reviews* 70, 660-703.
- [36] Anzai et al., Kim H., Park J.Y., Wakabayashi H., & Oyaizu H. (2000). Phylogenetic affiliation of the pseudomonads based on 16S rRNA sequence. *Int J Syst Evol Microbiol* 50, 1563-1589.
- [37] Chin-A-Woeng TF et al. (2000). Root colonization by phenazine-1-carboxamide-producing bacterium *Pseudomonas chlororaphis* PCL1391 is essential for biocontrol of tomato foot and root rot. *Mol Plant Microbe Interact* 13, 1340-1345.
- [38] G.M.York, J.Lupberger, J.Tian, A.G.Lawrence, J.A.Stubbe, & A.J.Sinskey (2003). *Ralstonia eutropha* H16 Encodes Two and Possibly Three Intracellular Poly[D-(L)-3-Hydroxybutyrate] Depolymerase Genes. *Journal of Bacteriology* 185, 3788-3794.

REFERENCES

- [39] Schwartz E., Henne A., Cramm R., Eitinger T., Friedrich B., & Gottschalk G. (2003). Complete nucleotide sequence of pHG1: a *Ralstonia eutropha* H16 megaplasmid encoding key enzymes of H₂-based lithoautotrophy and anaerobiosis. *J Mol Biol.* 332, 369-383.
- [40] Pohlmann A., Fricke W., Reinecke F., Kusian B., Liesegang H., Eitinger T., Ewering C., Pötter M., Schwartz E., Strittmatter A., Voß I., Friedrich B., Gottschalk G, Steinbüchel A., & Bowien B. (2006). Genome sequence of the bioplastic-producing "Knallgas" bacterium *Ralstonia eutropha* H16. *Nature Biotechnology* 24, 1257-1262.
- [41] Ahuja E., Janning P., Mentel M., Graebisch A., Breinbauer R., Hiller W., Costisella B., Thomashow L., Mavrodi D., & Blankenfeldt W. (2008). PhzA/B Catalyzes the Formation of the Tricycle in Phenazine Biosynthesis. *Journal of the American Chemical Society* 130, 17053-17061.
- [42] Blankenfeldt W. (2009). Skript zum „Wahlpflichtpraktikum Proteinexpression, Modifikation und Kristallisation“ an der Technischen Universität Dortmund, Studiengang Master Chemische Biologie.
- [43] K.Seong-Hoon, H.Tamao, T.Kazuki, I.Wakana, E.Akio, & M.Kunio (2007). Crystal Structure of the Oxygenase Component (HpaB) of the 4-Hydroxyphenylacetate 3-Monooxygenase from *Thermus thermophilus* HB8. *The Journal of Biological Chemistry* 282, 33107-33117.
- [44] Copeland R.A. (1994)., edited by N. Y. Chapman & Hall, pp. 62-71.
- [45] A.J.Messenger & J.M.Turner (1983). Phenazine-1,6-dicarboxylate and its dimethyl ester as precursors of other phenazines in bacteria. *FEMS Microbiology Letters* 18, 65-68.
- [46] M.E.Hernandez, A.Kappler, & D.K.Newman (2004). Phenazines and Other Redox-Active Antibiotics Promote Microbial Mineral Reduction. *Appl. Environ. Microbiol.* 70, 921-928.
- [47] A.Price-Whelan, L.E.Dietrich, & D.K.Newman (2006). Rethinking 'secondary' metabolism: physiological roles for phenazine antibiotics. *Nat. Chem. Biol.* 2, 71-78.
- [48] L.Thomashow & D.M.Weller (1988). Role of a phenazine antibiotic from *Pseudomonas fluorescens* in biological control of *Gaeumannomyces graminis* var. *tritici*. *J Bacteriol.* 180, 3499-3508.
- [49] F.C.Thomas Chin-A-Woeng, G.V.Bloemberg, & B.J.J.Lugtenberg (2003). Phenazines and their role in biocontrol by *Pseudomonas* bacteria. *New Phytologist* 157, 503-523.

REFERENCES

- [50] J.B.Laursen & J.Nielsen (2004). Phenazine natural products: biosynthesis, synthetic analogues and biological activity. *J. Chem. Rev.* *104*, 1663-1685.
- [51] P.Chaiyen, C.Suadee, & P.Wilairat (2001). A novel two-protein component flavoprotein hydroxylase. *Eur. J. Biochem* *268*, 5550-5561.
- [52] Thotsaporn K., Sucharitakul J., Wongratana J., Suadee C., & Chaiyen P. (2004). Cloning and expression of p-hydroxyphenylacetate 3-hydroxylase from *Acinetobacter baumannii*: evidence of the divergence of enzymes in the class of two-protein component aromatic hydroxylases. *Biochim Biophys Acta.* *1680*, 60-66.
- [53] Arunachalam U. & Massey V. (1994). Studies on the oxidative half-reaction of p - hydroxyphenylacetate 3-hydroxylase. *J. Biol. Chem.* *269*, 11795-11801.
- [54] Chakraborty S., Ortiz-Maldonado M., Eschenburg K., Entsch B., & Ballou D. (2005). Flavins and Flavoprotein. *Architect* 161-166.
- [55] Sucharitakul J., Chaiyen P., Entsch B., & Ballou D. (2005). The reductase of p-hydroxyphenylacetate 3-hydroxylase from *Acinetobacter baumannii* requires p-hydroxyphenylacetate for effective catalysis. *Biochemistry* *30*, 10434-10442.
- [56] Ballou D., Entsch B., & Cole L. (2005). Dynamics involved in catalysis by single-component and two-component flavin-dependent aromatic hydroxylases. *Biochemical and Biophysical Research Communications* *338*, 590-598.
- [57] Palfey B., Ballou D., & Massey V. (1995). Oxygen activation by flavins and pterins. Active Oxygen in Biochemistry. *Blackie Academic and Professional* 37-83.
- [58] G.R.Moran, B.Entsch, B.A.Palfey, & D.P.Ballou (1997). Electrostatic effects on substrate activation in *para*-hydroxybenzoate hydroxylase: studies of the mutant lysine 297 methionine. *Biochemistry* *36*, 7548-7556.
- [59] Palfey B. & Massey V. (1998). Flavin-dependent enzymes. *Comprehensive Biological Catalysis III*, 83-154.
- [60] Ruangchan N., Tongsook C., Sucharitakul J., & Chaiyen P. (2011). pH-dependent Studies Reveal an Efficient Hydroxylation Mechanism of the Oxygenase Component of p-Hydroxyphenylacetate 3-Hydroxylase. *J. Biol. Chem.* *286*, 223-233.
- [61] Webb B., Ballinger J., Kim E., Belchik S.M., Lam K.-S., Youn B., Nissen M.S., Xun L., & Kang C. (2010). Characterization of Chlorophenol 4-Monooxygenase (TftD) and NADH:FAD Oxidoreductase (TftC) of *Burkholderia cepacia* AC1100. *J. Biol. Chem.* *285*, 2014-2027.

REFERENCES

- [62] Belchik S.M. & Xun L. (2008). Functions of Flavin Reductase and Quinone Reductase in 2,4,6-Trichlorophenol Degradation by *Cupriavidus necator* JMP134. *J. Bacteriol.* 190, 1615-1619.
- [63] Galán B., Díaz E., Prieto M., & García J.L. (2000). Functional Analysis of the Small Component of the 4-Hydroxyphenylacetate 3-Monooxygenase of *Escherichia coli* W: a Prototype of a New Flavin:NAD(P)H Reductase Subfamily. *Journal of Bacteriology* 182, 636.
- [64] Jones K.C. & Ballou D. (1986). Reactions of the 4A-Hydroperoxide of Liver Microsomal Flavin-Containing Monooxygenase with Nucleophilic and Electrophilic Substrates. *J Biol Chem* 6, 2553-2559.
- [65] Ziegler D.M. (2002). An overview of the mechanism, substrate specificities, and structure of FMOs. *Drug Metab Rev.* 34, 503-511.
- [66] Phillips I.R. & Shephard E.A. (2008). Flavin-containing monooxygenases: mutations, diseases and drug response. *Trends Pharmacol Science* 29, 264-301.
- [67] Kim Y.M. & Ziegler D.M (2000). Size limits of thiocarbamides accepted as substrates by human flavin-containing monooxygenase 1. *Drug Metab Dispos* 8, 1003-1006.
- [68] Abramovitch R.A. & Capracotta M. (2003). Remediation of waters contaminated with pentachlorophenol. *Chemosphere* 50, 955-957.
- [69] Kot-Wasik, R.Kartanowicz, D.Dbrowska, & J.Namieczenik (2004). Determination of chlorophenols and phenoxyacid herbicides in the Gulf of Gdańsk, southern Baltic Sea. *Bulletin of Environmental Contamination and Toxicology* 73, 511-518.
- [70] Machera K., Miliadis G.E., Anagnostopoulos E., & Anastassiadou P. (1997). Determination of pentachlorophenol in environmental samples of the S. Euboic Gulf, Greece. *Bulletin of Environmental Contamination and Toxicology* 59, 909-916.
- [71] D.D.Jiayin, X.Muqi, C.Jiping, Y.Xiangping, & K.Zhenshan (2007). PCDD/F, PAH and heavy metals in the sewage sludge from six wastewater treatment plants in Beijing, China. *Chemosphere* 66, 353-361.
- [72] Virendra and Pandey S.D. (2004). Hazardous waste, impact on health and environment for development of better waste management strategies in future in India. *Environment International* 34, 417-431.

REFERENCES

- [73] R.Götz, O.-H.Bauer, P.Friesel, T.Herrmann, E.Jantzen, M.Kutzke, R.Lauer, O.Paepke, K.Roch, U.Rohweder, R.Schwartz, S.Sievers, & B.Stachel (2007). Vertical profile of PCDD/Fs, dioxin-like PCBs, other PCBs, PAHs, chlorobenzenes, DDX, HCHs, organotin compounds and chlorinated ethers in dated sediment/soil cores from flood-plains of the river Elbe, Germany. *Chemosphere* 67, 592-603.
- [74] Ahlborg U.G., Lindgren J.E., & Mercier M. (1974). Metabolism of pentachlorophenol. *Arch. Toxicol.* 32, 271-281.
- [75] Ahlborg U.H. & Thunberg T.M. (1980). Chlorinated phenols: Occurrence, toxicity, metabolism and environmental impact. *CRC Crit. Rev. Toxicol.* 7, 1-35.
- [76] Mitchell R.A., Loeschcke H.H., Massion W.H., & Severinghaus J.W. (1961). Physiologic significance of superficial medullary respiratory chemosensitivity. *Physiologist* 4, 74.
- [77] Kellner D.G., Mavest S.A., & Sligar S.G. (1997). Engineering cytochrome P450s for bioremediation. *Current Opinion in Biotechnology* 8, 274-276.
- [78] K.-H.van Pee & S.Unversucht (2003). Biological dehalogenation and halogenation reactions. *Chemosphere* 52, 299-312.
- [79] Lamar R.T., Glaser J.A., & Kirk T.K. (1990). Fate of pentachlorophenol in sterile soils inoculated with the white-rot basidiomycete *Phanerochaete chrysosporium*: mineralization, volatilization and depletion of PCP. *Soil Biology & Biochemistry* 22, 433-440.
- [80] Lestan, D. & Lamar, R. T. (1996). Development of fungal inocula for bioaugmentation of contaminated soils. *Applied and Environmental Microbiology* 62, 2045-2052.
- [81] BOLLAG J.-M. (1992). Decontaminating soil with enzymes. *Environmental Science Technology* 26, 1876-1881.
- [82] Vandamme P. & Coenye T. (2004). Taxonomy of the genus *Cupriavidus*: a tale of lost and found. *Int J Syst Evol Microbiol* 54, 2285-2289.
- [83] Kosako Y., Yano I., Hotta H., & Nishiuchi Y. (1995). Transfer of two *Burkholderia* and an *Alcaligenes* species to *Ralstonia* gen. nov.: proposal of *Ralstonia pickettii* (Ralston, Palleroni and Doudoroff 1973) comb. nov., *Ralstonia solanacearum* (Smith 1896) comb. nov. and *Ralstonia eutropha* (Davis 1969) comb. nov. *Microbiology and Immunology* 11, 897-904.
- [84] Plumeier I., Perez-Pantoja D., Heim S., Gonzalez B., & Pieper, D. H. (2002). Importance of different *tfd* genes for degradation of chloroaromatics by *Ralstonia eutropha* JMP134. *Journal of Bacteriology* 184, 4054-4064.

REFERENCES

- [85] Schneider J., Grosser RJ, Jayasimhulu K., Xue W., Kinkle B., & Warshawsky D. (2000). Biodegradation of carbazole by *Ralstonia* sp. RJGII.123 isolated from a hydrocarbon contaminated soil. *Can J Microbiol.* 46, 269-277.
- [86] <http://genome.jgi-psf.org/raleu/raleu.home.html> (2011).
- [87] Louie, T. M., C.M.Webster, & L.Xun (2002). Genetic and biochemical characterization of a 2,4,6-trichlorophenol degradation pathway in *Ralstonia eutropha* JMP134. *J. Bacteriol.* 184, 3492-3500.
- [88] Padilla L., Matus V., Zenteno P., & onzález B. (2002). Degradation of 2,4,6-trichlorophenol via chlorohydroxyquinol in *Ralstonia eutropha* JMP134 and JMP222. *J. Basic. Microbiol.* 40, 243-249.
- [89] Matus V., Sánchez M.A., Martínez M., & González B. (2003). Efficient Degradation of 2,4,6-Trichlorophenol Requires a Set of Catabolic Genes Related to tcp Genes from *Ralstonia eutropha* JMP134(pJP4). *Applied and Environmental Microbiology* 69, 7108-7115.
- [90] Sanchez M.A. & Gonzalez B. (2007). Genetic Characterization of 2,4,6-Trichlorophenol Degradation in *Cupriavidus necator* JMP134. *Applied and Environmental Microbiology* 73, 2769-2776.
- [91] Gisi M.R. & L.Xun (2005). Characterization of chlorophenol 4-monooxygenase (TftD) and NADH:flavin adenine dinucleotide oxidoreductase (TftC) of *Burkholderia cepacia* AC1100. *J. Bacteriol.* 185, 2786-2792.
- [92] Hübner A., Danganan C.E., Xun L., Chakrabarty A.M., & Hendrickson W. (1998). Genes for 2,4,5-trichlorophenoxyacetic acid metabolism in *Burkholderia cepacia* AC1100: characterization of the tftC and tftD genes and location of the tft operons on multiple replicons. *Appl. Environ. Microbiol.* 64, 2086-2093.
- [93] Bohuslavsek J., ayne J.W., olton H.Jr., & un L. (2001). Cloning, sequencing, and characterization of a gene cluster involved in EDTA degradation from the bacterium BNC1. *Appl. Environ. Microbiol.* 67, 688-695.
- [94] Eichhorn E., J.R.van der Ploeg, & T.Leisinger (1999). Characterization of a two-component alkanesulfonate monooxygenase from *Escherichia coli*. *J. Biol. Chem.* , 274, 26639-26646.
- [95] Xu Y., M.W.Mortimer, T.S.Fisher, M.L.Kahn, F.J.Brockman, & L.Xun (1997). Cloning, sequencing, and analysis of a gene cluster from *Chelatobacter heintzii* ATCC 29600 encoding nitrilotriacetate monooxygenase and NADH:flavin mononucleotide oxidoreductase. *J. Bacteriol.* 179, 1112-1116.

REFERENCES

- [96] Wieser M., B.Wagner, J.Eberspächer, & F.Lingens (1997). Purification and characterization of 2,4,6-trichlorophenol-4-monooxygenase, a dehalogenating enzyme from *Azotobacter* sp. strain GP1. *J. Bacteriol.* 179, 202-208.
- [97] Xun L. & C.M.Webster (2004). A monooxygenase catalyzes sequential dechlorinations of 2,4,6-trichlorophenol by oxidative and hydrolytic reactions. *J. Biol. Chem.* 279, 6696-6700.
- [98] Sanger F. et al. (1977). DNA sequencing with chain-terminating inhibitors. *Proceedings of the National Academy of Sciences U. S. A.* 74, 5463-5469.
- [99] Hansen L.H., Knudsen S., & Sørensen S.J. (1998). The effect of the lacY gene on the induction of IPTG inducible promoters, studied in *Escherichia coli* and *Pseudomonas fluorescens*. *Curr. Microbiol.* 6, 341-347.
- [100] Studier F.W. (2005). Protein production by auto-induction in high density shaking cultures. *Protein Expr Purif.* 1, 234.
- [101] Mihasan M., Ungureanu E., & Artenie V. (2004). Optimum parameters for overexpression of recombinant protein from tac promoters on autoinducible medium. *Romanian Biotechnological Letters.*
- [102] Bradford M. (1976). A Rapid and Sensitive Method for the Quantitation of Microgram Quantities of Protein Utilizing the Principle of Protein-Dye Binding. *Anal. Biochem.* 72, 248-254.
- [103] Lottspeich F. & Joachim W. (2006). *Bioanalytik*. München.
- [104] www.microcal.com (2011).
- [105] Wiseman T., Williston S., Brandts J.F., & Lin L.N. (1989). Rapid measurement of binding constants and heats of binding using a new titration calorimeter. *Anal. Biochem.* 179, 131-137.
- [106] Fisher H.F. & Singh N. (1995). Calorimetric methods for interpreting protein-ligand interactions. *Methods in Enzymology.* 259, 194-221.
- [107] Jelesarov I. & Bosshard H.R. (1999). Isothermal titration calorimetry and differential scanning calorimetry as complementary tools to investigate the energetics of bimolecular recognition. *J. Molec. Recog.* 12, 3-18.
- [108] www.chm.bris.ac.uk/ms/theory/quad-massspec.html (2011).
- [109] [www.umass.edu/karbon13/images/Link 1 ESI MS.JPG](http://www.umass.edu/karbon13/images/Link%201%20ESI%20MS.JPG) (2011).
- [110] www.med4you.at/ (2011)

REFERENCES

- [111] [www.edu/karbon13/images/Link 1 ESI MS.JPG](http://www.edu/karbon13/images/Link_1_ESI_MS.JPG) (2011).
- [112] Guimbaud C., Bartels-Rausch T., & Ammann M. (2003). An atmospheric pressure chemical ionization mass spectrometer (APCI-MS) combined with a chromatographic technique to measure the adsorption enthalpy of acetone on ice (226), 279-290. *International Journal of Mass Spectrometry* 226, 279-290.
- [113] McRee D.E. (1993). *Practical Protein Crystallography*. New York.
- [114] Rhodes C. (1993). *Crystallography Made Crystal Clear: A Guide For Users Of Macromolecular Models*. New York.
- [115] Ramachandran G.N., Ramakrishnan C, & Sasisekharan (1963). Stereochemistry of polypeptide chain configuration. *Journal Molecular Biology* 7, 95-99.
- [116] [www.butane.chem.uiuc.edu/pshapley/GenChem2/A3/electromagnetic spectrum.jpg](http://www.butane.chem.uiuc.edu/pshapley/GenChem2/A3/electromagnetic_spectrum.jpg) (2011)
- [117] <http://journals.iucr.org/d/issues/1998/01/00/gr0693/gr0693fig1.gif> (2011)
- [118] Kabsch W. (1993). Automatic processing of rotation diffraction data from crystal of initially unknown symmetry and cell constants. *Journal of Applied Crystallography* 26, 795-800.
- [119] Potterton L., McNicholas S., Krissinel E., Gruber J., Cowtan K., Emsley P., Murshudov G.N., Cohen S., Perrakis A., & Noble M. (2004). Developments in the CCP4 molecular-graphics project. *Acta Crystallographica D60* 2288-2294.
- [120] Emsley P. & Cowtan K. (2004). Coot: model-building tools for molecular graphics. *Acta Crystallographica D60* 2126-2132.
- [121] Murshudov G.N., Vagin A.A., & Dodson E.J. (1997). Refinement of macromolecular structures by the maximum-likelihood method. *Acta Crystallographica* 3, 240-255.
- [122] Brünger A.T. (1992). A System for X-ray Crystallography and NMR X-PLOR. Version 3.1.
- [123] Kim S.H., Miyatake H., Hisano T., Ohtani N., & Miki K. (2003). Crystallization and preliminary X-ray analysis of the small component of 4-hydroxyphenylacetate 3-monooxygenase (HpaC) and its cofactor complex from *Thermus thermophilus* HB8. *Acta Crystallographica D Biological Crystallography* 12, 2275-2278.

REFERENCES

- [124] Kim S.H., Miyatake H., Hisano T., Iwasaki W., Ebihara A., & Mikiab K. (2007). Crystallization and preliminary X-ray analysis of the oxygenase component (HpaB) of 4-hydroxyphenylacetate 3-monooxygenase from *Thermus thermophilus* HB8. *Acta Crystallographica Sect. F Struct. Biol. Commun.* 63, 556-559.
- [125] Winn M., Isupov M., & Murshudov G.N. (2001). Use of TLS parameters to model anisotropic displacements in macromolecular refinement. *Acta Cryst. D* 57, 122-133.
- [126] Tischler D., Kermer R., rönig A.D., aschabek S., illem J.H.van Berkel, & chlömänn M. (2010). StyA1 and StyA2B from *Rhodococcus opacus* 1CP: a Multifunctional Styrene Monooxygenase System. *Journal of Bacteriology* 192, 5220-5227.
- [127] Ukaegbu U.E. & Rosenzweig A.C. (2009). Structure of the redox sensor domain of *Methylococcus capsulatus* (Bath) MmoS. *Biochemistry* 48, 2207-2215.
- [128] Diederichs K. & Karplus P.A. (1997). Improved R-factors for diffraction data analysis in macromolecular crystallography. *Nature Structural Biology* 4, 269-275.
- [129] Emsley J. (2001). "Oxygen". *Nature's Building Blocks: An A-Z Guide to the Elements.* Oxford University Press. 297-304.
- [130] A.Kantz, F.Chin, N.Nallamotheu, T.Nguyen, & G.T.Gassner (2011). Mechanism of flavin transfer and oxygen activation by the two-component flavoenzyme styrene monooxygenase. *Archives of Biochemistry and biophysics* 442, 102-116.
- [131] Robert P.Hausinger (2004). Fe(II)/ α -Ketoglutarate-Dependent Hydroxylases and Related Enzymes. *Critical Reviews in Biochemistry and Molecular Biology* 39, 21-68.
- [132] Brolin SE & Agren A (1977). Assay of flavin nucleotides in pancreatic islets by a differential fluorimetric technique. *Biochem J.* 163, 159-162.

8. APPENDICES

Sequence alignment of PhzO, TcpA and HpaB

```

          10      20      30      40      50      60
          |      |      |      |      |      |
PhzOxx0  MLDFQNKRYLKSAESFKASLRDNR-TVIYQGVVEDVTTHFSTAGGISQVAEIEYEEQFS
TcpAxx1  -----MIRTKGQYLESLNDGR-NVWVGNEKIDNVATHPKTRDYAQRHADFYDLHHR
HpaBxx2  -----MARTGAEYIEALKTRPPNLWYKGEKVEDPTTHPVFRGIVRTMAALYDLQHD
          : : : : : * : : : : : : : : : : * : : : : :
Prim.cons. MLDFQNKRKM3RTG33Y3ESL3D3RPNVWY3GEKVEDVTTHP3TRG33333A33YDLQH3

          70      80      90      100     110     120
          |      |      |      |      |      |
PhzOxx0  GEHDDILTYVRPDGYLASSAYMPPRNKEDLASRRRAIMYVSQKTWG-THCRNLDMIASF
TcpAxx1  PDLQDVMTFVVDKDGERRTMQWFGHYDKQLRRKRKYHETIMREMAGASFPRTPDVNNYVL
HpaBxx2  PRYREVLTYEE-EGKRHGMSFLIPKTKEDLKRKGQAYKLWADQNLG-MMGRSPDYLNAV
          : : : : : * : : : : : * : : : : : * : : : : :
Prim.cons. P333DVLTYV32DG3R33M3333P33KEDL3RRR3A3333333333GA333R3PD33N3V3

          130     140     150     160     170     180
          |      |      |      |      |      |
PhzOxx0  VGMMGYLPTFR-----KKCPEYAEENITEYHDYAERNLSLYLSETIVDPQGYRARTHGTDLN
TcpAxx1  QTYIDDPSPWETQTIGAEGKVKAKNIVDFVNFVAKKHDLNCAAPQFVDPQMDRSNPDAQQRS
HpaBxx2  MAYAASADYFG-----EFAENVRNRYRRLDQDLATTHALTNPQVNRARPPSGQPD
          : : : : : * : : : : : : : : : : * : : : : :
Prim.cons. 33Y333333F3TQTIG2222E3AENI33Y33YA333DL333333VDPQ33RARP333Q33

          190     200     210     220     230     240
          |      |      |      |      |      |
PhzOxx0  LPPPDRAVMRINKQNAEGIWIISGVKGVGTAAPQSNEIFVGSLEFPAAPEES--FWAYVPVD
TcpAxx1  P-----GLRVIKNDKGIIVSVGKAI GTGVAFADWIIHIGVFFRPGIPGDQIIFAATPVN
HpaBxx2  PY----IPVGVVKQTEKGIIVRGARMTATFPLADEVLIFPSILLQAGSEKYALAFALPTS
          : : : : : * : : : : : * : : : : : : : : : : * : :
Prim.cons. P2PPDR233RV3KQN3KGIIVSVGK33GT3333333I33GS3F33A33E32233AA3PV3

          250     260     270     280     290     300
          |      |      |      |      |      |
PhzOxx0  APGVKIFCREIVSQPHASAYDHPLISKGEEAEAMVVFNDNVFIPRWRIMAANVPELAS-AG
TcpAxx1  TPGVTIVCRESVVKED--PIEHPLASQGDELDGMTVFDNVFIPWSHVFLGNPEHAK--L
HpaBxx2  TPGLHFVCREALVGGDS-PFDHPLSSRVEEMDCLVIFDDVLPWERVFILGNVELCNNAY
          : * : : : * : : : : * : : : : * : : : : * : : : : * : :
Prim.cons. TPGV3IVCRE3VV33D2SP3DHPL3S3GEE3D3MVVFNDNVFIPW3RVF3LGNPELA3NA3

          310     320     330     340     350     360
          |      |      |      |      |      |
PhzOxx0  FFSLWTSYSHWYTLVRLETKADLYAGLAKVIMEVLGLEGIADVVRQVSEIVQLAEIILKGM
TcpAxx1  YPQRVFDWLHYHALIRQSVRAELMAGLAILITEHIGTNKIPAVQTRVAKLIGFHQAMLAH
HpaBxx2  GATGALNHMAHQVVALKTAKTEAFLGVAALMAEGIGADVYGHVQEKIAEIIIVYLEAMRAF
          . : : : : * : : : : * : : : : * : : : : : : : :

```

```

Prim.cons.  333333333H333L3R333KAEL3AGLA3LI3E3IG333I33VQ3RVAEII333EAM3A3

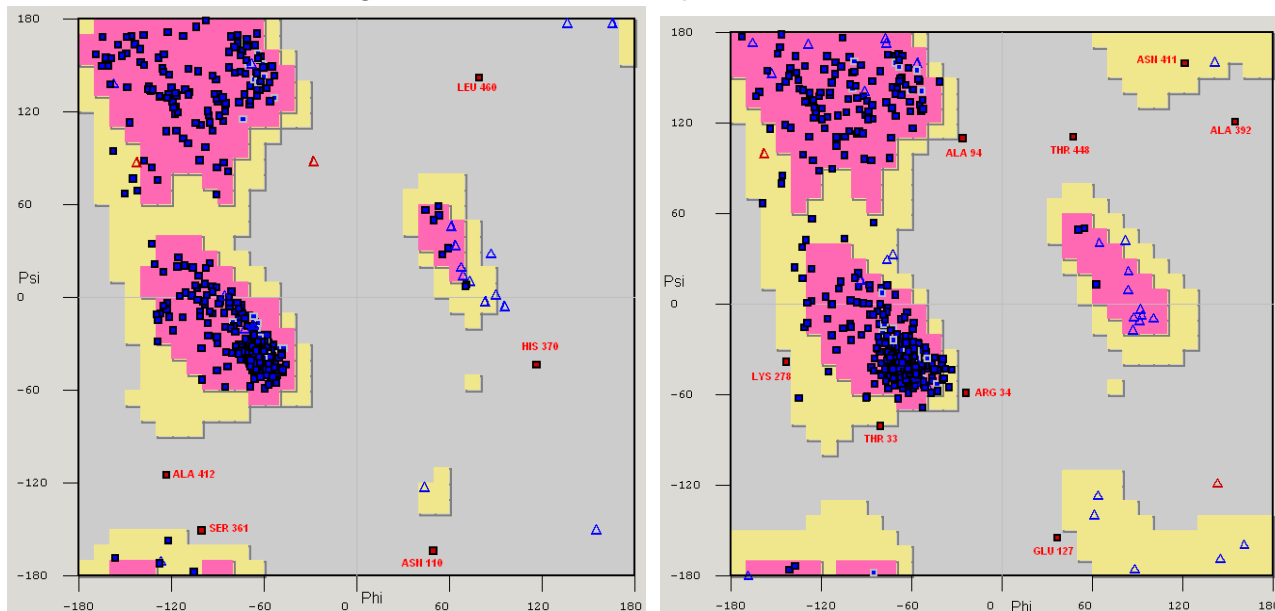
              370      380      390      400      410      420
              |       |       |       |       |       |
PhzOxx0     CIASIETAEMSDGDILLPGHNALAAGRVFAMEEKLPRVLHLLRELCQGLIILRFNEKDLAA
TcpAxx1     IVASEELGFHTPGGAYKPNILYDFGRALYLENFSQMIYELVDLSGRSALIFASE-DQWN
HpaBxx2     WTRAEEEAKENAYGLLVPDRGALDGARNLYPR-LYPRIREILEQIGASGLITLPS-EKDF
              : * . . . * . * : . : : : : * . : : . :
Prim.cons.  33ASEE3A3333GG3L3P333ALD3GR3LY3E2L333I3EL3EL3G3S3LI333EKD333

              430      440      450      460      470      480
              |       |       |       |       |       |
PhzOxx0     DAAFGQKFSWFLDTQSVGAREKNLLMNLVWDVAASEHSTRALVFEEQHALSEPLLRDNLV
TcpAxx1     DEALNGWFERMNNGPVQPHDRVKIGRVIRDLFLTDWGNRLFVENFNGTPLQAIRMLTM
HpaBxx2     KGPLGPFLEKFLQGAALEAKERVALFRLAWDMTLSGFGARQELYERFFFG--DPVRMYQT
              . . : . : : : . : : : * : : . * : : * . : *
Prim.cons.  D3ALG33FE3FL3G3333A3ERV3L3RL3WD33LS33G3R33VFE3F33322333RM333

              490      500      510      520      530
              |       |       |       |       |
PhzOxx0     LDYDYRES-----TSLIRRLVGLNAK---
TcpAxx1     QRAEFSAAGPYGTLARKVCGIELTEGHDSEYKATAGYAQALDSARHQEKLALSGTMTV
HpaBxx2     LYNVYNKE-----P-----YKERIHAFLKESLKVFEEVQA-
              :                               : . . : .
Prim.cons.  L333Y333GPYGTLARKVCGIELTEGHD2EYKATAGY2222233L333L33L33322V

```

The Ramachandran diagrams for PhzO and TcpA



PhzO	TCPA
In Preferred Regions: 614 (96.65%)	In Preferred Regions: 431 (92.89%)
In Allowed Regions: 9 (1.89%)	In Allowed Regions: 23 (4.96%)
Outliers: 7(1.47%)	Outliers: 10 (2.16%)

9. ACKNOWLEDGMENTS

I am very thankful to Prof. Dr. Wulf Blankenfeldt for accepting me as a PhD student in his group and for providing the kind of supervision any student would wish for. I sincerely thank him for his constant support, constructive guidance and active encouragement throughout my work that helped me visibly improve my knowledge.

I wish to thank Prof. Dr. Roland Winter (Technical University Dortmund, Department of Physical Chemistry I) for being my second supervisor and in the examination committee.

Special thanks to Prof. Dr. Roger S. Goody for giving me the chance to carry out my PhD studies at the Max Planck Institute Dortmund and also for his constant support throughout these years.

I wish to thank Dr. Linda Thomashow, Dr. Luying Xun and Dr. Dmitri Mavrodi, our collaborators in US who provided me with materials and useful informations.

I would like to thank Michael Weyand, Georg Holtermann, Ingrid Vetter and other members of MPI-Dortmund/Heidelberg X-ray community for qualified technical support in x-ray crystallography.

Special thanks go to members of the former AG Blankenfeldt in MPI Dortmund. Petra, thank you for your excellent technical assistance.

To my mother and sisters, my deep gratitude for their loving support and trust!

LEBENS LAUF

Persönliche Daten

Name	Emerich Mihai Gazdag
Geburtsdatum und -ort	20. Dezember 1978, Carei, Rumänien
Familienstand	ledig

Schul Ausbildung

09/1985 – 07/1989	Grundschule, Sanislau, Rumänien
09/1989 – 07/1993	Gymnasium, Sanislau, Rumänien
09/1993 – 07/1997	George-Cosbuc-Gymnasium, Cluj Napoca, Rumänien
07/1997	Abitur

Universitätsausbildung

10/1997 – 06/2002	Biologie und Chemie an der deutschen Fakultät der Universität "Babes Bolyai" in Cluj Napoca, Rumänien
10/2004 – 09/2006	Studiengang Chemische Biologie, Technische Universität Dortmund
01/2005 – 07/2005	Diplomarbeit, Max-Planck-Institut für Molekulare Physiologie und Universität Babes-Bolyai Cluj Napoca, Arbeitskreis Prof. Dr. W. Blankenfeldt: „Klonierung und Expression des Serin/Threonin kinase rezeptor assoziierten Proteins STRAP“
02/2006	Diplom in Biologie und Chemie an der Universität „Babes-Bolyai“ von Cluj Napoca (Klausenburg, Rumänien)
01/2007 – 06/2011	Promotionsstudium in der Arbeitsgruppe von Prof. Dr. Wulf Blankenfeldt am Max Planck Institut für Molekulare Physiologie Dortmund

EIDESSTATTLICHE ERKLÄRUNG

Hiermit versichere ich an Eides statt, dass ich die vorliegende Arbeit selbständig und nur mit den angegebenen Hilfsmitteln angefertigt habe.

Dortmund, den

Emerich Mihai Gazdag